University of Alberta

Modeling sea ice in Hudson Bay from a polar bear (*Ursus maritimus*) perspective

by

Laura Castro de la Guardia

A thesis submitted to the Faculty of Graduate Studies and Research
in partial fulfillment of the requirements for the degree of

Master of Science

Earth and Atmospheric Sciences

Fall 2012
Edmonton, Alberta

Abstract

Sea ice concentration (SIC), the length of the ice-free period, and the break-up date are correlated with the survival and reproduction success of polar bears (*Ursus maritimus*) in Western Hudson Bay (WH). I use a high-resolution sea ice-ocean model to predict these parameters through the 21st century and to assess the threat on polar bears in WH. The model was validated and calibrated with GPS-data from polar bears in WH. Predictions are based on the IPCC greenhouse gas-emission scenarios: B1, A1B and A2. The model predicted significant changes in WH spring SIC in A1B and A2, and in the seasonal ice cycle in B1, A1B and A2. From 2061-2100, the mean break-up date advances 15.7 days (B1), 31.5 days (A1B), and 46 days (A2), and the mean ice-free period lengthens by 4.5 weeks (B1), 8.4 weeks (A1B), and 12.5 weeks (A2). Should the model projections be realized, a viable population of polar bears will not likely persist in WH until the end of this century.

Acknowledgments

A large part of my gratitude is to my supervisors Paul Myers and Andrew Derocher, for their guidance, patience, funding, and encouragements. Also to Arjen Terwisscha van Scheltinga for his assistance with the sea ice-ocean model, and Matlab-coding, and to Nick Lunn from Environment Canada, for assisting in the polar bear data collection and his tutorship during field-trip and in posters and abstracts presentations. Big big thanks to my parents (Elena de la Guardia & Rafael Castro) who help me with their guidance and also funding, and to all my family and friends, in Cuba and Canada, that even from a distance where able to transmit the feeling of support, encouraging, and love: Lourdes, Emma, Ele, Ruth, Lazaro, Tere, Cristy, Ayla, Tani, Lisi, Anu, Alo, Lily, Mario, Mayito, Erne, Carmen, Ale, Lina, Alia, Dany and Rafy and others.

A special gratitude and thanks to friends like: Julian Beaudry who spent many hours proofed-reading the thesis and all other assignments during the Master's degree, Jean-Baptiste Tary, who helped in the editing of the final versions of the thesis, and Qian Duanni, for her company during late hours and weekends while writing in our office: thank you for keeping the office's light ON! Other friends who also made a difference are Xianmin Hu, Anna Katavouta, Veluthedath Kuzhiyil Praveen, Qiang Wang, Veronique Lago, Colin More, from the physics department, and Stephen Hamilton, Barry Robinson, Marie Auger-Methe, Nick Pilfold, Alysa McCall, Evan Richardson, Pat Mislan, Vicki Sahanatien, from the biology department. They all helped in many ways to shape the final version of this thesis.

Lastly, I will like to recognize the institutions and associations that contributed to found this project: EnviroNorth, ArcticNet, International Association for Impact Assessment-Western and Northern Canada, Environement Canada, Polar Bears International, WWF Canada, Quark Expeditions, and NSERC, and the University of Alberta through the Department of Earth and Atmospheric Sciences, the Faculty of Graduate Studies (FGSR): J Gordin Kaplan Graduate Student Award, the Graduate Students Association (GSR): Professional Development Grant, and the Institute for Geophysical Research (IGR): Hibb's Student Conference Travel Award.

I am thankful to all for making this journey an enjoyable and exciting learning experience.

TABLE OF CONTENTS

LIST OF TABLES

LIST OF FIGURES

LIST OF ABBREVIATIONS

20C3M	Refers to the 20st century run of the CGCM
A1B	IPCC scenario in which CO_2 concentrations increases to 720 ppm
A2	IPCC scenario in which CO_2 concentrations increases to 800 ppm
B1	IPCC scenario in which CO_2 concentrations increases to 550 ppm
CCCma	Canadian Center of Climate modeling and analysis
CGCM	Canadian Global Climate Model
CIS	Canadian Ice Service
EVP	Elastic-Viscous-Plastic rheology
FESOM	Finite element sea ice ocean model
Gmsh	Mesh generator from Wessel and Smith (1996)
Gmsh	Unstructured triangular mesh generator
GPS	Global Positioning System
HB	Hudson Bay
IPCC	Intergovernmental Panel for Climate Change
JB	James Bay
NCAR /NCEP	National Center of Atmospheric Research/National Center of Environmental prediction
NCEP/DOE	National Center of Atmospheric Research/Department of Energy
NH	Northern Hemisphere
NOAA/OAR/ESRL PSD	National Oceanic Atmospheric Research/ Office of Oceanic and Atmospheric research/ Earth System Research Laboratory, Physical Science Division
	In conjunction, these offices (in Boulder, Colorado, USA) developed and provide the NCEP/NCAR and NCEP/DOE

data sets.

CO_2	Carbon dioxide
PHC	Polar Science Center of Hydrographic Climatology
PMW-BS	Passive Microwave - Bootstrap algorithm
RMSE	Root Mean Square Error
SH	Southern Hudson Bay
SIC	Sea Ice Concentration
VP	Viscous Plastic rheology
WH	Western Hudson Bay

Chapter 1. Introduction

1.1 On the importance of sea ice

Sea ice became a feature of the Arctic Ocean about 47 million years ago in response to significant cooling of the Earth, caused by declining carbon dioxide (CO_2) concentrations in the atmosphere (Polyak et al., 2010, Miller et al., 2010). From this early time and until recently, variations in sea ice were controlled by non-anthropogenic changes in weather conditions that affected atmospheric circulation (Magnusdottir et al., 2004), temperatures, and/or solar irradiance (Kinnard et al., 2006, Gillett et al., 2008, Miller et al., 2010). Since the mid-19th century, however, atmospheric surface temperatures in the Northern Hemisphere (NH) have increased nearly monotonically (Przybylak, 2007, Shein et al., 2006). The greatest changes in temperature have occurred in autumn and spring, and post 1990, over the Canadian and Pacific sectors of the Arctic (Comiso, 2002, Przybylak, 2007). In these two regions the mean temperatures rose 1.26ºC and 1.48ºC since 1995 compared to the period of 1951-90 (Przybylak, 2007). This warming, associated with the rapid anthropogenic development and the increase in CO_2 concentrations (Gillett et al., 2008, Shein et al., 2006, Gearheard, 2008, Polyak et al., 2010), is causing large declines in sea ice concentration, thickness, and area throughout the NH (Polyak et al., 2010, Alekseev et al., 2008, Deser and

Teng, 2008, Parkinson and Cavalieri, 2008, Comiso, 2002). In the Arctic Ocean, for example, sea ice area declined by 45,100 km^2/yr between 1979 and 2006 (Parkinson and Cavalieri, 2008), and within only 25 years (1982-2007), 56% of the multiyear sea ice melted (Polyak et al., 2010). In the Canadian Arctic, negative trends in the Sea Ice Concentration (SIC) are some of the largest: the SIC declined at 3.6% per decade from 1980 to 2004 (Kinnard et al., 2006), and this trend seems to be much larger during the last decade of the 20^{th} century (Kinnard et al., 2006).

The loss of sea ice from the NH is concerning, because the sea ice is an important modulator of the world climate (Paeth and Pollinger, 2010, Perovich et al., 2002, Serreze et al., 2007, Miller et al., 2010, Meehl et al., 2006) and it is also an integral part of the Arctic ecosystem (Lunn et al., 1997, Chambellant, 2010, Derocher, 2005, Sibert et al., 2010, Juhl et al., 2011). The sea ice acts as a blanket over the ocean limiting oceanic heat absorption: sea ice has an albedo of 50% during summer and up to 80% during winter (Perovich et al., 2002). Therefore the melt of sea ice from the Arctic results in lower albedo that will likely lead to positive feedbacks that could cause a warming amplification in the Arctic (Serreze and Francis, 2006, Bitz and Roe, 2004, Holland and Bitz, 2003). This amplification would lead to greater and much faster changes in the atmosphere-ocean interactions (Paeth and Pollinger, 2010) with the potential to affect significantly the known atmospheric and oceanic circulation (Serreze et al., 2007, Meehl et al., 2006). An example is the capping of deep convection zones,

predicted as a consequences of the freshening of the North Atlantic and Labrador Sea resulting from higher freshwater export from the Arctic Ocean either because of the increase sea ice drift (Rampal et al., 2011) or of longer melting seasons and thus more liquid freshwater available to export (Lee et al., 2011). This is hypothesized to have the potential to change global heat distribution.

The loss of sea ice is also an imminent threat to the Arctic pagophilic species (Johannessen and Miles, 2011, Moore and Huntington, 2008, Laidre et al., 2008, Durner et al., 2009), especially the polar bear (*Ursus maritimus*). Polar bears are the top predators of the Arctic ecosystem and a specialized species that uses the sea ice as a platform to access and hunt their marine prey. Prey diversity includes ringed seals (*Pusa hispida*), bearded seals (*Erignathus barbatus*), harp seals (*Pagophilis groenlandicus*), harbour seals (*Phoca vitulina*), hooded seals (*Cystophora cristata*), belugas (*Delphinapterus leucas*), and walrus (*Odobenus rosmarus*) (Thiemann et al., 2008b). These species are also largely pagophilic, and therefore, are also threatened by the loss of sea ice (Thiemann et al., 2008b, Slater et al., 2010). Polar bears feed predominantly on the blubber (thick layer of adipose tissue) of their prey (Stirling and McEwan, 1975), and they can consume between 35 kg and 40 kg of blubber in a single meal. The large amounts of blubber in their diet allow polar bears to more rapidly increase their own fatty tissue (Pond et al., 1992). The body mass of polar bears is 35% fat (Cattet, 1990). Adipose tissue is important for energy storage and insulation: it allow polar bears to survive prolonged fasting periods and to survive in the cold and harsh

environment of the North. For populations in seasonal ice environments, large fat stores ensure survival during on land periods where there is very little access to marine prey (Derocher et al., 1992).

The global population of polar bears was estimated stable with 20,000 to 25,000 individuals in 2010 (PBSG, 2010). However, the global population is subdivided into 19 management units/populations which are all distributed in the NH (Figure 1.1) and in regions where sea ice is present most of the year (DeMaster and Stirling, 1981). The difference in sea ice habitat leads to population-specific trends in response to global warming: 1 of the 19 management units is increasing, 3 are stable, and 8 are declining (PBSG, 2010). The 7 remaining management units have unknown status because of insufficient data (PBSG, 2010). These management units are created based on polar bear's denning and movement behaviour (Thiemann et al., 2008a). In regions occupied by the southernmost populations such as Western Hudson Bay (WH) and Southern Hudson Bay (SH) (Figure 1.1), the sea ice is seasonal and it melts completely during the summer. There, polar bears are forced on land every summer where they have no access to the marine prey. In more Arctic populations such as the Arctic Ocean, the East Greenland, and the Lancaster Sound polar bears spend their entire lives on the sea ice, however, they move from multiyear sea ice to new-year sea ice near the continental shelf where productivity and abundance of prey is highest (Smith, 1980, Harwood and Stirling, 1992).

1.2 Polar bears and climate change in WH

The WH population is among the best studied populations of polar bears. Research on this population consisting of continuous data collection started early in the 1980s (Regehr et al., 2007). In 1984 the WH population was estimated at 1194 individuals, and in 2004 at 935 individuals (Regehr et al., 2007); a decline of near 20%. This decline was associated with changes in sea ice condition such as the SIC reductions and lengthening of the ice-free period and the harvest of population in Nunavut (Derocher and Stirling, 1995a, Regehr et al., 2007, Rockwell and Gormezano, 2009, Scott and Marshall, 2010, Stirling et al., 2008a, Stirling et al., 1999, Molnár et al., 2010, Parks et al., 2006, Molnár et al., 2011). From 1979-2007, winter SIC in HB decline at a rate of ~3% per decade, but from 1993-2007 it declined at a rate of 9% per decade (Deser and Teng, 2008). The declines in SIC, however, have been largest in July and November, ranging from 20 to 30% per decade (Hochheim and Barber, 2010, Hochheim et al., 2011); as a result the ice cycle is changing rapidly: the ice-free period is increasing (at 12.9 days per decade), the break-up date is advancing (at a rate of 5.3 days per decade), and the freeze-up date delayed (at a rate of 7.2 days per decade) (Markus et al., 2009). Changes in SIC are strongly correlated with the increase in atmospheric surface temperature (Hochheim et al., 2010, Wang et al., 1994b, Saucier and Dionne, 1998, Joly et al., 2011), being averaging 0.4ºC to 0.8ºC per decade in

summer (Hochheim et al., 2011) and 1.2ºC to 1.6ºC per decade in autumn (Hochheim and Barber, 2010) for all HB.

During the ice-free period, which lasts about 4 months (Watts and Hansen, 1987), polar bears depend almost exclusively on their fat stores, and can lose about 0.9 kg of body mass per day (Derocher and Stirling, 1995b). The fasting period is longer and more energetically demanding for pregnant females who enter maternity dens in November to give birth to 1 to 3 cubs (DeMaster and Stirling, 1981, Derocher and Stirling, 1995b). The female and her cubs do not return to the sea ice to feed until late February to March (Watts and Hansen, 1987). The litter size and survival of cubs depend on the female body condition (weight) at onshore arrival (Derocher et al., 1992, Molnár et al., 2011, Rode et al., 2010).

Polar bears accumulate a large part of their body fat during spring and early summer (March-July) (Dyck and Kebreab, 2009, Derocher et al., 2004, Cherry et al., 2009). Early summer is the best hunting period for polar bears (Derocher et al., 2002), because of the higher abundance of seals and their accessibility on the sea ice; between March and April ringed seals give birth within snow layers built on the sea ice (Ferguson et al., 2005), and after April and through July, seals haul out on the surface of the sea ice to molt (Lunn et al., 1997), thereby becoming more vulnerable to polar bear predation. The end of the spring hunting season in HB is dictated by break-up, when polar bears are forced ashore due to low SIC and the absence of sea ice. Poor condition of polar bears on

land is correlated to earlier break-up day (Derocher and Stirling, 1995a, Stirling et al., 1999), and polar bears survival during the summer season is related to both, their condition and to the length of the ice-free period (Regehr et al., 2007). Low SIC during the spring can negatively affect the hunting success of polar bears (Stirling et al., 2008b).

The effects of advancing break-up date and lengthening of the ice-free period on polar bears survival in WH was examined using a dynamic energy budget model (Molnár et al., 2010, Molnár et al., 2011). The model suggested that if break-up date in WH advances by one month relative to 1990s, 40 - 73% of the pregnant females could have insufficient fat-stores and litter size could decrease 22 - 67% (Molnár et al., 2011). The model also predicted that if the ice-free period increases to 180 days, 28 - 48% of the adult male population in WH could die of starvation because of insufficient fat-stores to survive the extended ice-free period (Molnár et al., 2010). Further, the authors suggested that adult males would be among the groups less threaten by the extension of the ice-free period (Molnár et al., 2010). Reproductive failure and mortality associated with these critical levels suggests that one or two years reaching either of these levels (critical years) could dramatically change the demographic structure of the WH population. Therefore, altered sea ice dynamics is a major concern, especially considering that current and predicted trends of atmospheric surface temperatures (Meehl et al., 2006, Koenigk et al., 2011, Gagnon and Gough, 2005, Rampal et al., 2011) could result in critical years before the end of this century. It is still unclear however,

how often and when critical years will occur. Having this information is critical to the conservation of polar bears. Reaching these thresholds determines when WH habitat will become unsuitable for polar bears.

In HB, a doubling of CO_2 concentration is predicted to increase temperatures resulting in significant losses of SIC (50-100%) in all months, but especially in spring and autumn (Gough and Wolfe, 2001, Gagnon and Gough, 2005). The advances in break-up and delays in freeze-up dates resulting from this warming will b about 1 month, leading to a 2 months lengthening of the ice-free period compared to current conditions (Gough and Wolfe, 2001). Similar sea ice results were obtained in a recent study that measured the effects of warming proposed for scenario A1B of the Intergovernmental Panel on Climate Change (IPCC) during the period 2040-70 (Joly et al., 2010). They showed that atmospheric temperatures would increase 3.9ºC causing a 50% decline of mean annual sea ice thickness and maximum sea ice volume compared to estimates for 1961-1990. The mean loss of annual sea ice extent was estimated at 2.6% (32,3500 km^2) and sea ice volume at 31% (592 km^3) (Joly et al., 2010). These changes in the sea ice cover lead to lower albedo and thus, a higher accumulation of heat in the water column that resulted in the advance of the break-up date by 24 days, and a 49 day increase in the length of the ice-free period compared to the same parameters estimated for 1961-90. These studies suggest that polar bear populations in HB will lose their habitat as CO_2 concentrations continue to increase. However, these predictions were general for HB and not made to

specifically to WH as defined by (Molnár et al., 2010, Molnár et al., 2011) and one cannot infer when and how frequent critical thresholds will become under predicted warmer climate of the 21st century.

1.3 Thesis objectives

The first objective is to evaluate the performance of a recently developed high-resolution sea ice-ocean model in HB focusing on the SIC and the seasonal cycle and exploring the use of polar bear telemetry data from WH as an additional tool in the validation of the model (Chapter II). Based on the polar bear dependence on sea ice, locations offshore are assumed to indicate the presence of sea ice, and the movements of polar bears from land to sea ice and vice versa, is use to indicate seasonality of the sea ice in WH. This is the first time polar bear-telemetry data is used to asses a sea ice model's results, and although still simplistic, the approach has applications in most Arctic regions were accurate sea ice data during summer is missing and polar bear telemetry data is available.

My second objective is to use this model to predict the 21st century sea ice in HB, focusing on the changes in the seasonal cycle in WH (length of the fasting period and break-up date) and the spring SIC in HB (Chapter 3). The predictions are based on CO_2 emission scenarios proposed by the IPCC: B1, A1B, A2 and Committed. This research is in part driven by the need to improve conservation of polar bear populations in HB, and to raise the awareness on the potential effects of

future warming on polar bear habitat. The thesis focuses on the WH population, but has direct application to the Southern Hudson Bay population, further south, and the Foxe Basin population, further north. And, as a microcosm of the worldwide circumstances of the species (Peacock et al., 2011), what is learned in HB could be applied to the circumpolar region.

1.4 Previous modeling studies in HB

To investigate polar bear future habitat loss in HB it is important to use sea ice models that can accurately predict the sea ice seasonal cycle so that one can infer the effects on polar bear migration offshore and ashore. Coupled sea ice-ocean models are becoming increasingly successful at reproducing ice and ocean properties and processes, however relatively little interest has been given to the HB region. These models have been used to increase the understanding of the physical environment, such as: what drives sea ice drift? What is the pattern of sea ice formation and melting? What are the effects of atmospheric forcing on sea ice cover? And only few have been used to predict the effect of future climate conditions. Of these, none has yet been used to predict sea ice changes throughout the length of the 21st century in ways that can be use to interpret the effects on polar bears. Nonetheless, these studies have contributed to identifying the most

important parameters that affect sea ice and that must be considered in models if realistic predictions of SIC are desired.

A series of sensitivity experiments in HB using coarse resolution two-layer sea ice-ocean dynamic-thermodynamic model (55 km) with a multilevel-3D-baroclinic ocean revealed that the dominant force to accurately simulate ice drift were the winds, except in eastern HB, where ocean currents played an important role in the export of sea ice into Hudson Strait (Wang et al., 1994c). The authors also found that realistic temperatures of the mixed layer were necessary to correctly simulate the seasonal ice cycle. In their simulations, the mixed layer temperature plays a major role in the timing of sea ice formation and thickness. The model was later used to estimate changes in the sea ice in southeastern HB under warmer climate with doubled the CO_2 concentration (Ingram et al., 1996). Results showed dramatic changes in the sea ice cycle and a reduction of maximum sea ice thickness of ~35%.

To improved the understanding of the sea ice cycle in HB and the effects of warming other models have been developed with increase resolution and different complexity (Saucier and Dionne, 1998, Saucier et al., 2004, Joly et al., 2010). Using dynamic-thermodynamic sea ice model coupled to a 3D ocean model 80 m deep and a resolution of 40 km, Saucier and Dionne showed that atmospheric temperature was among the most important factors regulating the amount of sea ice in HB (Saucier and Dionne, 1998). They predicted that a $2^{o}C$ increase in atmospheric temperature could reduce winter sea ice volume by over

20%. To understand the influence of oceanographic processes on sea ice declines, Saucier and Dionne's model was improved by allowing realistic bathymetry and ocean depth and increasing horizontal resolution to 10 km and the vertical resolution to 10 m (Saucier et al., 2004). This new model also incorporated realistic tidal, atmospheric, hydrologic and oceanographic currents. The model simulations of the seasonal ice cycle were similar to the earlier model, but with improved results during the late-spring-summer period (Saucier and Dionne, 1998, Saucier et al., 2004). The results suggested that ocean circulation has an important role in the export of sea ice along the eastern coast (Saucier et al., 2004). This model was recently used to predict the effects of global warming in HB marine system using IPCC scenario A1B from 2041–70 (Joly et al., 2010). Even though the greater complexity of the ocean model, the results (discussed in detail section 1.2), were similar to those obtained in the simpler and earlier version of Saucier and Dionne (1998). To date, this model is the most complete sea ice-ocean model tested in HB (Saucier et al., 2004).

Other studies have shown that the complexity of the ocean model (2D vs. 3D) does not have a strong effect on the response of sea ice to climate change (Gough and Allakhverdova, 1998, Gough and Allakhverdova, 1999, Gough and Wolfe, 2001). These studies used coarse resolution global climate models to predict changes in sea ice. Differences between these studies were more associated with parameterization of the vertical diffusivity and that the atmospheric forcing had a dominant role in sea ice response (Gough and

Allakhverdova, 1999, Gough and Wolfe, 2001) regardless of the complexity of the ocean component (Gough and Wolfe, 2001).

In this study, I used a sea ice model coupled to a 2D ocean model. The model has a horizontal resolution ranging from 10 to 25 km within HB. The sea ice is a two-layer sea ice model that is fully dynamic and thermodynamic. The ocean model is fully thermodynamics, and represents the mixed layer: it has only one level of depth 30 m. The ocean model is restored to climatological values to prevent drifting because dynamic processes are not considered. Considering the previous modeling research in HB, I should expect to obtain accurate SIC results with this model by using typical values of vertical diffusivity.

1.5 Hudson Bay physical environment

Current understanding of HB physical environment is mostly derived from observations and model simulations. However, research on the physical environment in HB is relatively scarce and most of the *in situ* observations are from the 1970s-80s. These have helped validate modeling studies that have served to understand recent declines in sea ice cover (section 1.6 contains the thesis dissertation outline).

1.5.1 Bay bathymetry and ocean circulation

HB is the largest bay in Canada, located in north-eastern Canada and land-bounded by the Canadian provinces of Quebec in the east, Ontario in the south, Manitoba in the west, and the Nunavut Territory in the northwest (Figure 1.2). HB is a relatively shallow basin with an average depth of 250 m (Pelletier, 1986). The basin topography is smooth: shallower near the coast and deeper towards the north. The two major topographic features are located in the southwest and are the Midbay Bank and the Winisk Trough (Pelletier, 1986). The Midbay Bank is a broad ridge that rises up to 40 m between Severn River estuary and Winisk River estuary. It extends north almost half the length of the Bay (Figure 1.2). The Winisk Trough is a deep trench of several 100 meters that extent north from Winisk River estuary to Coats Island (Figure 1.2).

HB is open in the north and connected to Foxe Basin in the northwest and Hudson Strait in the northeast through relatively narrow channels at each side of Southampton Island (Martini, 1986). The relatively shallow channel (Pelletier, 1986) west of Southampton Island, Roes Welcome Sound, is an important route of cold and fresh Arctic water inflow into HB (Prinsenberg, 1986a). This inflow is an important modulator of surface water properties (Prinsenberg, 1986b) and of the regional atmospheric temperatures (Maxwell, 1986) in northwest HB. The wider channels on the east are an important route for the export of sea ice into Hudson Strait (Prinsenberg, 1986a). This outflow has also an important role in the advection of heat and sea ice from James Bay to Hudson Strait during late-spring-

summer (Wang et al., 1994c, Saucier et al., 2004). The inflow/outflow currents are among the main drivers of the marine cyclonic circulation of HB, winds, tides and buoyancy currents strengthen the cyclonic circulation. Some dense waters overflows into HB from Foxe Basin through a deep channel between Southampton Island and Coats Island (Defossez et al., 2008). This deep water inflow modulates the deep water properties in HB (Prinsenberg, 1986b), but its influence on the surface waters or sea ice formation is poorly understood.

1.5.2 Wind forcing

Winds are the major contributors of the sea ice motion during winter, and during summer they strengthen the ocean surface circulation (Maxwell, 1986). The strength and direction of the wind field is regulated by a persistent low pressure vortex over northern Baffin Island during winter (Maxwell, 1986). The location and intensity of the low pressure vortex affects winter severity and wind strength. Intrusion of cold Arctic air masses in HB and strong wind are common during autumn and winter when the vortex is at its southernmost location (Maxwell, 1986). As the low pressure moves northward in summer the wind speed declines (Maxwell, 1986). The intrusion of the Arctic air masses are a strong modulator of the mixed layer temperature in HB (Maxwell, 1986, Prinsenberg, 1986b), while the role of upward ocean-heat flux is small due to the small heat content in Hudson Bay during winter (Saucier et al., 2004).

The mean winds in WH are generally north-westerlies to westerlies, and in eastern HB, they blow from the west and the southwest (Maxwell, 1986). These wind patterns often results in winds blowing offshore from land or land-fast ice creating a complex system of leads and polynyas along the western shores and eastern islands of HB. Leads develop yearly along the western coast (Maxwell, 1986) while polynyas are more common on the southeast side of the islands in eastern HB and along the southwest coast of Akimiski Island (Stewart and Barber, 2010). Leads and polynyas are important regions of dense water formation and first-year sea ice production throughout the winter, and as an interface between air, ice and water, they are also important sites for energy transfer, mixing and upwelling (Stewart and Barber, 2010). High biological productivity is associated with these sites. Landfast ice forms early in the season and is common along the eastern shores of HB where waters are shallow, well mixed, and with low salinity (Stewart and Barber, 2010).

1.5.3 Sea ice cycle

The sea ice cycle is mainly controlled by atmospheric temperatures (Hochheim et al., 2010, Wang et al., 1994b, Saucier and Dionne, 1998, Joly et al., 2011), this is evident when comparing past and present literature. For example, studies conducted during the 1970s calculated a mean freeze-up date in late October to early November (Prinsenberg, 1986b, Maxwell, 1986), while in recent decades the freeze-up date is between mid and late November (Hochheim and

Barber, 2010). The trends in atmospheric temperatures have led to the delay (advance) of the formation (melting) of sea ice by almost 1 month since the 1970s (Markus et al., 2009).

Sea ice forms first in northwest HB in early November and it rapidly expands southeast, such that by December and January sea ice covers almost entirely the Bay (Maxwell, 1986, Hochheim and Barber, 2010). Typical SIC in January are over 80% (Wang et al., 1994c, Saucier et al., 2004). Maximum sea ice cover and SIC occur between April and May (Maxwell, 1986, Hochheim et al., 2011). In northwest HB, sea ice growth is mostly due to thermodynamic processes. In southeast HB, the initial sea ice formation is mostly due to dynamic processes that advected sea ice formed in northwest HB to the southeast before thermodynamic processes dominate sea ice formation in the region (Saucier et al., 2004, Wang et al., 1994c). Melting of the sea ice usually starts in late-spring and continues until all sea ice melts in summer. James Bay becomes ice free first, and is followed by northern HB. Last sea ice to melt is found along the south-western shore (Hochheim et al., 2011, Stirling et al., 2004). By August, HB is ice-free. The progression of melting results from the combination of the cyclonic wind and oceanic circulation: as the sea ice cover starts melting in SH, the pack ice becomes loose allowing the north-westerly winds to advect sea ice from north-western HB to SH. At the same time, ocean currents strengthen with the disappearance of the sea ice cover and the stronger coast to offshore density gradient as a result of freshening of the coastal waters from increased runoff.

These density gradient currents are especially important in eastern HB advecting sea ice northward into Hudson Strait (Saucier et al., 2004, Wang et al., 1994c).

Sea ice thickness data is scarce, but suggests that the ice grows from south to north, and that the maximum thickness (March-May) is estimated to be 1 m in southern James Bay and 2 m in northern HB. However, this could be significantly underestimated, with errors reaching 90% because it is calculated based on the large freshwater input in HB (Prinsenberg, 1986b).

1.5.4 Freshwater input

Mean annual freshwater input into HB is 12.5 m^3/s (Martini, 1986), which is approximately 12% of the total Arctic runoff (St-Laurent et al., 2011). Fresh water input is subject to a strong seasonal cycle (St-Laurent et al., 2011, Prinsenberg, 1986a); it is highest in spring and summer, ~45.5 m^3/s, and lowest in winter, ~5m^3/s (Martini, 1986). Sources of freshwater are: sea ice melt, runoff, and precipitation-evaporation. Ice melt is a significant source of freshwater offshore, while runoff is more important along the coast and within 100 km of the shore line (St-Laurent et al., 2011). Runoff dilutes the water nearshore, setting-up strong gradients and density-driven currents during spring and summer. These currents have an important role in sea ice and heat advection north from James Bay into Hudson Strait (Wang et al., 1994a, Wang et al., 1994c). The runoff increases from north to south, reaching a maximum in James Bay (Prinsenberg,

1986b). Precipitation is highest in southern HB-James Bay (Prinsenberg, 1986b) and increases from winter to summer and from north to south. Maximum evaporation occurs in summer and decreases from west to east (Prinsenberg, 1986b). As a result, during summer and early fall, there are distinct salinity gradients: offshore-inshore and northeast-southwest (Prinsenberg, 1986b). The salinity of the surface layer is lowest along the coast (Prinsenberg, 1986b, St-Laurent et al., 2011), and on the southwest between the Churchill estuary and the Belcher Islands were salinity reaches its lower values (Roff and Legendre, 1986).

The large amount of freshwater entering the system causes pronounced vertical stratification of the water column, with a pycnocline that can reach 20 to 28 m deep between August and September (Prinsenberg, 1986b, Roff and Legendre, 1986). The deep pycnocline limits the mixing between the surface and bottom water layers, resulting in a homogeneous mixed layer (Prinsenberg, 1986b) with pronounced seasonal changes in temperature and salinity (St-Laurent et al., 2011). The annual mean mixed layer temperature ranges from 1 to 9ºC and its salinity ranges from 21 to 32 g/kg (St-Laurent et al., 2011), while the bottom waters remain close to freezing at -1.7ºC and 34 g/kg salinity throughout the year (Roff and Legendre, 1986, Prinsenberg, 1986b).

The volume and timing of freshwater influences thermodynamic and dynamic processes within HB: increasing runoff in spring strengthens baroclinic currents which contribute to sea ice break-up, melt and advection along the

eastern coast. The diluted surface waters in autumn have a higher freezing temperature, and thus sea ice forms faster where salinity is lower.

1.6 Dissertation outline.

Model validation is necessary to determine its strengths and weaknesses before using it for predictions. The details of the validation are in Chapter II where I show the model's simulation of the seasonal cycle and SIC. I compared the model results of the SIC to Canadian Ice Service (CIS) charts and Passive Microwave (PMW) data, and to validate the timing of seasonal cycle I used GPS telemetry data from collared polar bears. Based on the polar bear's known dependence of sea ice, I used the polar bear migration to obtain insight about the seasonal changes of the sea ice habitat. This is the first time polar bear telemetry data is used in this manner, and in this study it was especially important during freeze-up and break-up when PMW SIC had its lowest accuracy.

Chapter III describes the application of the model in future climate predictions. It contains the results of three climate scenarios that measure the effect of increased CO_2 concentration throughout the 21^{st} century. The focus is given to the parameters that have been linked to polar bear ecology. Global warming effects on sea ice were assessed using IPCC climate scenarios B1, A1B

and A2. The results of this Chapter examines the conservation and proactive management of polar bears.

Chapter IV is the general conclusion. It consists of a summary of the main results with the implications and future areas for research that can expand and/or improve on my findings.

Chapter V /Appendix 1 contains a detail description of the model with some of the main equations.

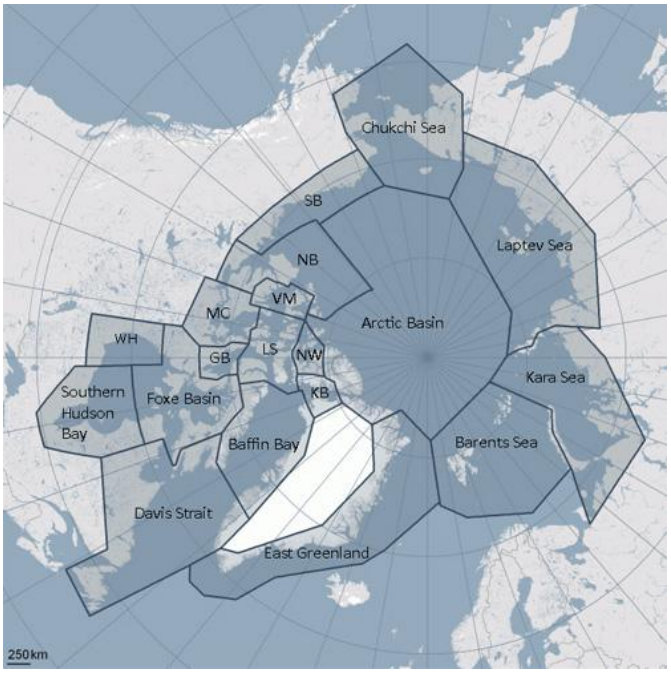

Figure 1.1. Global polar bear population distribution showing subdivisions for the 19 management units. Abbreviations: Viscount Melville Sound (VM), Norwegian Bay (NW), Kane Basin (KB), Lancaster Sound (LS), Western Hudson Bay (WH), Gulf of Boothia(GB), M'Clintock Channel (MC), Southern Beaufort Sea (SB), and Northern Beaufort Sea (NB) (http://pbsg.npolar.no; IUCN Polar Bear Specialist Group (03/2010))

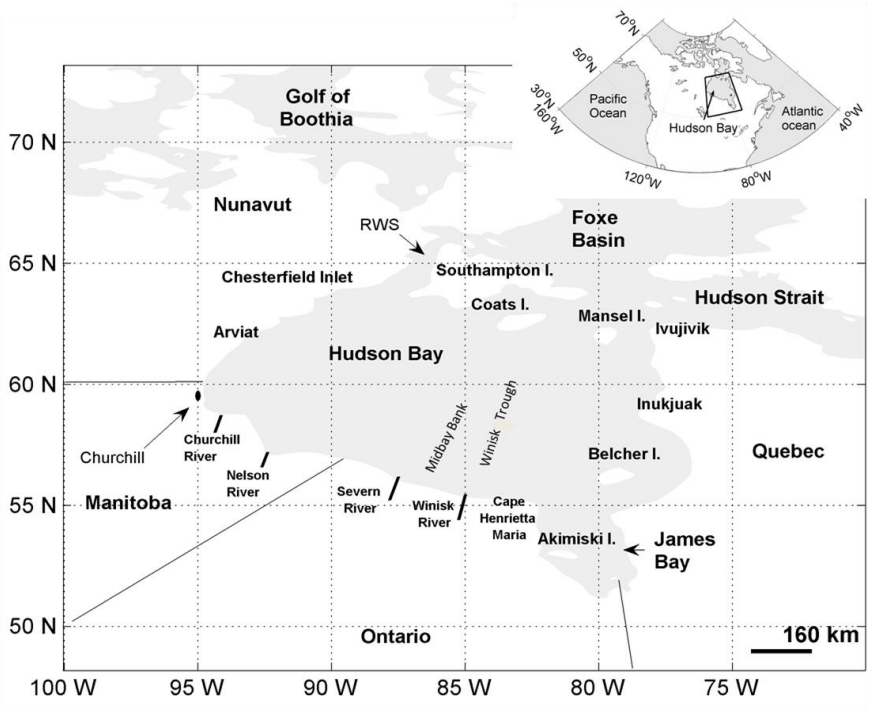

Figure 1.2. Study area. The inset, on the top-right corner, shows the location of Hudson Bay in North America. The enlarged map depicts the approximate location of major topographic features of Hudson Bay: Midbay Bank ridge and Winisk Trough. Abbreviation: Roes Welcome Sound (RWS).

1.7 References

Alekseev, G. V., Kuzmina, S. I., Nagurny, A. P. & Ivanov, N. E. 2008. Arctic sea ice data sets in the context of climate change during the 20th century. *In:* Bronnimann, S., Luterbacher, J., Ewen, T., Diaz, H. F., Stolarski, R. S. & Neu, U. (eds.) *Climate Variability and Extremes during the Past 100 Years*, 47-63 pp.

Bitz, C. M. & Roe, G. H. 2004. A mechanism for the high rate of sea ice thinning in the Arctic Ocean. *Journal of Climate,* 17, 3623-3632.

Cattet, M. 1990. Predicting condition in black bears and polar bears on the basis of morphological and physiological measurments. *Canadian Journal of Zoology*, 68, 32-39.

Chambellant, M. 2010. Hudson Bay Ringed Seal: Ecology in a Warming Climate, *Springer-Verlag Berlin, Berlin,* 137-158 pp.

Cherry, S. G., Derocher, A. E., Stirling, I. & Richardson, E. S. 2009. Fasting physiology of polar bears in relation to environmental change and breeding behavior in the Beaufort Sea. *Polar Biology,* 32, 383-391.

Comiso, J. C. 2002. Correlation and trend studies of the sea-ice cover and surface temperatures in the Arctic. *In:* Winther, J. G. & Solberg, R. (eds.) *Annals of Glaciology, Vol 34, 2002.*

Defossez, M., Saucier, F. J., Myers, P. G., Caya, D. & Dumais, J. F. 2008. Multi-Year Observations of Deep Water Renewal in Foxe Basin, Canada. *Atmosphere-Ocean,* 46, 377-390.

Demaster, D. P. & Stirling, I. 1981. *Ursus Maritimus*. *Mammalian Species,* 145, 1-7.

Derocher, A. E. 2005. Population ecology of polar bears at Svalbard, Norway. *Population Ecology,* 47, 267-275.

Derocher, A. E., Lunn, N. J. & Stirling, I. 2004. Polar bears in a warming climate. *Integrative and Comparative Biology,* 44, 163-176.

Derocher, A. E. & Stirling, I. 1995a. Estimation of polar bear population-size and survival in western Hudson-Bay. *Journal of Wildlife Management,* 59, 215-221.

Derocher, A. E. & Stirling, I. 1995b. Temporal variation in reproduction and body-mass of polar bears in western Hudson-Bay. *Canadian Journal of Zoology,* 73, 1657-1665.

Derocher, A. E., Stirling, I. & Andriashek, D. 1992. Pregnancy rates and serum progesterone levels of polar bears in western Hudson-Bay. *Canadian Journal of Zoology,* 70, 561-566.

Derocher, A. E., Wiig, Ø. & Andersen, M. 2002. Diet composition of polar bears in Svalbard and the western Barents Sea. *Polar Biology,* 25, 448-452.

Deser, C. & Teng, H. 2008. Evolution of Arctic sea ice concentration trends and the role of atmospheric circulation forcing, 1979-2007. *Geophysical Research Letters,* 35.

Durner, G. M., et al. 2009. Predicting 21st-century polar bear habitat distribution from global climate models. *Ecological Monographs,* 79, 25-58.

Dyck, M. G. & Kebreab, E. 2009. Estimating the energy contribution of polar bear (*Ursus Maritimus*) summer diets to the total energy budget. *Journal of Mammalogy,* 90, 585-593.

Ferguson, S. H., Stirling, I. & Mcloughlin, P. 2005. Climate change and ringed seal (*Phoca hispida*) recruitment in western Hudson Bay. *Marine Mammal Science,* 21, 121-135.

Gagnon, A. S. & Gough, W. A. 2005. Climate change scenarios for the Hudson Bay region: An intermodel comparison. *Climatic Change,* 69, 269-297.

Gearheard, S. 2008. A change in the weather. *Natural History,* 117, 32-38.

Gillett, N. P., Stone, D. A., Stott, P. A., Nozawa, T., Karpechko, A. Y., Hegerl, G. C., Wehner, M. F. & Jones, P. D. 2008. Attribution of polar warming to human influence. *Nature Geoscience,* 1, 750-754.

Gough, W. A. & Allakhverdova, T. 1998. Sensitivity of a coarse resolution ocean general circulation model under climate change forcing. *Tellus Series a-Dynamic Meteorology and Oceanography,* 50, 124-133.

Gough, W. A. & Allakhverdova, T. 1999. Limitations of using a coarse resolution model to assess the impact of climate chance on sea ice in Hudson Bay. *Canadian Geographer,* 43, 415-422.

Gough, W. A. & Wolfe, E. 2001. Climate change scenarios for Hudson Bay, Canada, from general circulation models. *Arctic,* 54, 142-148.

Harwood, L. A. & Stirling, I. 1992. Distributrion of ringed seals in the southeastern Beaufort Sea during late summer. *Canadian Journal of Zoology,* 70, 891-900.

Hochheim, K. P. & Barber, D. G. 2010. Atmospheric forcing of sea ice in Hudson Bay during the fall period, 1980-2005. *Journal of Geophysical Research-Oceans,* 115.

Hochheim, K. P., Barber, D. G. & Lukovich, J. V. 2010. *Changing Sea Ice Conditions in Hudson Bay, 1980-2005,* Berlin, Springer-Verlag Berlin, 39-51 pp.

Hochheim, K. P., Lukovich, J. V. & Barber, D. G. 2011. Atmospheric forcing of sea ice in Hudson Bay during the spring period, 1980–2005. *Journal of Marine Systems,* 88, 476-487.

Holland, M. M. & Bitz, C. M. 2003. Polar amplification of climate change in coupled models. *Climate Dynamics,* 21, 221-232.

Ingram, R. G., Wang, J., LIN, C., Legendre, L. & Fortier, L. 1996. Impact of freshwater on a subarctic coastal ecosystem under seasonal sea ice (southeastern Hudson Bay, Canada) .1. Interannual variability and predicted global warming influence on river plume dynamics and sea ice. *Journal of Marine Systems,* 7, 221-231.

Johannessen, O. M. & Miles, M. W. 2011. Critical vulnerabilities of marine and sea ice-based ecosystems in the high Arctic. *Regional Environmental Change,* 11, S239-S248.

Joly, S., Senneville, S., Caya, D. & Saucier, F. J. 2010. Sensitivity of Hudson Bay Sea ice and ocean climate to atmospheric temperature forcing *Climate Dynamics,* 36, 1835-1849.

Joly, S., Senneville, S., Caya, D. & Saucier, F. J. 2011. Sensitivity of Hudson Bay Sea ice and ocean climate to atmospheric temperature forcing. *Climate Dynamics,* 36, 1835-1849.

Juhl, A. R., Krembs, C. & Meiners, K. M. 2011. Seasonal development and differential retention of ice algae and other organic fractions in first-year Arctic sea ice. *Marine Ecology-Progress Series,* 436, 1-16.

Kinnard, C., Zdanowicz, C. M., Fisher, D. A., Alt, B. & McCourt, S. 2006. Climatic analysis of sea-ice variability in the Canadian Arctic from operational charts, 1980-2004. *In:* Langhorne, P. & Squire, V. (eds.) *Annals of Glaciology, Vol 44, 2006.* Cambridge: International Glaciological Society.

Koenigk, T., Doscher, R. & Nikulin, G. 2011. Arctic future scenario experiments with a coupled regional climate model. *Tellus Series a-Dynamic Meteorology and Oceanography,* 63, 69-86.

Laidre, K. L., Stirling, I., Lowry, L. F., Wiig, Ø., Heide-Jorgensen, M. P. & Ferguson, S. H. 2008. Quantifying the sensitivity of arctic marine mammals to climate-induced habitat change. *Ecological Applications,* 18, S97-S125.

Lee, S. Y., Chiang, J. C. H., Matsumoto, K. & Tokos, K. S. 2011. Southern Ocean wind response to North Atlantic cooling and the rise in atmospheric CO2:

Modeling perspective and paleoceanographic implications. *Paleoceanography,* 26.

Lunn, N. J., Stirling, I. & Nowicki, S. N. 1997. Distribution and abundance of ringed (*Phoca hispida*) and bearded seals (*Erignathus barbatus*) in western Hudson Bay. *Canadian Journal of Fisheries and Aquatic Sciences,* 54, 914-921.

Magnusdottir, G., Deser, C. & Saravanan, R. 2004. The effects of North Atlantic SST and sea ice anomalies on the winter circulation in CCM3. Part I: Main features and storm track characteristics of the response. *Journal of Climate,* 17, 857-876.

Markus, T., Stroeve, J. C. & Miller, J. 2009. Recent changes in Arctic sea ice melt onset, freezeup, and melt season length. *Journal of Geophysical Research-Oceans,* 114.

Martini, I. P. 1986. Coastal feature of Canadian Inland Seas. *In:* Martini, I. P. (ed.) *Canadian Inland Seas.* New York: Elsevier Science Publishers Company Inc.

Maxwell, J. B. 1986. A climate overview of the Canadian Inland Seas. *In:* Martini, I. P. (ed.) *Canadian Inland Seas.* New York: Elsevier Science Publishers Company Inc.

Meehl, G. A., Washington, W. M., Santer, B. D., Collins, W. D., Arblaster, J. M., Hu, A. X., Lawrence, D. M., Teng, H. Y., Buja, L. E. & Strand, W. G. 2006. Climate change projections for the twenty-first century and climate change commitment in the CCSM3. *Journal of Climate,* 19, 2597-2616.

Miller, G. H., et al. 2010. Temperature and precipitation history of the Arctic. *Quaternary Science Reviews,* 29, 1679-1715.

Molnár, P. K., Derocher, A. E., Klanjscek, T. & Lewis, M. A. 2011. Predicting climate change impacts on polar bear litter size. *Nature Communications,* 2 (DOI: 18610.1038/ncomms1183).

Molnár, P. K., Derocher, A. E., Thiemann, G. W. & Lewis, M. A. 2010. Predicting survival, reproduction and abundance of polar bears under climate change. *Biological Conservation,* 143, 1612-1622.

Moore, S. E. & Huntington, H. P. 2008. Arctic marine mammals and climate change: Impacts and resilience. *Ecological Applications,* 18, S157-S165.

Paeth, H. & Pollinger, F. 2010. Enhanced evidence in climate models for changes in extratropical atmospheric circulation. *Tellus Series a-Dynamic Meteorology and Oceanography,* 62, 647-660.

Parkinson, C. L. & Cavalieri, D. J. 2008. Arctic sea ice variability and trends, 1979-2006. *Journal of Geophysical Research-Oceans,* 113.

Parks, E. K., Derocher, A. E. & Lunn, N. J. 2006. Seasonal and annual movement patterns of polar bears on the sea ice of Hudson Bay. *Canadian Journal of Zoology,* 84, 1281-1294.

Peacock, E., Derocher, A. E., Thiemann, G. W. & Stirling, I. 2011. Conservation and management of Canada's polar bears (*Ursus maritimus*) in a changing Arctic. *Canadian Journal of Zoology,* 89, 371-385.

Pelletier, B. R. 1986. Seafloor morphology and sediments. *In:* Martini, I. P. (ed.) *Canadian Inland Seas.* New York: Elsevier Science Publishers Company Inc.

Perovich, D. K., Grenfell, T. C., Light, B. & Hobbs, P. V. 2002. Seasonal evolution of the albedo of multiyear Arctic sea ice. *Journal of Geophysical Research-Oceans,* 107.

Polyak, L., et al. 2010. History of sea ice in the Arctic. *Quaternary Science Reviews,* 29, 1757-1778.

Pond, C. M., Mattacks, C. A., Colby, R. H. & Ramsay, M. A. 1992. The anatomy, chemical-composition, and metabolism of adipose-tissure in wild polar bears (*Ursus maritimus*). *Canadian Journal of Zoology,* 70, 326-341.

Prinsenberg, S. J. 1986a. The circulation pattern and current structure of Hudosn Bay. *In:* Martini, I. P. (ed.) *Canadian Inland Seas.* New York: Elsevier Science Publishers Company Inc., 163-182 pp.

Prinsenberg, S. J. 1986b. Salinity and temperature distribution of Hudson Bay and James Bay. *In:* MARTINI, I. P. (ed.) *Canadian Inland Seas.* New York: Elsevier Science Publishers Company Inc.,187-204 pp.

Przybylak, R. 2007. Recent air-temperature changes in the Arctic. *In:* Sharp, M. (ed.) *Annals of Glaciology, Vol 46, 2007.*

Rampal, P., Weiss, J., Dubois, C. & Campin, J. M. 2011. IPCC climate models do not capture Arctic sea ice drift acceleration: Consequences in terms of projected sea ice thinning and decline. *Journal of Geophysical Research-Oceans,* 116.

Regehr, E. V., Lunn, N. J., Amstrup, S. C. & Stirling, L. 2007. Effects of earlier sea ice breakup on survival and population size of polar bears in western Hudson bay. *Journal of Wildlife Management,* 71, 2673-2683.

Rockwell, R. F. & Gormezano, L. J. 2009. The early bear gets the goose: climate change, polar bears and lesser snow geese in western Hudson Bay. *Polar Biology,* 32, 539-547.

Rode, K. D., Amstrup, S. C. & Regehr, E. V. 2010. Reduced body size and cub recruitment in polar bears associated with sea ice decline. *Ecological Applications,* 20, 768-782.

Roff, J. C. & Legendre, L. 1986. Physio-Chemical and biological oceanography of Hudson Bay. *In:* Martini, I. P. (ed.) *Canadian Inland Seas.* New York: Elsevier Science Publishers Company Inc., 265-292 pp.

Saucier, F. J. & Dionne, J. 1998. A 3-D coupled ice-ocean model applied to Hudson Bay, Canada: The seasonal cycle and time-dependent climate response to atmospheric forcing and runoff. *Journal of Geophysical Research-Oceans,* 103, 27689-27705.

Saucier, F. J., Senneville, S., Prinsenberg, S. J., Roy, F., Smith, G., Gachon, P., Caya, D. & Laprise, R. 2004. Modelling the sea ice-ocean seasonal cycle in Hudson Bay, Foxe Basin and Hudson Strait, Canada. *Climate Dynamics,* 23, 303-326.

Scott, J. B. T. & Marshall, G. J. 2010. A step-change in the date of sea-ice breakup in western Hudson Bay. *Arctic,* 63, 155-164.

Serreze, M. C., Barrett, A. P., Slater, A. G., Steele, M., Zhang, J. L. & Trenberth, K. E. 2007. The large-scale energy budget of the Arctic. *Journal of Geophysical Research-Atmospheres,* 112.

Serreze, M. C. & Francis, J. A. 2006. The arctic amplification debate. *Climatic Change,* 76, 241-264.

Shein, K. A., et al. 2006. State of the climate in 2005. *Bulletin of the American Meteorological Society,* 87, S6-S102.

Sibert, V., Zakardjian, B., Saucier, F., Gosselin, M., Starr, M. & Senneville, S. 2010. Spatial and temporal variability of ice algal production in a 3D ice-ocean model of the Hudson Bay, Hudson Strait and Foxe Basin system. *Polar Research,* 29, 353-378.

Slater, G. J., Figueirido, B., Louis, L., Yang, P. & van Valkenburgh, B. 2010. Biomechanical consequences of rapid evolution in the polar bear lineage. *Plos One,* 5.

Smith, T. G. 1980. Polar bear predation of ringed and bearded seals in the land-fast sea ice habitat. *Canadian Journal of Zoology,* 58, 2201-2209.

St-Laurent, P., Straneo, F., Dumais, J. F. & Barber, D. G. 2011. What is the fate of the river waters of Hudson Bay? *Journal of Marine Systems,* 88, 352-361.

Stewart, D. B. & Barber, D. G. 2010. The Ocean-Sea Ice-Atmosphere System of the Hudson Bay Complex. In: Ferguson, S. H., Loseto, L. L. and Mallory, M. L. (eds) *Little less Arctic: Top predators in the world's largest northern inland sea, Hudson Bay,* 1-37 pp.

Stirling, I., Derocher, A. E., Gough, W. A. & Rode, K. 2008a. Response to Dyck et al. (2007) on polar bears and climate change in western Hudson Bay. *Ecological Complexity,* 5, 193-201.

Stirling, I., Lunn, N. J. & Iacozza, J. 1999. Long-term trends in the population ecology of polar bears in western Hudson Bay in relation to climatic change. *Arctic,* 52, 294-306.

Stirling, I., Lunn, N. J., Iacozza, J., Elliott, C. & Obbard, M. 2004. Polar bear distribution and abundance on the Southwestern Hudson Bay Coast during open water season, in relation to population trends and annual ice patterns. *Arctic,* 57, 15-26.

Stirling, I. & Mcewan, E. H. 1975. Caloric value of whole ringed seals (*Phoca hyspida*) in relation to polar bear (*Ursus maritimus*) ecology and hunting behavior. *Canadian Journal of Zoology,* 53, 1021-1027.

Stirling, I., Richardson, E., Thiemann, G. W. & Derocher, A. E. 2008b. Unusual predation attempts of polar bears on ringed seals in the southern Beaufort Sea: Possible significance of changing spring ice conditions. *Arctic,* 61, 14-22.

Thiemann, G. W., Derocher, A. E. & Stirling, I. 2008a. Polar bear (*Ursus maritimus*) conservation in Canada: an ecological basis for identifying designatable units. *Oryx,* 42, 504-515.

Thiemann, G. W., Iverson, S. J. & Stirling, I. 2008b. Polar bear diets and Arcitc marine food webs: insights from fatty acid analysis. *Ecological Monographs,* 78, 591-613.

Wang, J., Mysak, L. A. & Ingram, R. G. 1994a. A 3-Dimensional numerical-simulation of Hudson-Bay summer ocean circulation- topographic gyres, separations and coastal jets. *Journal of Physical Oceanography,* 24, 2496-2514.

Wang, J., Mysak, L. A. & Ingram, R. G. 1994b. Internal variability of sea ice cover in Hudson Bay, Baffin Bay and the Labrador Sea. *Atmosphere-Ocean,* 32, 421-447.

Wang, J., Mysak, L. A. & Ingram, R. G. 1994c. A numerical-simulation of sea ice in Hudson Bay. *Journal of Physical Oceanography,* 24, 2515-2533.

Watts, P. D. & Hansen, S. E. 1987. Cyclic starvation as a reproductive stratergy in the polar bear, *Symposia of the Zoological Sociaty of London,* 57, 305-318.

Chapter 2 . Polar bear-GPS-telemetry data as a tool to calibrate and validate a sea ice model in Hudson-Bay.

2.1 Introduction

Numerical models improve the understanding of ecosystems that are poorly accessible to humans and help predict future environmental conditions (Molnár et al., 2010, Molnár et al., 2011, Saucier and Dionne, 1998, Hunke and Dukowicz, 1997, Holland and Bitz, 2003). In the Arctic and subarctic ecosystems sea ice-ocean models have contributed substantially to the understanding of both physical and biological processes (Saucier et al., 2004, Amstrup et al., 2009, Yakovlev, 2009b, Yakovlev, 2009a, Sibert et al., 2010). The recent sea ice and temperature trends are threatening the integrity of these ecosystems (Learmonth et al., 2006, Prowse et al., 2009, Chapman and Walsh, 1993). As an integral part of these ecosystems, the sea ice is essential to the survival of a wide range of species. Polar bears (*Ursus maritimus*), for example, are strongly dependent on the sea ice as a platform to access their marine prey (Derocher et al., 2004). Studies on the Western Hudson Bay (WH) polar bear population in Hudson Bay (HB), Canada, have shown that declines in number of individuals (Regehr et al., 2007), body mass and recruitment (Derocher and Stirling, 1995) are associated to recent decline in sea ice concentration (SIC) and changes in the sea ice cycle (Derocher et al., 1992, Stirling et al., 1999). This is one of the southernmost populations of

polar bears (Peacock et al., 2010), for which the deleterious effects of climate change may appear earlier. Similar threats have been suggested for other populations (Stirling and Derocher, 1993).

In WH, polar bears are on the sea ice during winter but are forced ashore in summer (Derocher and Stirling, 1990) when the sea ice cover melts completely (Maxwell, 1986, Gough et al., 2004). These migrations on and off the sea ice are highly correlated to changes in SIC during freeze-up and break-up (Cherry, 2011). Future changes in the seasonal ice cycle of HB are of concern because polar bears depend on the sea ice to hunt ringed seals (*Pusa hispida*) and bearded seals (*Erignathus barbatus*) (Thiemann et al., 2008), and on land they have limited access to these prey (Watts and Hansen, 1987, Derocher and Stirling, 1995).

In this chapter I validate a recently developed sea ice model for the Arctic and Subarctic (Terwisscha van Scheltinga et al., 2010). The model is prognostic and has high temporal and spatial resolution within HB, and thus could be used to predict the 21st century changes in sea ice parameters that are most important to polar bears such as the seasonal cycle and the SIC. Validation of the seasonal sea ice cycle is the most challenging because satellite-derived SIC data can either lack the desired temporal resolution or accuracy during break-up and freeze-up in HB. The Canadian Ice Service (CIS) is one of the most reliable sources of SIC in HB (Hochheim and Barber, 2010, Hochheim et al., 2011), however, the charts have low temporal resolution (weekly), and therefore cannot be used to compare to the daily estimates of SIC. This limits the identification of the break-up and freeze-up

dates which are necessary to define the ice-free period length. Passive microwave (PMW) data, in contrast, contains daily fields of SIC, however it has lowest accuracy during melting and freezing (Cavalieri et al., 1991, Comiso et al., 1997, Markus and Cavalieri, 2000, Markus and Dokken, 2002, Agnew and Howell, 2003), and during heavy cloud weather conditions, which are typically observed during break-up (Shokr et al., 2003, Liu et al., 2008, Liu et al., 2009, Markus and Cavalieri, 2000). Incorporating polar bear data in the validation of the model could surmount these limitations. Polar bear GPS data from Argos' radio collars have temporal resolution of 4 hours, spatial resolution of less than or equal to 10 m (Patterson et al., 2010, Tomkiewicz et al., 2010), and the accuracy is unaffected by weather conditions (Tomkiewicz et al., 2010). Based on the dependence of polar bears on sea ice (Stirling et al., 2008, Parks et al., 2006, Arthur et al., 1996) the GPS-locations offshore can be considered as *in situ* measurements of the presence of sea ice at those locations.

The objective of this Chapter is to determine the accuracy of the model simulation of the SIC in HB, with emphasis on the timing of break-up and freeze-up which will be validated using the polar bear GPS data. In addition I will look at the relation between the SIC and the WH polar bear migration to calibrate the model's seasonal cycle with the length of the polar bear fasting period. The focus on these parameters pertains to the application of the model in predictive studies regarding the impact of climate change on polar bear sea ice habitat in WH (see Chapter 3). If successfully applied, the method has the potential to contribute to

the validation of the sea ice models in other Arctic regions as GPS technology is widely used nowadays in polar bear research (Amstrup et al., 2001, Amstrup et al., 2000, Durner et al., 2009, Born et al., 1997, Mauritzen et al., 2001).

2.2 Methods

2.2.1 Study area

HB is a large shallow basin in north-eastern Canada with an area of approximately 10^6 km^2 and a mean depth of 150 m (Prinsenberg, 1986a). In the following, I define the HB area as the oceanic region within 51ºN - 64ºN and 76ºW - 95ºW (Figure 2.1a). HB sea ice and oceanic circulation is cyclonic. The inflow of cold Arctic water through a shallow channel west of Southampton Island and the export via two channels to the east side of Southampton Island are fundamental to the oceanic circulation (Wang et al., 1994a, Wang et al., 1994c, Prinsenberg, 1986a). This circulation is enhanced by the winds, and by the tidal and density currents. The winds have an important role in the advection of sea ice during ice covered months, the ocean currents' role is more important in the east once the sea ice pack breaks down (Wang et al., 1994c, Saucier et al., 2004). The predominant winds in HB are from the north and northwest (Maxwell, 1986) causing the advection of sea ice in a south-eastward direction. The ocean currents are strongest during summer due to the melt of sea ice and the increase in runoff that strengthen the density currents along coastal regions (Prinsenberg, 1986a).

Tidal and density currents are dampened during winter with the formation of the sea ice cover and are not influential in the sea ice drift (Prinsenberg and Freeman, 1986). However, during late spring and summer, coastal currents strengthen and are important for advecting heat and exporting sea ice northward from James Bay into Hudson Strait along the east coast (Wang et al., 1994c, Saucier et al., 2004). Surface winds and the intrusion of Arctic air masses are important modulators of the sea ice formation as they accelerate the cooling of the regional surface temperatures during autumn (Maxwell, 1986).

2.2.2 Model details

The model domain is the Arctic and subarctic Seas north of 50ºN, only excluding the Bering Sea and the Baltic Sea. Closed boundary conditions are applied at Bering Strait and in the North Atlantic Ocean at 50ºN (Terwisscha van Scheltinga et al., 2010) (Supplementary-Fig.5.1a). This sea-ice ocean model is similar to the Finite Element Sea Ice-Ocean Model (FESOM) described in (Timmermann et al., 2009). The main distinction is that the ocean model is a slab-ocean model, similar to Lietaer *et al.* (2008), instead of the multi-level ocean model used in FESOM (Danilov et al., 2004). The sea ice model is the same as FESOM. Sea ice thermodynamics ignore internal heat storage (Semtner, 1976), and thermodynamic equations are calculated using energy balances at three interfaces: air-ice, ice-ocean, air-ocean. Sea ice dynamics are based on the elastic-viscous-plastic (EVP) rheology of (Hunke and Dukowicz, 2002, Hunke and

Dukowicz, 1997), where the physical behaviour of the sea ice is treated as a non-linear compressible fluid that can deform depending on thickness and pressure.

The slab ocean model has a constant depth of 30 m and it is characterized by a unique temperature and salinity. Ocean dynamics is simplified by neglecting ocean currents and sea-surface height gradient. Therefore, temperature and salinity of the ocean are restored to climatological values to prevent model drift. The restoring is done using a relaxation time scale of 180 days. Restoring terms are included in the equations for temperature and salinity fluxes (Terwisscha van Scheltinga et al., 2010). These simplifications in the ocean dynamics are not expected to significantly affect the SIC outputs, because the contribution of the oceanic circulation to changes in SIC in HB are small compared to the effect of the atmospheric forcing (Wang et al., 1994b, Wang et al., 1994c, Joly et al., 2010, Hochheim and Barber, 2010, Mysak et al., 1996, Saucier and Dionne, 1998, Gough and Allakhverdova, 1998). However, one may noticed that sea ice drift is slower compared to observations, because in the ice drift equation only winds provides input to the ice momentum. A more thorough description of the model's equations can be found in Appendix 1. For the list of the model parameters and constant values see Table 2.1.

The model runs on an unstructured triangular mesh, generated with the Gmsh generator (Geuzaine and Remacle, 2009, Terwisscha van Scheltinga et al., 2011). The unstructured grid gives more flexibility to the horizontal resolution, avoids pole singularities, and enhances the delineation of the coastline (Lietaer et

al., 2008). The spatial resolution is 200 km in the centre of the Arctic Basin, and becomes linearly finer towards the coast and narrow channels. Finest resolution is found within the channels of the Canadian Arctic Archipelago, were horizontal resolution is of 200 m. In HB, the coarsest resolution is of 25 km at the center of the Bay and finest is of 10 km near the coasts, for a total of 3134 elements within HB (Supplementary-Fig 5.1b). The coastline delineation data used by Gmsh is taken from Global Self-consistent Hierarchical High-Resolution Shoreline data base with a mean resolution of 178 m (Wessel and Smith, 1996). The model simulation of SIC, sea ice extent and thickness were validated in the Canadian Arctic Archipelago and they showed good agreement with PMW SIC data and other model estimates (Terwisscha van Scheltinga et al., 2010).

2.2.3 Initialization and forcing data

The model was initialized on January 1, 1973 and ran until December 31, 2010. Both atmospheric and oceanic forcing data are required to run the model. Atmospheric data was obtained from the National Center of Environmental Prediction and the National Center of Atmospheric Research (NCEP/NCAR; Boulder, Colorado, USA). These have a resolution of 1.975° by 1.975° (online access http://www.esrl.noaa.gov/psd/). Atmospheric forcing data included daily wind field at 10 m, air temperature and specific humidity at 2m, total cloudiness, and net precipitation. The model is forced with NCEP/NCAR reanalysis I (Kalnay et al., 1996) for the first 6 years (1973-79) and with NCEP-DOE reanalysis II

(Kanamitsu et al., 2002) from 1979 to 2010. Ocean forcing was obtained from the Polar Science Center of Hydrographic Climatology (PHC 3.0 (Steele et al., 2001), at http://dss.ucar.edu/datasets/ds285.2/). The PHC monthly climatological values of temperature and salinity of the mixed layer were linearly interpolated to obtain daily values. These have a resolution of 1° by 1°.

Initial sea ice conditions were prescribed as in Timmermann *et al.* (2009) where nodes with an ocean temperature < -1ºC are prescribed with an ice thickness of 1 m, a snow thickness of 10 cm, and a SIC of 90%. The SIC is defined by the percentage of the area cover by sea ice of thickness > 0.05 cm. The mean monthly fields of SIC were compared to satellite-derived data (CIS and PMW) from 1979-2006, and the daily SIC fields were compared to the polar bear GPS data and PMW data from 2004-10.

2.2.4 Satellite-derived SIC fields

The CIS produces weekly mean SIC charts derived from a combination of satellite measures from synthetic aperture radar, high resolution radiometer, airborne sea ice data, forecaster expertise, and, in some regions, *in situ* observations. The CIS charts have a horizontal resolution of 0.25^{o}x 0.25^{o} and are reproduced on a stereographic grid (25 x 25 km). To compared to PMW and model results I used the charts from 1979-2006. The CIS charts are considered reliable source of SIC in HB and in most studies they are treated as observations

(Hochheim and Barber, 2010, Hochheim et al., 2011). The SIC is given in tenths. The temporal and regional availability of weekly charts depends on the severity of the ice period, whereby fewer charts are produced during winter conditions. Therefore, to avoid discontinuities in the data set monthly means SIC have been calculated from the weekly SIC charts. The monthly means were calculated by averaging 2 or more weeks per month; in months when there were less than two weeks worth of fields no monthly average was produced. March was the month with most missing data, and monthly means are not available every year. CIS SIC monthly fields will be considered as the most accurate fields of SIC in HB, and they are compared to both, the model's and PMW's monthly fields of SIC to evaluate their accuracy.

The PMW SIC data is derived from brightness temperature readings of PMW satellites using a mathematical algorithm that links the brightness temperature to the SIC of the ice cover. The PMW SIC used is derived from brightness surface temperature readings (from Nimbus-7 Scanning Multichannel Microwave Radiometer, and the Defense Meteorological Satellite Program -F8, -F11 and -F13 Special Sensor Microwave/Imager radiances) using the Bootstrap (BS) algorithm (Comiso, 1999, updated 2008) (hereafter this data is called PMW-BS). The temporal resolution is of daily and monthly mean fields, and the horizontal resolution is 25 by 25 km on a polar stereographic grid. PMW-BS monthly mean fields were compared to those of the CIS to identify estimation errors of the PMW-BS data in HB. An error of minus 25-30% has been suggested

in the Arctic Ocean during break-up (Markus and Cavalieri, 2000, Comiso and Kwok, 1996). The error of the PMW data is identified by comparing with CIS. This is important as a reference, because the PMW data is use to validate the model results of the daily SIC fields and seasonal ice cycle. Although the CIS charts would have been preferred, these cannot be use because it has no daily SIC fields.

2.2.5 Polar bear GPS telemetry data

Polar bear telemetry data (Table 2.2) was obtained from 74 global positioning system (GPS) Argos® satellite-linked collars (Telonics Genration III and IV, Mesa, Arizona) that were deployed on 68 adult females with either cubs-of-the-year or one-year-old cubs. Females were captured from 2004 to 2009 in WH, between Churchill, Manitoba and the Ontario border. These collars provided a total of 97,227 GPS locations over the entire study period (Figure 2.1b, Table 2.2). Captures occurred on land either in August/September when female bears were ashore. Captured polar bears were located from a helicopter and immobilized via remote injection of tiletamine hydrochloride and zolazepam hydrochloride (Zoletil®, Laboratoires Virbac, Carros, France; (Stirling et al., 1989)). Capture and handling methods were approved by animal care committees at the University of Alberta and Environment Canada and were in accordance with the Canadian Council on Animal Care. The accuracy of Argos Satellite-GPS locations is < 10 m (Patterson et al., 2010, Tomkiewicz et al., 2010).

Offshore locations are defined as GPS-locations more than 10 km from the shoreline to avoid introducing false-offshore locations due to inaccuracies in the model's delineation of the coastline and the large tidal flats. This also contributed to ensure that most offshore locations where on sea ice and not polar bears swimming in open water. Data from collars with a gap of more than 3 days between consecutive GPS location are not including for the calculations of the migration dates. These precautions are meant to reduce the bias of including GPS locations from a polar bear swimming. Long distance swims are rare but are becoming more common, however, during long distances swimming the collars do not transmit continuously because the antenna is submerged under water (Monnett and Gleason, 2006, Durner et al., 2011).

2.2.6 Data analysis

To quantify the differences between estimated SIC by the CIS, the model, and the PMW-BS data, the root mean square error (RMSE) was calculated: $RMSE_i = \sqrt{\frac{SSE}{N-p}}$, per month ($i$) for N=28 year period (1979-2006), p=1, and SSE is the sum of square errors, calculated as $SSE = \sum e_i^2$, where e are the residuals ($e = y - \hat{y}$) per month. In the calculation of the residuals, the CIS estimates are the observations (y) and the model and PMW-data are the predicted variable ($\hat{y}$). Results of RMSE are in Table 2.3.

In months where the RMSE was large (June, July, November, December), the model simulation of the interannual variability of SIC was assessed using the Pearson product-moment correlation coefficient (r^2). This correlation tested the strength of the linear relation between model SIC and CIS SIC for each of these months; the r^2 between PMW-BS and CIS SIC was also calculated for comparison. Correlations will be high (r^2 =1 is maximum) if simulation of the interannual variability is similar to CIS. Similar r^2 for PMW-BS and a model is also expected and will assist assessing the model accuracy. Correlation results are shown in Figure 2.3.

Polar bear GPS-data were used as a categorical variable (presence/absence of sea ice). Locations offshore were assumed to indicate the presence of sea ice. This assumption is based on the dependence of polar bears on the sea ice (DeMaster and Stirling, 1981, Regehr et al., 2007) and the physiological limitations of long distance swimming (Durner et al., 2011, Monnett and Gleason, 2006). Moreover, observations of polar bears behaviour in WH that have found that polar bears migration on and off the sea ice are highly correlated to SIC (Stirling et al., 1999, Derocher and Stirling, 1990, Cherry, 2011). Therefore, when polar bear locations are on land it is assumed that there is no polar bear habitat offshore. From this analysis I exclude pregnant female's from November – February, because they stay on land for parturition and nourishment of the cubs during this time (Watts and Hansen, 1987). The daily fields of SIC obtained from the PMW-BS (2004-07) data and the model (2004-09) were evaluated using the

GPS-data. GPS locations were compared with SIC charts by plotting them together and determining the SIC at each location with each data set. Locations on < 10% SIC were considered as being on open water and as it is assumed that all locations offshore must be on sea ice, the error of the data set was quantified by determining the percentage of locations offshore on open water per month (Table 2.4).

The polar bear data during freeze-up (November-December.) and break-up (June-July) was used to estimate the mean day the WH population migrated offshore and ashore. The migration ashore was estimated by averaging the date individual females migrated onto land. Individual migration date was defined as the first day when locations on land were not followed by locations offshore until the next ice period. Similarly, I estimated the date the bears migrated offshore, as the first day locations offshore where not followed by locations on land until the next ice-free period. The mean dates were estimated using at least 2 collared polar bears. Therefore, I was only able to calculate the dates of migration ashore from 2006-09 and the dates of migration offshore from 2004-08.

I determined the linear correlation between SIC in WH and the migration of polar bears. This was done to evaluate the model's ability to predict trends that are ecologically important to polar bears. In particular, I was interested in the changes to the fasting period, which I defined as the period between the migrations ashore and offshore of the same year. A previous study found a high correlation between the migration ashore and the 30% SIC in WH, and the

migration offshore and the 10% SIC in WH (Cherry, 2011). I calculated the correlation of the migration of polar bears and these two values of SIC using the model estimates, but also included two addition SIC values above and below (Cherry, 2011)'s reference value to account for differences between data sets (e.g., the 10%, 20%, 30%, 40% and 50% during break-up and the 10%, 20% and 30% during freeze-up). The best correlation is that with the highest r-square and lowest p-value, and it is compared to Cherry (2011); these results are shown in Figure 2.7. These values of SIC are used to predict the polar bear migration in the past and to examined the trend in the length of the fasting period over 1979-2010 (Figure 2.8).

2.3 Results

The SIC monthly means simulated by the model and PMW-BS are in good agreement with the CIS estimates (within 15%) between 1979 and 2006 (Figure 2.2, Table 2.3). The 28 year-mean SIC estimates are within 5% of the CIS mean in all months, except July, June, November and December. During these months, the model overestimates the SIC in June +8.5% (σ=6.7) and July +12.4% (σ=6.9), and underestimates it in November -9.7% (σ=9.5), and December -9.6% (σ=13.6). The model and PMW-BS errors in June and July are similar in magnitude (Table 2.3) although of opposite sign when compared to the CIS estimates: the PMW-BS underestimates the SIC in June -8.6% (σ=6.9) and July -16.0% (σ=6.6) compared

to CIS estimates (Figure 2.2). Despite differences, both data sets simulated the interannual variability of the mean SIC well (Figure 2.3) with strong positive correlations when compared to CIS and significant ($p \leq 0.5$): the correlations coefficient (r^2) between CIS and PMW-BS are 0.86 in June, 0.88 in July, 0.85 in November, 0.83 in December; and between CIS and the model output are 0.66 in June, 0.86 in July, and 0.74 in both November and December.

In June and July, the model simulates well the gradient of SIC observed in CIS: the highest SIC is in the southwest and the lowest SIC in the northwest and James Bay where there are ice-free conditions (Figures 2.4). The CIS also estimates almost ice-free conditions in the area immediately east and north-east of the Belcher Islands; the model does not capture this. In these months, the model overestimates the SIC in eastern HB by roughly 20%. The PMW-BS SIC represents well the SIC gradient in June and July but it underestimates the SIC in the southwest by roughly 25%, and overestimates the size of the ice-free regions in northern and eastern HB. In November and December, the model did not represent well the SIC nearshore. In November, the model showed almost no ice nearshore. These results contrast with those of CIS and PMW-BS which show sea ice in up to 50% SIC along all the western shore of HB, including the western shores of James Bay. Model simulation was better in offshore regions. In December, the model continued to underestimate the SIC nearshore, by about 40% compared to CIS data. The PMW-BS SIC is, in generally good agreement

with the CIS estimates during freeze-up months, except for a small overestimation of the SIC in north-western HB (Figure 2.4).

As expected, all offshore polar bear locations during winter and spring were on the sea ice, however, some locations in July, November, and December where in open water. This suggested that both, the model and the PMW-BS data could be underestimating the amount of sea ice on these months periodically. During July, only 0.1% of the GPS locations were in open water using the model daily SIC fields, while when using the PMW-BS SIC fields 95.2% of the locations were in open water (Table 2.4). This result indicated that the PMW-BS data is significantly underestimating the amount of sea ice in HB during break-up, a critical period to study the migration ashore. In November, 15.0% of the locations were in open water using the model simulation of SIC. Most of these locations were nearshore and related to land fast ice, which the model fails to represent. In December, the percentage of locations in open water is smaller, only 0.2%. Similar percentage errors were obtained using PMW-BS SIC data: 15.2% in November and 0.1% in December, but in November these locations in open water were more associated with the sea ice further offshore (Table 2.4).

Migration ashore occurred between July 6th and Aug 5th in 2006-09. Last locations offshore where usually in southwest HB, between Churchill and Cape Henrietta Maria (Figure.2.5), suggesting the presence of sea ice along the southwest coast. Our model correctly simulates sea ice in the southwest, and most locations during the migration ashore were on sea ice (Figure.2.6). The PMW-BS

SIC data, on the other hand, shows almost no sea ice in this region during the migration ashore, and thus, most locations offshore are in open water (Figure.2.5). The migration offshore occurred between Nov 26th and Dec 2nd in 2004-08. First locations offshore were usually close to or north of Churchill, Manitoba and associated with the sea ice that forms along the coast (Figure 2.6). A delay of 5days (σ=1.5) was detected in the model formation of sea ice in 2004-09. This delay is the difference between the date the polar bear was located in open water and the time sea ice formed at those location.

The migration on land is best correlated to the date of 50% SIC in WH (r^2=0.99) and the migration offshore was correlated to the day of 10% SIC in WH (r^2=0.80) (Figure 2.7). Polar bears migrated on land almost simultaneously (0.7days (σ=1.7)) when SIC in WH reached 50% (Figure 2.7a), and migrated offshore on average 1.2days (σ=1.2) before the date of 10% SIC in WH (Figure 2.7b). Therefore, the period between the date of 50% SIC and the date of 10% SIC in WH, represents the fasting period of polar bears. From 1980-2000, the ice-free period lengthened at a rate of one week per decade, with a steeper trend of 2 weeks per decade after 1990. It was estimated that the fasting period was 2 weeks longer in 2000-10 compared to 1980-90 (Figure.2.8).

2.4 Discussion

The use of animals to sample their environment is a recent development. Several studies have used marine mammals, such as seals and whales, to monitor oceanographic parameters in remote areas where data is difficult to obtain (Lydersen et al., 2002, Laidre et al., 2008, Simmons et al., 2009, Boehlert et al., 2001). This is the first time polar bears have been used to sample sea ice characteristics to assist in the validation of sea ice models. Using GPS locations of polar bears in WH, I obtained information that aids in the validation of a sea ice-ocean model in HB. The use of GPS-locations as a categorical variable suggested that PMW-BS data is significantly underestimating the amount of sea ice in July. Telemetry data showed polar bears offshore while PMW-BS estimated that HB was ice-free. GPS-locations also suggested that the model overestimates sea ice in July and underestimates in November.

Overall, the model simulates the mean SIC in good agreement with the CIS data in every month from 1979-2006. Those months in which there are larger differences (June, July, November and December) are characterized by partial sea ice cover and the estimation errors could arise from simplification in the ocean dynamics that under-estimate the importance of ocean currents during partial ice cover (Prinsenberg and Freeman, 1986, Prinsenberg, 1986a, Prinsenberg, 1986b). In June and July, for example, the overestimation of SIC are likely due to the accumulation of sea ice in eastern HB, (1) because in the model's main force driving sea ice drift is wind stress, and between May and August, winds blow from the northwest and west (Maxwell, 1986). Wang et al. (1994c) arrived at a

similar conclusion while conducting sensitivity experiments with a coarse resolution sea-ice ocean model. And (2) because spring and summer are characterized by well-developed baroclinic currents on the eastern coast that are thought to advect sea ice (Wang et al., 1994c, Saucier et al., 2004) and heat (Prinsenberg, 1984) northward along the eastern coast of HB, from James Bay to Hudson Strait. The model's simplified dynamics ignores the ocean currents that contribute to accelerated rate of sea ice disappearance, through melt or export, in eastern HB (Wang et al., 1994c, Saucier et al., 2004), and thus the slower ice melt in eastern HB.

An intermodel comparison using two sea ice-ocean models that differed only in the configuration of the ocean component (slab-ocean vs. full ocean model) showed that the vertical parameterization of thermal diffusivity has a more important role in the response of sea ice to global warming than including a several vertical levels in a dynamic ocean model (Gough and Wolfe, 2001). These authors suggested that a higher value of thermal diffusivity was associated with faster sea ice thickness declines. Other authors also agree that the parameterization of ocean thermodynamics has a strong influence in SIC (Gough and Allakhverdova, 1999, Gagnon and Gough, 2005). Ocean currents appear to be more important in the advection of sea ice in eastern HB, where unresolved ocean dynamic have led to over-estimation of sea ice concentration during break-up (Wang et al., 1994c, Saucier et al., 2004). The simplifications of the model do not

appear to cause overestimations of the sea ice in WH, because polar bear locations in July were occupying the entire area covered by sea ice in WH.

The GPS-data suggests that the PMW-BS data is significantly underestimating the sea ice area and probably also the SIC during break-up making it inappropriate to evaluate the model-daily SIC outputs. These findings emphasize the need for a careful examination of studies using daily PMW-BS SIC data during break-up in HB. In November and December some GPS locations were near the coast or offshore in proximity to the ice edge. Using PMW-BS data it was noted that polar bears nearshore moved offshore as soon as the sea ice formed near their location, and that those further offshore follow the southeast drift of the sea ice pack, spending most of their time near the ice edge. Such behaviour indicated the delays in the model formation of sea ice. In November, polar bears often move south or offshore before sea ice was predicted in the area. With PMW-BS data, a similar delay was only present near the ice-edge and during the first days of the migration, but estimating the ice edge with PMW data is challenged by the higher evaporation and cloud formation in the proximity of the edge that affect the brightness surface temperature readings (Hunewinkel et al., 1998, Dokken et al., 2002). Based on the noted behaviour of polar bears to stay near the ice edge during freeze-up (region above 10% SIC immediately next to the open water), I think it is possible that GPS telemetry data can be use to help identify the expansion of sea ice at freeze-up, complementing with satellite data. It would also be interesting to explore the applications of telemetry data in the

identification of polynyas, as polar bears are known to frequent polynyas because of the abundance of prey (Schliebe et al., 2008, Harwood and Stirling, 1992, Stirling, 1997).

The model delay of sea ice formation could be explained by the simplification in the ocean model's dynamic and the use of a constant mixed layer depth of 30 m. In northwest HB, there is an inflow of cold Arctic water through Roes Welcome Sound (Prinsenberg, 1986a) that is an important modulator of surface water properties in north-western HB (Prinsenberg, 1986b). The relaxation constant used to adjust the water properties may need to be smaller (< 190 day) to capture the effect of the inflow and increase the accuracy in the timing of the sea ice formation. However, stronger restoring may compromise the prognostic characteristic of the sea ice model. The northwest inflow also contributes to the advection of sea ice south (Wang et al., 1994c, Prinsenberg, 1987, Saucier et al., 2004). Therefore, omitting ocean currents from the sea ice momentum equation, leads to slower sea ice drift. Moreover, because the typical winds in autumn are westerly (Maxwell, 1986), the model advect the newly form sea ice away from shore (east) instead of the more realistic southeast advection (Wang et al., 1994c, Prinsenberg, 1987, Saucier et al., 2004). The absence of sea ice nearshore could also be a result of using a slab-ocean with a constant depth of 30 m, in contrast with the varying depth of the ocean nearshore (<10 m) (Martini, 1986, Pelletier, 1986). A homogenous but thicker layer of water takes longer to cool down to freezing.

Similar to Cherry (2011), I found a strong correlation between the SIC in WH and the migration of polar bears from WH population. In both studies, the migration ashore was more strongly correlated to a freeze-up date of 10% SIC. In contrast, I found that the migration ashore was more strongly correlated, and occured almost simultaneously, with 50% SIC. In Cherry (2011), the migration ashore was more strongly correlated to 30% SIC and occured about one month later. The differences between the studies during break-up could arise from differences in SIC data, or from differences in the polar bear telmetry data used in each study. Cherry (2011) used a combination non-GPS telemetry data from 1991-97 and GPS data from 2004-07, while I used only the GPS locations. Differences in the selected SIC to return on land could indicate a change in the polar bears selection to maximize the time offshore. Therefore, one would expect polar bears to select a lower SIC rather than the higher SIC found when compared both studies. Therefore, it is more likely that differences between the two studies are associated with differences in the source of SIC used. Cherry (2011) used PMW SIC data, and this was demonstrated to significantly underestimate the SIC in July, while the model overestimate the SIC in July. The PMW data is also known to have larger underestimation errors in the Arctic during melting (Markus and Cavalieri, 2000, Comiso and Kwok, 1996). Further, in Cherry (2011) the migration ashore was occuring ~25 days after the 30% SIC in WH, therfore, by the date polar bears returned onland, PMW charts were showing no sea ice. In contrast, the model results although overestiamting the avaraged SIC in HB, in WH, results matched the CIS charts. Moreover, observations of the polar bear

migration in WH, indicate that polar bears abandoned sea ice for land when SIC are near 50% (Stirling et al., 1999). These results suggest that the model estimating SIC with better accuracy than PMW data in July.

The positive and steep trend of ~1.5 week per decade found for the length of the ice-free period in WH (1980-2010), is similar to the 10 days per decade calculated for the whole HB in a previous study (Markus et al., 2009). This trend is also in accordance with polar bear demographic studies that have shown a decline in WH bear population from 1984 to 2004 that was associated to the changing sea ice conditions (Regehr et al., 2007).

2.5 Conclusions

In this chapter I explored the use of polar bear GPS data for the validation of the SIC output from a new sea ice-ocean model. This is the first time GPS polar bear data has been used to provide information about sea ice condition. The approach taken is based in the high dependence of polar bears on sea ice, and the strong correlation between the migration of polar bears and the SIC in WH that has been found by previous studies.

The sea ice-ocean model presented in this study demonstrates proficiency in simulating the intra-annual and interannual changes in the SIC in HB, aside from small overestimations during June and July, and small underestimations

during November and December compared to the CIS SIC data. The estimation errors, however, are relatively small (< 15%) and similar in magnitude to those of the PMW data when compared to CIS. The SIC overestimations were associated to with regions where ocean currents are strongest; and the SIC underestimations were associated with the absence of land-fast ice. It is likely that these errors arise from the simplifications in the ocean dynamics of the slab ocean component of the model. Sensitivity studies to measure the effect of resorting are recommended to evaluate the model's performance in estimating the land-fast ice, and to gain insight into causes of sea ice absence nearshore.

The polar bear GPS-data proved to be a powerful tool in conjunction with satellite data to detect uncertainties in SIC estimates, and timing of the sea ice cycle in WH. The contribution of GPS-data was especially important during break-up when I was unable to use PMW-BS SIC data to infer the daily changes of the SIC. Further, analysis of the model in eastern HB using telemetry data from polar bears in the SH population could serve to quantify the delays in the melting of the sea ice in the east. The tendency of polar bears in WH to remain near the ice edge during freeze-up suggests that the GPS-data can be use to contour the ice edge; a technique that can be applied in other regions of the Arctic if polar bear's behaviour is similar. The positive results obtained with the GPS-data suggest that it could be used to complement satellite SIC data in the validation of sea ice models in other regions.

The seasonal migration of polar bears matched closely seasonality of the sea ice. There is a strong correlation between the polar bear migration and the SIC in WH, whereas polar bears abandon the sea ice when SIC in WH declined to 50%. This implies that polar bears will be at risk in a warmer climate where the tendency is to lower SIC. Considering the satisfactory results obtained with the sea ice-ocean model in WH, it is suggested that this model be used to predict future sea ice conditions WH. There are currently no studies that predict the 21st century sea ice changes in HB using a polar bear habitat perspective. In an attempt to fill-in this gap, I follow-up with a study using this same sea ice model to predict the 21st century SIC and seasonal cycle in HB and WH, in ways that can be interpreted to help anticipate the effects of global warming on polar bears.

(A)

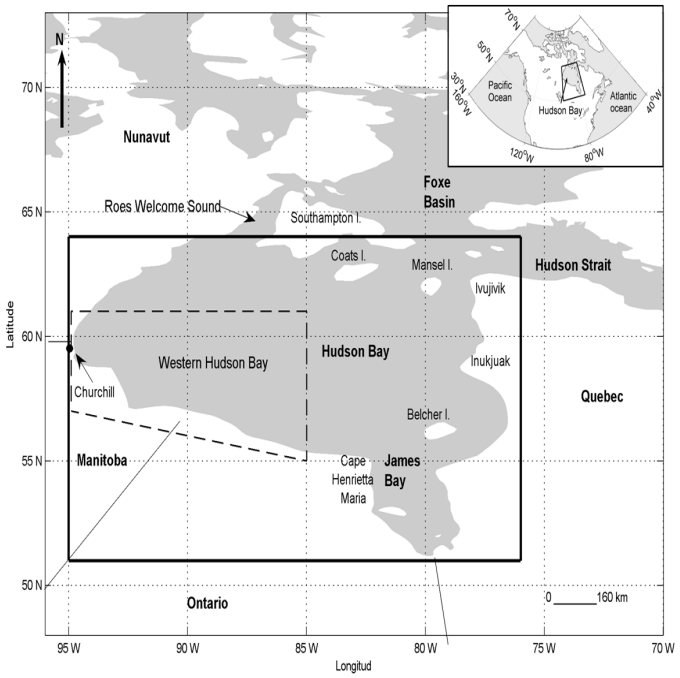

(B)

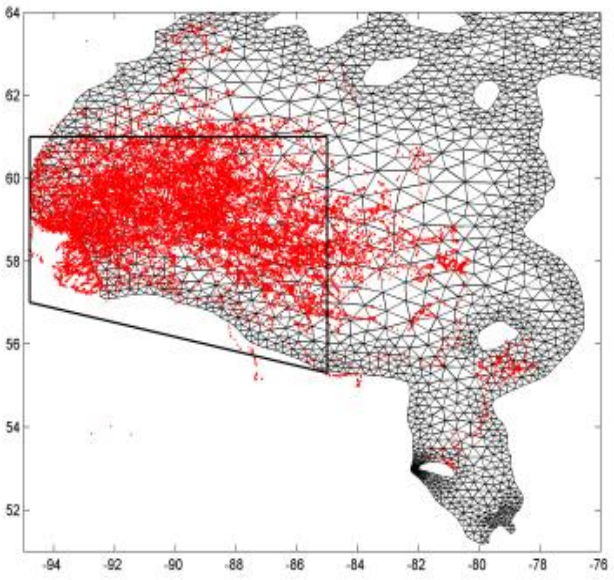

Figure 2.1 Hudson Bay (solid line) and Western Hudson Bay (dashed line) domains (A). The location of Hudson Bay (HB) within the North American sub-continent is shown on the inset on the top-right corner of (A). The model grid within HB is range from 10 to 25 Km (B). Available polar bear GPS locations from western Hudson Bay (solid line) and from 2004 -09 are shown using red dots. Western Hudson Bay is the 95% area used by the polar bears.

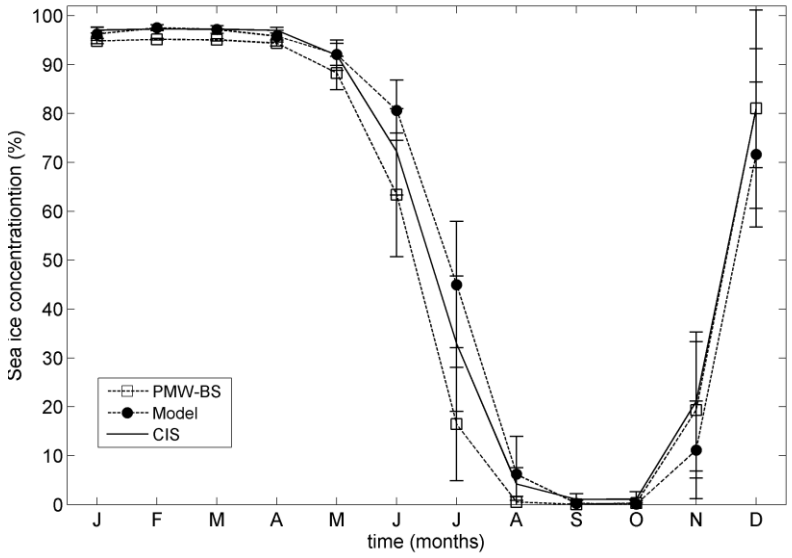

Figure 2.2 Mean monthly SIC in HB from 1979-2006. Error bars are ± one standard deviation. Estimates from Canadian Ice Service (CIS), are compared to Passive Microwave - Bootstrap algorithm (PMW-BS; (Comiso, 1999, updated 2008)), and model results (model).

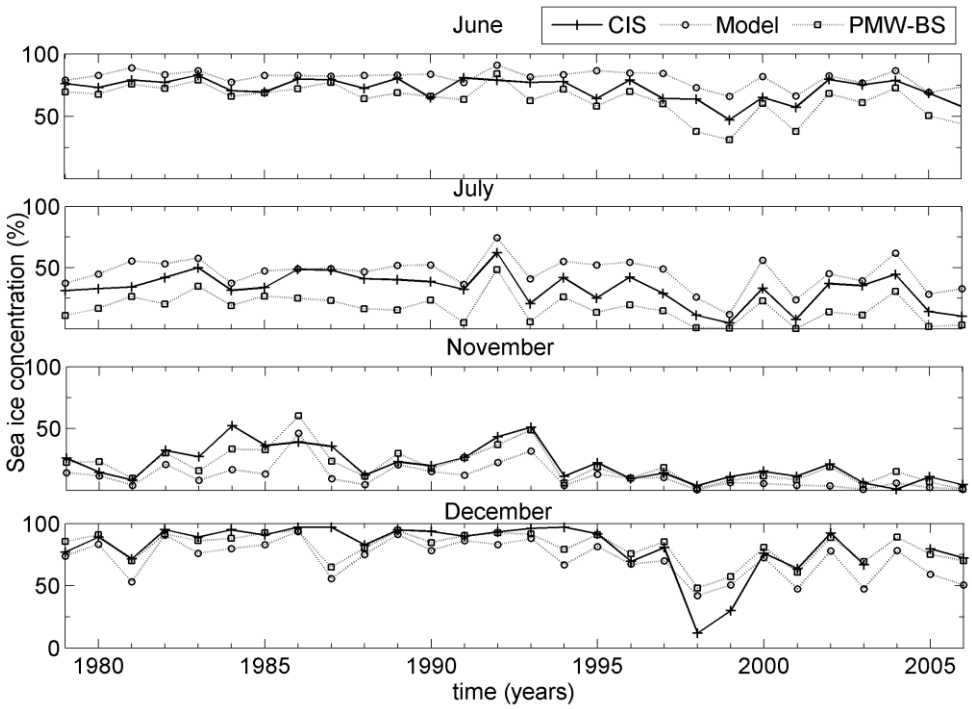

Figure 2.3 Interannual variation of mean SIC in HB for 1979-2006 and months: June, July, November, and December, estimated by Canadian Ice Service (CIS), Passive Microwave with bootstrap algorithm (PMW-BS;(Comiso, 1999, updated 2008)) and the Model simulation. Eventhough model and PMW-BS errors compared to CIS, the correlation coefficients (r^2) are high: r^2 between CIS and PMW-BS are 0.86 in June, 0.88 in July, 0.85 in November, 0.83 in December; and r^2 between CIS and Model are 0.66 in June, 0.86 in July, 0.74 in November and December.

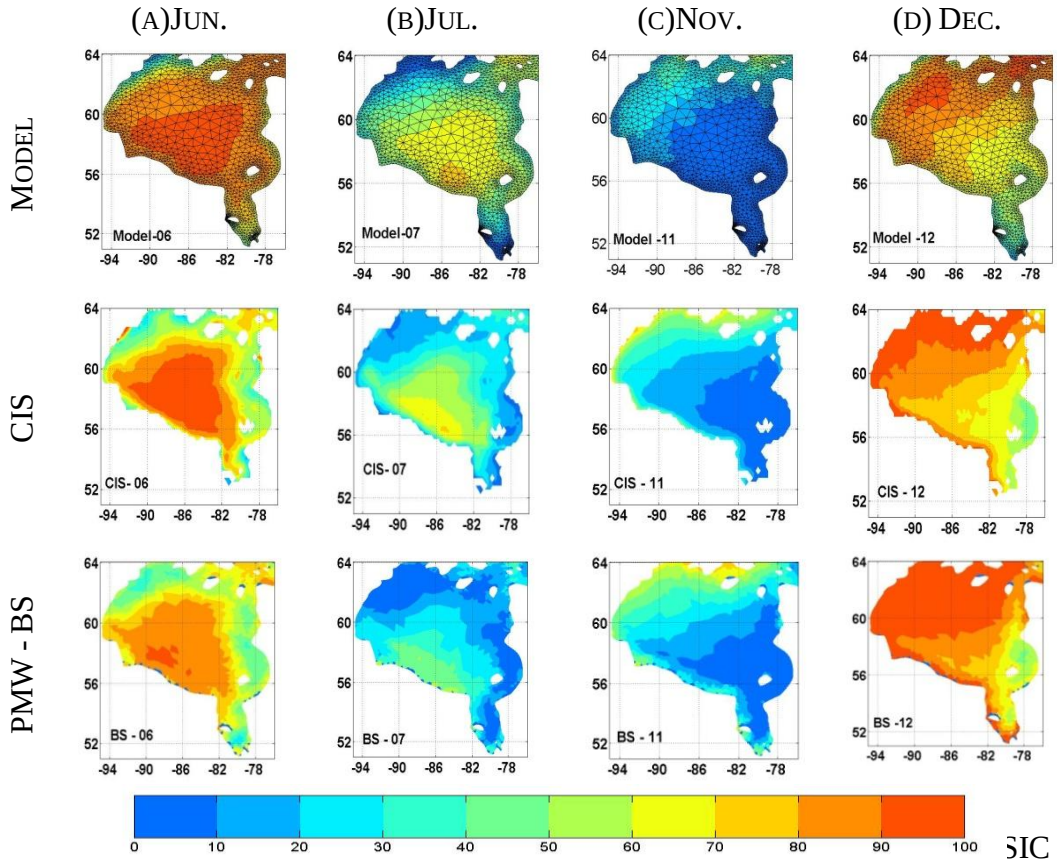

Figure 2.4 Spatial distribution of the mean sea ice concentration (SIC) (1979-2006) in June (a), July (b), November (c), and December (c) estimated by the model, Canidian Ice Service (CIS), and Passive Microwave data (PMW-BS; (Comiso, 1999, updated 2008)).

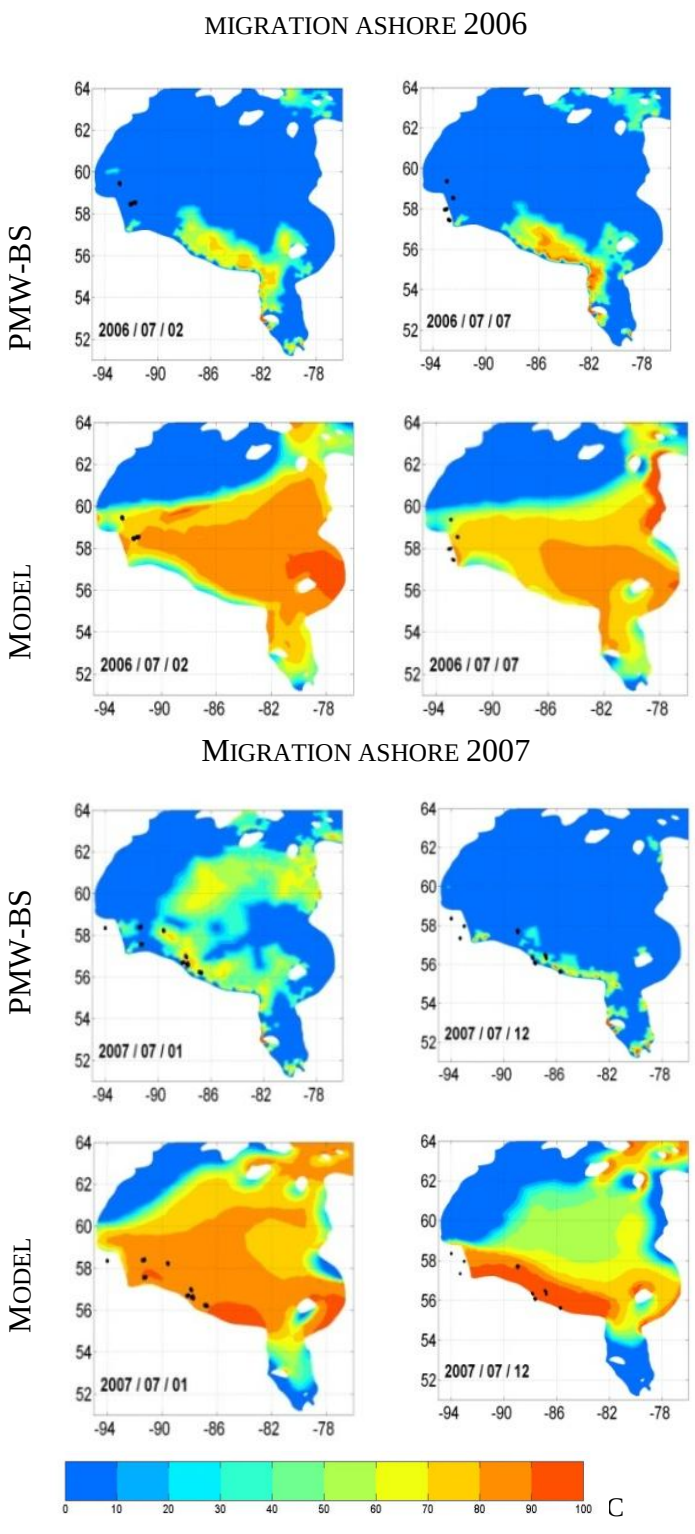

Figure 2.5 Two examples of sea ice concentration (SIC) during the polar bear migration ashore in 2006 and 2007. Polar bear locations are the black dots. On the left column, is the first day a bear was found on land, and on the right column, is the last day a bear was found offshore. SIC estimates by the PMW-BS data are compared to Model estimates. Polar bears on dark blue (<10% SIC) are the included in the estimation errors of July in Table 2.4.

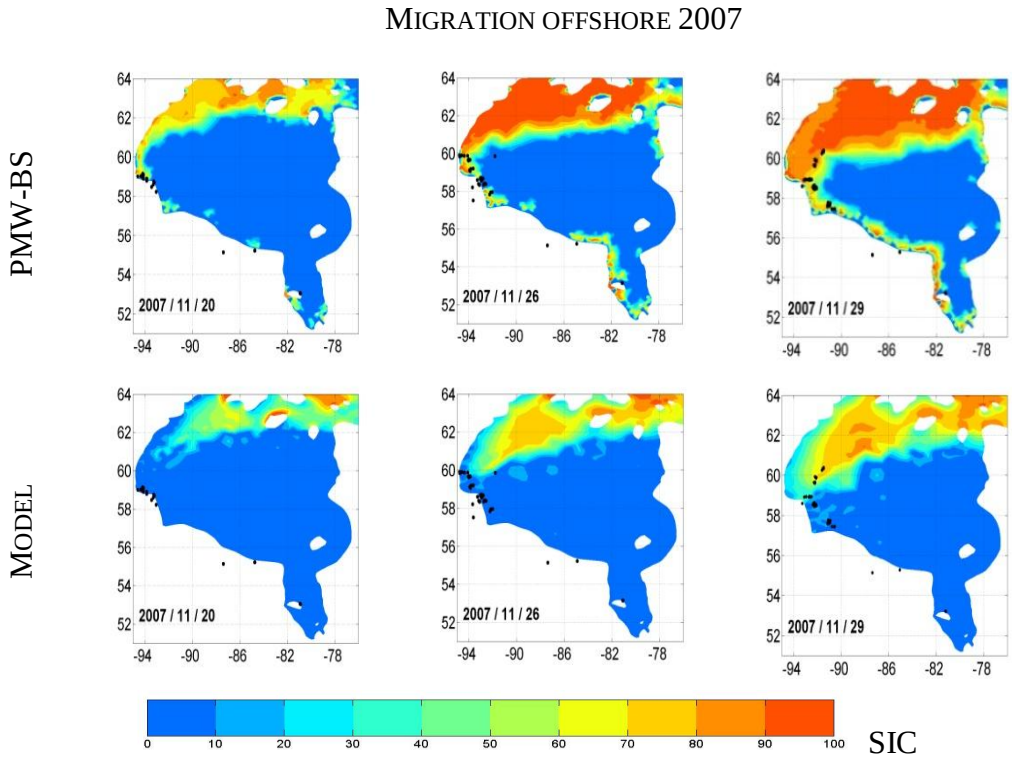

Figure 2.6 Examples of sea ice concentration (SIC) during the polar bear migration offshore in 2007. The example shows that the first day a location was found offshore, and that the last day locations where found ashore (excluding GPS locations from pregnant females) (e.g. length of the migration 20-29 of November 2007). The SIC is estimated by the PMW-BS data (top) and this model (bottom). Polar bear GPS locations are indicated by black dots. The GPS-locations of polar bears on open water (dark blue) are included in the estimation errors of November in Table 2.4.

(A)

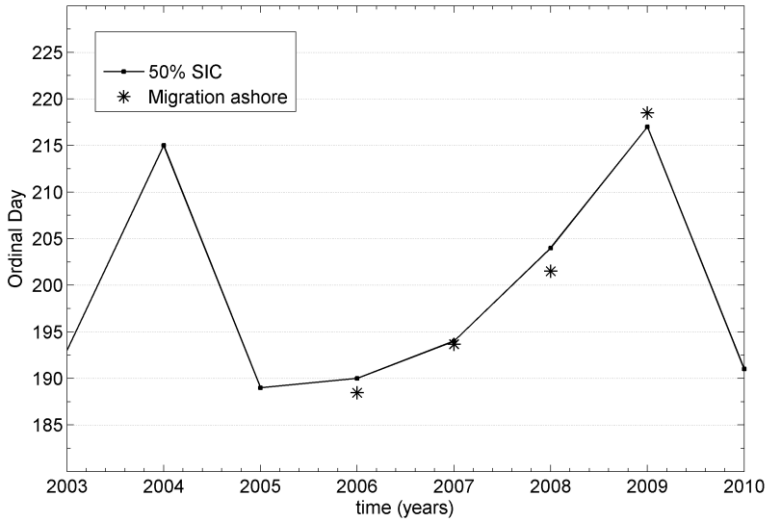

(B)

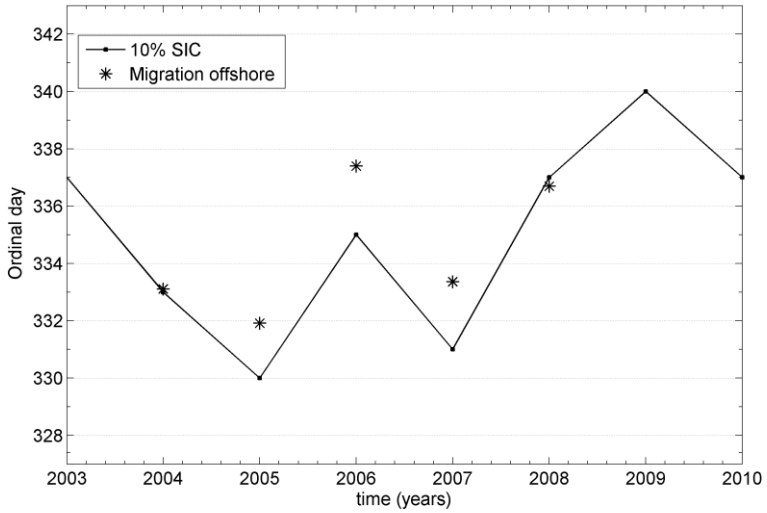

Figure 2.7 Relation between the polar bear migration ashore (A) and offshore (B) and SIC in WH. The correlation coefficient between the date of 10% SIC and the migration offshore was $r^2 = 0.80$, $p = 0.04$, and between migration ashore and the day of 50% SIC $r^2 = 0.99$, $p = 0.01$.

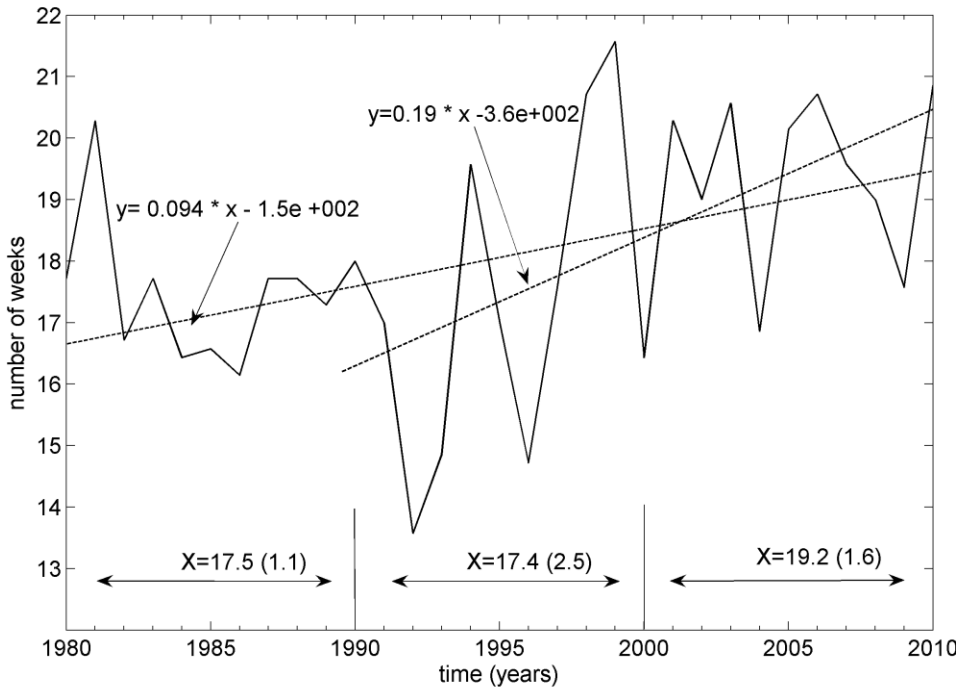

Figure 2.8 Model simulation of the duration of the ice-free period (solid line) in Western Hudson Bay (WH) from 1980-2010. Linear trends (dashed lines) calculated for the complete period (1980-2010), and for the last 2 decades (1990-2010). The mean lengths of the ice-free period are calculated for each of decade and are indicated at the bottom (standard deviation in parenthesis). The ice-free period is the period between the day of 50% SIC during break-up and the day of 10% SIC during freeze-up.

Table 2.1 Selection of parameters and values used in the model run.

PARAMETER	VALUE
Grid spacing	200 M – 25 KM
Mixed layer depth	H_{ML}= 30.0 M
Critical ice thickness	H_O= 0.05 M
Critical ice concentration	A_O= 0.15
Melting temperature	T_{AMELT}= 273.16 K
Laplacian diffusivity	K= 1000 M/S
Emissivity of water, ice, snow	$\epsilon_O = \epsilon_I = \epsilon_S$ =0.97
Stefan Boltzmann's constant	Σ= 5.67E-8 W/M^2K^4
Thermal conductivity ocean-ice	K_{OI}= 1.0E^{-3}
Thermal conductivity ice	K_I= 2.17 W / M K
Thermal conductivity snow	K_S= 0.31 W / M K
Albedo frozen snow $T_A \leq$ 273.16 K	A_{SD}= 0.85
Albedo melting snow $T_A \geq$ 273.16 K	A_{SW}= 0.73
Albedo frozen ice	A_{ID}= 0.75
Albedo melting ice	A_{IW}= 0.66
Albedo sea water	A_O= 0.10
Water density	P_O=1025 KG/M^3
Ice density	P_I= 910 KG/M^3
Snow density	P_S= 290 KG/M^3
Air density	P_A= 1.3 KG/M^3
Amplification factor	G=1.0
Volumetric Heat capacity of water	CC=4.20E^6 J/M^3K
Volumetric latent heat of sea ice	C_I= 3.02E8 J/M^3
Specific heat capacity of air	C_{PA}=1004 J/KGK
Latent heat of evaporation	L_V= 2.500E^6 J/KG
Latent heat of sublimation	L_S= 2.834E^6 J/KG
Bulk sensible and latent heat transfer coefficients	$C_{DS}=C_{DL}$= 1.75E^{-3}
Heat transfer coefficient ocean-sea ice	Γ_T= 1.0E^{-4}
Constant latent heat fluxes over ocean	Q_{SO}= 17.2694
Constant latent heat fluxes over ice	Q_{SI}= 21.8745
Latent heat over water	T_{QO}= 237.3 K
Latent heat over ice	T_{QI}= 265.5 K
Drag coefficient of wind over ice	C_{DAI}= 1.32E^{-3}
Drag coefficient of wind over ocean	C_{DAO}= 1.0E^{-3}
Drag coefficient of ocean over ice	C_{DOI}= 3.0E^{-3}
Rheology time step	2000 S
EVP rheology time step	150 S
Yield curve eccentricity	E=2

Table 2.2 Telemetry data from polar bears in Western Hudson Bay from 2004-09. The table shows the total number of polar bears and the GPS locations available per sampling year (season), in relation to the number of GPS locations during break-up (Jun.-Jul.) and freeze-up (Nov.-Dec.).

SEASON	NUMBER OF POLAR BEARS	TOTAL NUMBER OF LOCATIONS	AVAILABLE LOCATIONS JUN-JUL	AVAILABLE LOCATIONS NOV.-DEC.
09/2004- 08/2005	9	48881	44	1536
09/2005-08/2006	10	10755	983	2508
09/2007-08/2008	19	18428	4101	1194
09/2008-08/2009	15	19163	4520	1573

Table 2.3 Root Mean Square Errors (RMSE)* of monthly SIC fields (1979-2006). RMSE are calculated for the model and the PMW-BS data using the CIS fields as the observations.

	MODEL	PMW-BS
JANUARY	1.20	2.11
FEBRUARY	0.59	2.29
MARCH	2.91	2.72
APRIL	1.59	2.70
MAY	3.12	5.01
JUNE	10.77	10.96
JULY	14.12	17.23
AUGUST	5.65	4.48
SEPTEMBER	1.43	1.50
OCTOBER	1.72	1.47
NOVEMBER	13.48	7.64
DECEMBER	16.39	11.87

*$\mathrm{RMSE_i} = \sqrt{\frac{\mathrm{SSE}}{\mathrm{N-p}}}$, where N=28, p=1, and $\mathrm{SSE} = \sum \mathrm{e_i^2}$ where e are the residuals ($\mathrm{e} = \mathrm{y} - \hat{\mathrm{y}}$), i is the month, $\hat{\mathrm{y}}$ is the simulated SIC by this model or PMW-BS and y is CIS SIC.

Table 2.4 Comparing sea ice fields with telemetry data. On the table are the total number of polar bear-GPS locations offshore (N) and number of those locations that were found in open water (O) for each months shown and for each data set. The estimated error (E) is a measure of how accurate the sea ice fields from each data set are: E = (O/N)*100. To calculate "O", the daily fields of SIC were plotted together with locations. Different years were used to calculate number of "O" for the MODEL (2004-09) and PMW-BS (2004-07); this depended on the availability of sea ice fields. Only the months were the MODEL error was greater than cero are shown in the table.

	JULY			NOVEMBER			DECEMBER		
	N	O	E	N	O	E	N	O	E
MODEL	1000	1	0.1	967	147	15.2	6000	12	0.2
PMW-BS	105	100	95.2	636	96	15.0	3333	4	0.1

2.6 References

Agnew, T. & Howell, S. 2003. The use of operational ice charts for evaluating passive microwave ice concentration data. *Atmosphere-Ocean,* 41, 317-331.

Amstrup, S. C., Caswell, H., Deweaver, E., Stirling, I., Douglas, D. C., Marcot, B. G. & Hunter, C. M. 2009. Rebuttal of "Polar Bear Population Forecasts: A Public-Policy Forecasting Audit". *Interfaces,* 39, 353-369.

Amstrup, S. C., Durner, G. M., McDonald, T. L., Mulcahy, D. M. & Garner, G. W. 2001. Comparing movement patterns of satellite-tagged male and female polar bears. *Canadian Journal of Zoology,* 79, 2147-2158.

Amstrup, S. C., Durner, G. M., Stirling, I., Lunn, N. N. & Messier, F. 2000. Movements and distribution of polar bears in the Beaufort Sea. *Canadian Journal of Zoology,* 78, 948-966.

Arthur, S. M., Manly, B. F. J., McDonald, L. L. & Garner, G. W. 1996. Assessing habitat selection when availability changes. *Ecology,* 77, 215-227.

Boehlert, G. W., Costa, D. P., Crocker, D. E., Green, P., O'brien, T., Levitus, S. & Le Boeuf, B. J. 2001. Autonomous pinniped environmental samplers: Using instrumented animals as oceanographic data collectors. *Journal of Atmospheric and Oceanic Technology,* 18, 1882-1893.

Born, E. W., Wiig, Ø. & Thomassen, J. 1997. Seasonal and annual movements of radio-collared polar bears (*Ursus maritimus*) in northeast Greenland. *Journal of Marine Systems,* 10, 67-77.

Cavalieri, D. J., Crawford, J. P., Drinkwater, M. R., Eppler, D. T., Farmer, L. D., Jentz, R. R. & Wackerman, C. C. 1991. Aircraft active and passive microwave validation of sea ice concentration from defense metereological satellite program special sensor microwave imager. *Journal of Geophysical Research-Oceans,* 96, 21989-22008.

Chapman, W. L. & Walsh, J. E. 1993. Recent variations of sea ice and air-temperature in high-latitudes. *Bulletin of the American Meteorological Society*, 74, 33-47.

Cherry, S. G. 2011. *The ecology of polar bears in relation to sea ice dynamics.* Ph.D. Thesis, University of Alberta.

Comiso, J. C. 1999, updated 2008. Bootstrap Sea Ice Concentrations from Nimbus-7 SMMR and DMSP SSM/I, [1979-2007]. Boulder, Colorado USA: National Snow and Ice Data Center.

Comiso, J. C., Cavalieri, D. J., Parkinson, C. L. & Gloersen, P. 1997. Passive microwave algorithms for sea ice concentration: A comparison of two techniques. *Remote Sensing of Environment,* 60, 357-384.

Comiso, J. C. & Kwok, R. 1996. Surface and radiative characteristics of the summer Arctic sea ice cover from multisensor satellite observations. *Journal of Geophysical Research-Oceans,* 101, 28397-28416.

Danilov, S., Gennady, K. & Schröter, J. 2004. A finite-element ocean model: principles and evaluation. *Ocean Modelling,* 125-150.

Demaster, D. P. & Stirling, I. 1981. *Ursus maritimus*. *Mammalian Species,* 145, 1-7.

Derocher, A. E., Lunn, N. J. & Stirling, I. 2004. Polar bears in a warming climate. *Integrative and Comparative Biology*, 44, 163-176.

Derocher, A. E. & Stirling, I. 1990. Distribution of polar bears (*Ursus maritimus*) during the ice-free period in western Hudson Bay. *Canadian Journal of Zoology* 68, 1395-1403.

Derocher, A. E. & Stirling, I. 1995. Temporal variation in reproduction and body-mass of polar bears in western Hudson-Bay. *Canadian Journal of Zoology*, 73, 1657-1665.

Derocher, A. E., Stirling, I. & Andriashek, D. 1992. Pregnancy rates and serum progesterone levels of polar bears in western Hudson-Bay. *Canadian Journal of Zoology*, 70, 561-566.

Dokken, S. T., Winsor, P., Markus, T., Askne, J. & Bjork, G. 2002. ERS SAR characterization of coastal polynyas in the Arctic and comparison with SSM/I and numerical model investigations. *Remote Sensing of Environment*, 80, 321-335.

Durner, G. M., et al. 2009. Predicting 21st-century polar bear habitat distribution from global climate models. *Ecological Monographs*, 79, 25-58.

Durner, G. M., Whiteman, J. P., Harlow, H. J., Amstrup, S. C., Regehr, E. V. & Ben-david, M. 2011. Consequences of long-distance swimming and travel over deep-water pack ice for a female polar bear during a year of extreme sea ice retreat. *Polar Biology*, 34, 975-984.

Gagnon, A. S. & Gough, W. A. 2005. Climate change scenarios for the Hudson Bay region: An intermodel comparison. *Climatic Change*, 69, 269-297.

Geuzaine, C. & Remacle, J. F. 2009. Gmsh: A 3-D finite element mesh generator with built-in pre- and post-processing facilities. *International Journal for Numerical Methods in Engineering,* 79, 1309-1331.

Gough, W. A. & Allakhverdova, T. 1998. Sensitivity of a coarse resolution ocean general circulation model under climate change forcing. *Tellus Series a-Dynamic Meteorology and Oceanography,* 50, 124-133.

Gough, W. A. & Allakhverdova, T. 1999. Limitations of using a coarse resolution model to assess the impact of climate chance on sea ice in Hudson Bay. *Canadian Geographer,* 43, 415-422.

Gough, W. A., Cornwell, A. R. & Tsuji, L. J. S. 2004. Trends in seasonal sea ice duration in southwestern Hudson Bay. *Arctic,* 57, 299-305.

Gough, W. A. & Wolfe, E. 2001. Climate change scenarios for Hudson Bay, Canada, from general circulation models. *Arctic,* 54, 142-148.

Harwood, L. A. & Stirling, I. 1992. Distributrion of ringed seals in the southeastern Beaufort Sea during late summer. *Canadian Journal of Zoology-Revue Canadienne De Zoologie,* 70, 891-900.

Hochheim, K. P. & Barber, D. G. 2010. Atmospheric forcing of sea ice in Hudson Bay during the fall period, 1980-2005. *Journal of Geophysical Research-Oceans,* 115.

Hochheim, K. P., Lukovich, J. V. & Barber, D. G. 2011. Atmospheric forcing of sea ice in Hudson Bay during the spring period, 1980–2005. *Journal of Marine Systems,* 88, 476-487.

Holland, M. M. & Bitz, C. M. 2003. Polar amplification of climate change in coupled models. *Climate Dynamics,* 21, 221-232.

Hunewinkel, T., Markus, T. & Heygster, G. C. 1998. Improved determination of the sea ice edge with SSM/I data for small-scale analyses. *Ieee Transactions on Geoscience and Remote Sensing,* 36, 1795-1808.

Hunke, E. C. & Dukowicz, J. K. 1997. An elastic-viscous-plastic model for sea ice dynamics. *Journal of Physical Oceanography,* 27, 1849-1867.

Hunke, E. C. & Dukowicz, J. K. 2002. The elastic-viscous-plastic sea ice dynamics model in general orthogonal curvilinear coordinates on a sphere-incorporation of metric terms. *Monthly Weather Review,* 130, 1848-1865.

Joly, S., Senneville, S., Caya, D. & Saucier, F. J. 2010. Sensitivity of Hudson Bay Sea ice and ocean climate to atmospheric temperature forcing *Climate Dynamics,* 1835-1849.

Kalnay, E., et al. 1996. The NCEP/NCAR 40-year reanalysis project. *Bulletin of the American Meteorological Society,* 437-470.

Kanamitsu, M., Ebisuzaki, W., Woollen, J., Yang, S., Hnilo, J. & Potter, G. 2002. NCEP-DOE AMIP II reanalysis (R-2). *Bulletin of the American Meteorological Society,* 83, 1631-1642.

Laidre, K. L., Stirling, I., Lowry, L. F., Wiig, Ø., Heide-Jorgensen, M. P. & Ferguson, S. H. 2008. Quantifying the sensitivity of arctic marine mammals to climate-induced habitat change. *Ecological Applications,* 18, S97-S125.

Learmonth, J. A., Macleod, C. D., Santos, M. B., Pierce, G. J., Crick, H. Q. P. & Robinson, R. A. 2006. Potential effects of climate change on marine mammals. *In:* Gibson, R. (ed.) *Oceanography and Marine Biology - an Annual Review, Vol 44.*

Lietaer, O., Fichefet, T. & Legat, V. 2008. The effects of resolving the Canadian Arctic Archipelago in a finite element sea ice model. *Ocean Modelling,* 24, 140-152.

Liu, J. P., Zhang, Z. H., Hu, Y. Y., Chen, L. Q., Dai, Y. J. & Ren, X. B. 2008. Assessment of surface air temperature over the Arctic Ocean in reanalysis and IPCC AR4 model simulations with IABP/POLES observations. *Journal of Geophysical Research-Atmospheres,* 113.

Liu, Y. H., Key, J. R. & Wang, X. J. 2009. Influence of changes in sea ice concentration and cloud cover on recent Arctic surface temperature trends. *Geophysical Research Letters,* 36.

Lydersen, C., Nost, O. A., Lovell, P., McConnell, B. J., Gammelsrod, T., Hunter, C., Fedak, M. A. & Kovacs, K. M. 2002. Salinity and temperature structure of a freezing Arctic fjord - monitored by white whales (*Delphinapterus leucas*). *Geophysical Research Letters,* 29.

Markus, T. & Cavalieri, D. J. 2000. An enhancement of the NASA Team sea ice algorithm. *Ieee Transactions on Geoscience and Remote Sensing,* 38, 1387-1398.

Markus, T. & Dokken, S. T. 2002. Evaluation of late summer passive microwave Arctic sea ice retrievals. *Ieee Transactions on Geoscience and Remote Sensing,* 40, 348-356.

Markus, T., Stroeve, J. C. & Miller, J. 2009. Recent changes in Arctic sea ice melt onset, freezeup, and melt season length. *Journal of Geophysical Research-Oceans,* 114.

Martini, I. P. 1986. Coastal feature of Canadian Inland Seas. *In:* Martini, I. P. (ed.) *Canadian Inland Seas.* New York: Elsevier Science Publishers Company Inc.

Mauritzen, M., Derocher, A. E. & Wiig, Ø. 2001. Space-use strategies of female polar bears in a dynamic sea ice habitat. *Canadian Journal of Zoology-Revue Canadienne De Zoologie,* 79, 1704-1713.

Maxwell, J. B. 1986. A climate overview of the Canadian Inland Seas. *In:* Martini, I. P. (ed.) *Canadian Inland Seas.* New York: Elsevier Science Publishers Company Inc, 79-99 pp.

Molnár, P. K., Derocher, A. E., Klanjscek, T. & Lewis, M. A. 2011. Predicting climate change impacts on polar bear litter size. *Nature Communications,* 2, DOI: 18610.1038/ncomms1183.

Molnár, P. K., Derocher, A. E., Thiemann, G. W. & Lewis, M. A. 2010. Predicting survival, reproduction and abundance of polar bears under climate change. *Biological Conservation,* 143, 1612-1622.

Monnett, C. & Gleason, J. S. 2006. Observations of mortality associated with extended open-water swimming by polar bears in the Alaskan Beaufort Sea. *Polar Biology,* 29, 681-687.

Mysak, L. A., Ingram, R. G., Wang, J. & Vanderbaaren, A. 1996. The anomalous sea-ice extent in Hudson Bay, Baffin Bay and the Labrador Sea during three simultaneous NAO and ENSO episodes. *Atmosphere-Ocean,* 34, 313-343.

Parks, E. K., Derocher, A. E. & Lunn, N. J. 2006. Seasonal and annual movement patterns of polar bears on the sea ice of Hudson Bay. *Canadian Journal of Zoology,* 84, 1281-1294.

Patterson, T. A., McConnell, B. J., Fedak, M. A., Bravington, M. V. & Hindell, M. A. 2010. Using GPS data to evaluate the accuracy of state-space methods for correction of Argos satellite telemetry error. *Ecology,* 91, 273-285.

Peacock, E., Derocher, A. E., Lunn, N. J. & Obbard, M. 2010. Polar bear ecology and management in Hudson Bay in the face of climate change *In:* Ferguson, S. H., Loseto, L. L. & Mallory, M. L. (eds.) *A little less Arctic: Top predators in the world's largest northern inland sea, Hudson Bay.* London: Springer, 95-115 pp.

Pelletier, B. R. 1986. Seafloor morphology and sediments. *In:* Martini, I. P. (ed.) *Canadian Inland Seas.* New York: Elsevier Science Publishers Company Inc., 143-162 pp.

Prinsenberg, S. J. 1984. Fresh-water contents and heat budgets of James Bay and Hudson Bay. *Continental Shelf Research,* 3, 191-200.

Prinsenberg, S. J. 1986a. The circulation pattern and current structure of Hudosn Bay. *In:* Martini, I. P. (ed.) *Canadian Inland Seas.* New York: Elsevier Science Publishers Company Inc.

Prinsenberg, S. J. 1986b. Salinity and temperature distribution of Hudson Bay and James Bay. *In:* Martini, I. P. (ed.) *Canadian Inland Seas.* New York: Elsevier Science Publishers Company Inc.

Prinsenberg, S. J. 1987. Seasonal current variations observed in western Hudson Bay. *Journal of Geophysical Research-Oceans,* 92, 10756-10766.

Prinsenberg, S. J. & Freeman, N. G. 1986. Tidal heights and currents in Hudson Bay and James Bay. *In:* Martini, I. P. (ed.) *Canadian Inland Seas.* New York: Elsevier Science Publishers Company Inc.

Prowse, T. D., Furgal, C., Wrona, F. J. & Reist, J. D. 2009. Implications of Climate Change for Northern Canada: Freshwater, Marine, and Terrestrial Ecosystems. *Ambio,* 38, 282-289.

Regehr, E. V., Lunn, N. J., Amstrup, S. C. & Stirling, L. 2007. Effects of earlier sea ice breakup on survival and population size of polar bears in western Hudson bay. *Journal of Wildlife Management,* 71, 2673-2683.

Saucier, F. J. & Dionne, J. 1998. A 3-D coupled ice-ocean model applied to Hudson Bay, Canada: The seasonal cycle and time-dependent climate response to atmospheric forcing and runoff. *Journal of Geophysical Research-Oceans,* 103, 27689-27705.

Saucier, F. J., Senneville, S., Prinsenberg, S. J., Roy, F., Smith, G., Gachon, P., Caya, D. & Laprise, R. 2004. Modelling the sea ice-ocean seasonal cycle in Hudson Bay, Foxe Basin and Hudson Strait, Canada. *Climate Dynamics,* 23, 303-326.

Schliebe, S., Rode, K. D., Gleason, J. S., Wilder, J., Proffitt, K., Evans, T. J. & Miller, S. 2008. Effects of sea ice extent and food availability on spatial and temporal distribution of polar bears during the fall open-water period in the Southern Beaufort Sea. *Polar Biology,* 31, 999-1010.

Semtner, A. J. 1976. Model for thermodynamic growth of sea ice in numerical intestigations of climate. *Journal of Physical Oceanography,* 6, 379-389.

Shokr, M., Markus, T. & Ieee 2003. *Evaluation of ice concentration algorithms using data fusion of SSM/I and radarsat*, 65-67 pp.

Sibert, V., Zakardjian, B., Saucier, F., Gosselin, M., Starr, M. & Senneville, S. 2010. Spatial and temporal variability of ice algal production in a 3D ice-ocean model of the Hudson Bay, Hudson Strait and Foxe Basin system. *Polar Research,* 29, 353-378.

Simmons, S. E., Tremblay, Y. & Costa, D. P. 2009. Pinnipeds as ocean-temperature samplers: calibrations, validations, and data quality. *Limnology and Oceanography-Methods,* 7, 648-656.

Steele, M., Morley, R. & Ermold, W. 2001. PHC: A Global Ocean Hydrography with a High-Quality Arctic Ocean. *Journal of Climate,* 14, 2079-2087.

Stirling, I. 1997. The importance of polynyas, ice edges, and leads to marine mammals and birds. *Journal of Marine Systems,* 10, 9-21.

Stirling, I. & Derocher, A. E. 1993. Possible impacts of climatic warming on polar bears. *Arctic,* 46, 240-245.

Stirling, I., Lunn, N. J. & Iacozza, J. 1999. Long-term trends in the population ecology of polar bears in western Hudson Bay in relation to climatic change. *Arctic,* 52, 294-306.

Stirling, I., Richardson, E., Thiemann, G. W. & Derocher, A. E. 2008. Unusual predation attempts of polar bears on ringed seals in the southern Beaufort Sea: Possible significance of changing spring ice conditions. *Arctic,* 61, 14-22.

Stirling, I., Spencer, C. & Andriashek, D. 1989. Immobilization of polar bears (*Ursus maritimus*) with Telazol in the Canadian Arctic. *Journal of Wildlife Diseases,* 25, 159-168.

Terwisscha van Scheltinga, A. D., Myers, P. G. & Pietrzak, J. D. 2010. A finite element sea ice model of the Canadian Arctic Archipelago. *Ocean Dynamics,* 60, 1539-1558.

Terwisscha van Scheltinga, A. D., Myers, P. G. & Pietrzak, J. D. 2011. Mesh generation in archipelagos. *Ocean Dynamics Topical Collections on Multiscale Modeling,* (submitted Dec. 2011).

Thiemann, G. W., Derocher, A. E. & Stirling, I. 2008. Polar bear (*Ursus maritimus*) conservation in Canada: an ecological basis for identifying designatable units. *Oryx,* 42, 504-515.

Timmermann, R., Danilov, S., Schroter, J., Boning, C., Sidorenko, D. & Rollenhagen, K. 2009. Ocean circulation and sea ice distribution in a finite element global sea ice-ocean model. *Ocean Modelling,* 27, 114-129.

Tomkiewicz, S. M., Fuller, M. R., Kie, J. G. & Bates, K. K. 2010. Global positioning system and associated technologies in animal behaviour and ecological research. *Philosophical Transactions of the Royal Society B-Biological Sciences,* 365, 2163-2176.

Wang, J., Mysak, L. A. & Ingram, R. G. 1994a. A 3-Dimensional numerical-simulation of Hudson-Bay summer ocean circulation- topographic gyres, separations and coastal jets. *Journal of Physical Oceanography,* 24, 2496-2514.

Wang, J., Mysak, L. A. & Ingram, R. G. 1994b. Internal variability of sea-ice cover in Hudson-Bay, Baffin-Bay and the Labrador Sea. *Atmosphere-Ocean,* 32, 421-447.

Wang, J., Mysak, L. A. & Ingram, R. G. 1994c. A numerical-simulation of sea-ice in Hudson-Bay. *Journal of Physical Oceanography,* 24, 2515-2533.

Watts, P. D. & Hansen, S. E. 1987. Cyclic starvation as a reproductive stratergy in the polar bear *Symposia of the Zoological Society of London,* 57, 305-318.

Wessel, P. & Smith, W. H. F. 1996. A global, self-consistent, hierarchical, high-resolution shoreline database. *Journal of Geophysical Research,* 101, 8741-8743.

Yakovlev, N. G. 2009a. Reproduction of the large-scale state of water and sea ice in the Arctic Ocean from 1948 to 2002: Part II. The state of ice and snow cover. *Izvestiya Atmospheric and Oceanic Physics,* 45, 478-494.

Yakovlev, N. G. 2009b. Reproduction of the large-scale state of water and sea ice in the Arctic Ocean in 1948-2002: Part I. Numerical model. *Izvestiya Atmospheric and Oceanic Physics,* 45, 357-371.

Chapter 3 Predicting sea ice dynamics in Hudson Bay and impacts on polar bears.

3.1 Introduction

Polar bears (*Ursus maritimus*) are an ice-obligated species that depend on the sea ice as a platform to access and hunt their marine prey (Smith, 1980, Stirling and McEwan, 1975, Derocher et al., 2002). The species has a circumpolar distribution in close association with the presence of sea ice (DeMaster and Stirling, 1981). In Hudson Bay (HB), Canada, the southernmost range of polar bears (Smith, 1980, Stirling and McEwan, 1975, Derocher et al., 2002, Peacock et al., 2010), the populations are challenged by the seasonal melt of their sea ice habitat in summer (Gough et al., 2004). The melt of the sea ice cover during summer forces polar bears on land (Derocher and Stirling, 1990), from where their marine prey with high energy content are inaccessible (Rode et al., 2010b, Ramsay and Stirling, 1988): ringed seals (*Pusa hispida*) and bearded seals (*Erignathus barbatus*)(Thiemann et al., 2008). During summer, polar bears rely on their fat stores to survive the ice-free period and in Western Hudson Bay (WH) lose up to 1 kg of body weight per day while fasting (Derocher and Stirling, 1995b). The onland period is about 4 months for males and non-pregnant females, and nearly 8 to 9 months for pregnant females who enter maternity dens in November at the time other bears return to the sea ice (Watts and Hansen, 1987).

The fat stores needed to survive the fasting period are accumulated through hunting on the sea ice. The most important hunting period is spring (Molnár et al., 2010, Rode et al., 2010a, Stirling and Øritsland, 1995) and more generally, high sea ice concentration (SIC) increases the hunting success of polar bears (Stirling, 2002).

Over the last 30 years, positive temperature anomalies in the northern hemisphere (Shein et al., 2006, Manabe et al., 2011) have caused changes in the seasonal ice cycle and significant losses of SIC in HB (Markus et al., 2009, Hochheim and Barber, 2010, Hochheim et al., 2011, Gagnon and Gough, 2005b). These changes are correlated with declines in body condition, recruitment, and survival of polar bears in WH (Stirling and Parkinson, 2006, Derocher et al., 2004, Molnár et al., 2010, Regehr et al., 2007, Stirling et al., 1999). Between 1987 and 2004 the WH polar bear population declined from 1,194 to 935 individuals; a drop largely attributed to the advances in the break-up date and SIC losses in WH and to a lesser degree excess harvest (Regehr et al., 2007). Years with earlier break-up date (date of 50% SIC) are correlated with poor physical conditions of polar bears (i.e., thinner) on land in summer (Derocher and Stirling, 1995a). Thinner polar bears, at the same time, have less fat stores and thus lower probability of surviving the ice-free period (Molnár et al., 2010). Other changes in the seasonal cycle include later freeze-up and thus a longer ice-free period (Markus et al., 2009, Hochheim and Barber, 2010), which are associated with

increase food stress and risk of starvation of polar bears (Regehr et al., 2007, Parks et al., 2006).

Dynamic energy budget studies predict that in a year in which the WH ice-free period lengthens to 180 days (~6 months), 28-48% of the adult males in the WH population will die of starvation before the end of summer (Molnár et al., 2010); and that in any year in which the break-up date advances 1- 2 months relative to the 1990s, 40-100% of the pregnant females in the WH population will fail to reproduce (Molnár et al., 2011). Hereafter years either one such events are called "critical years" based on their predicted deleterious impact on WH polar bears. Estimating both the occurrence and frequent critical years in the future is important for the conservation and management of the WH population. However there are many sea ice models that study the effects of climate change on the Arctic through the 21st century, only a few focused on HB, and none focus on the impact of the sea ice changes on polar bears.

Previous modeling in HB includes mainly sensitivity studies that measure the response of the sea ice cover to different forcing (Wang et al., 1994b, Wang et al., 1994c, Mysak et al., 1996, Saucier and Dionne, 1998). These studies showed that the atmospheric temperature is the main contributor to the changes in the SIC, and seasonality of the sea ice in HB. For example, increasing the temperature by 2^{o}C lengthen the ice-free period by 1 month (Saucier and Dionne, 1998). As well, climate change studies that measured the response of HB's sea ice cover to global warming support this finding and showed a strong inverse relationship between

temperature and sea ice concentration in HB (Gough and Allakhverdova, 1998, Gough and Wolfe, 2001, Gagnon and Gough, 2005a, Joly et al., 2010). A doubling of the CO_2 concentration, for example, results in a warming predicted to caused a lengthening of the ice-free period to a total of about 6 months, and an advance in the break-up date of about 1 month relative to the 1 x CO_2 run (Gough and Wolfe, 2001). These means were calculated for the whole HB and are not specific to WH, they were also obtained from a 20 year output of two global circulation models: GCM I and GCM II, which have a coarse resolution. A recent study obtained similar results using a higher resolution sea ice-ocean model and the warming proposed for scenario A2 of the Intergovernmental Panel on Climate Change (IPCC) for 2041-70 relative to 1971-90 (~1.5 x CO_2) (Joly et al., 2010). While these studies provide a sense of how the sea ice might change with global warming, no studies have examined how critical life history events for polar bears may be affected.

In this Chapter, I predict the response of the seasonal ice cycle and SIC to climate change in the 21st century proposed by the IPCC in scenarios Committed, B1, A1B and A2. I used a high-resolution finite element sea ice-ocean model (FESOM) with varying spatial resolution and atmospheric forcing from the CGCM models. The model's simulation of SIC in the 20th century was validated before proceeding with the predictions. My objectives are to predict (1) the maximum SIC in HB, (2) the trends in the break-up date and (3) length of the ice-free period in WH. From these three aspects of sea ice dynamics I will determine

the timing and occurrence of critical years during the 21st century in each of the warming scenarios.

3.2 Methods

3.2.1 Study area

Hudson Bay is defined as the area between 52ºN - 64ºN and 76ºW - 95ºW, an area of approximately 10^6 km^2. WH is a subdivision of HB: 55ºN - 61ºN and 85ºW - 95ºW, which is the closest approximation to the 95% minimum convex polygon of the area used by polar bears in the WH population (Peacock et al., 2010) (Figure 3.1).

HB is a seasonally ice covered body of water. The maximum SIC occurs in spring, March – May, and ice-free conditions last from mid-July to early November. The seasonal and interannual changes in the SIC are mainly driven by atmospheric conditions such as temperature and wind (Wang et al., 1994b, Mysak et al., 1996). Arctic-like conditions during winter, when HB is ice covered, are a result of the frequent intrusion of cold Arctic air masses (Maxwell, 1986). The inflow of Arctic waters from Foxe Basin play a secondary role, but it is important for cooling the surface water in northwestern HB (Prinsenberg, 1986a, Prinsenberg, 1986b).

The oceanic and sea ice circulation in HB are cyclonic, and mainly driven by the inflow/outflow through channels east and west of Southampton Island (Figure 3.1), the winds, the density currents, and the tidal currents (Maxwell, 1986, Prinsenberg, 1986a, Prinsenberg, 1986b, Prinsenberg and Freeman, 1986, Wang et al., 1994a). The influence of the inflow/outflow, density currents, and tidal currents are dampened with the formation of the sea ice cover in winter (Prinsenberg and Freeman, 1986, Prinsenberg, 1986a) and therefore play a minor role in the circulation of sea ice, except during melting when density currents are strengthened by the increased runoff and freshwater, especially in eastern HB (Wang et al., 1994a, Saucier et al., 2004). Therefore, it is possible that the model simplifications in the ocean dynamics have implications that may affect the model results (see following section).

3.2.2 Model description

The finite element sea ice-ocean model is a version of the FESOM (Timmermann et al., 2009), however the sea ice model is here coupled to a slab-ocean model (Terwisscha van Scheltinga et al., 2010) instead of the original multilevel ocean of FESOM. The sea ice dynamics are based on the elastic-viscous plastic rheology (Hunke and Dukowicz, 2002) and the thermodynamics are calculated at several interfaces (Parkinson and Washington, 2007), using a zero-layer approach to describe heat diffusion through thick ice (Semtner, 1976). The zero-layer approach considers a linear temperature profile between the

surface and the bottom of sea ice, neglecting heat storage within the ice. The slab-ocean model has similar configuration to the one describe in Lietaer et al. (2008). It has a constant depth of 30 m, it is vertically homogenous, it does not consider ocean currents, and it assumes equal ocean dynamic height and thus no sea surface height gradient (Lietaer et al., 2008, Terwisscha van Scheltinga et al., 2010). The main distinction between ocean models, is that Terwisscha van Scheltinga et al. (2010)'s slab-ocean is characterized by temperature and salinity, rather than only temperature. The slab-ocean represents the mixed layer of the Arctic and subarctic Ocean. The simplified dynamics reduce the ocean surface stress to a drag of the ocean on the sea ice. Thus, sea ice drift is mainly governed by the surface winds. The ocean temperature and salinity are restored to time-varying climatology through a term added to the heat and salinity fluxes (Terwisscha van Scheltinga et al., 2010). Restoring timescale is 180 days. Other model parameters and constants are shown in Table 3.1.

The model domain includes the Arctic and subarctic seas north of 50ºN, excluding the Bering Sea and the Baltic Seas (Supplementary-Fig 5.1a). It has closed boundary conditions at the Bering Strait and in the North Atlantic Ocean at 50ºN. The spatial resolution in the central Arctic is 200 km but becomes finer (up to 100 m) towards the coast and within narrow channels where higher resolution is important to resolve small scale processes. Within HB, the spatial resolution is 25 km in the central offshore regions, linearly increasing to 10 km near the coast (Supplementary-Fig 5.1b). The model results of SIC, thickness, and fluxes were validated in the Canadian Arctic Archipelago and were shown to have reasonable

agreement with available observations from passive microwave satellite (PMW) data (Terwisscha van Scheltinga et al., 2010). The model simulation of SIC in HB was also shown to be in good agreement with the CIS SIC (Chapter 2).

3.2.3 Initialization and forcing data

The model initializes on January 1, 1954 with initial sea ice thickness, snow thickness, and sea ice concentration following the criteria of (Timmermann et al., 2009) with at nodes where ocean temperature is below -1ºC, designated sea ice thickness of 1 m, snow thickness 10 cm, and sea ice concentration of 90%, and at nodes where the ocean temperature was above -1ºC, no sea ice was prescribed. These are also typical climatological values for sea ice parameters in HB during winter (Prinsenberg, 1986b). The hindcast run continues to December 31, 2000. Sea ice parameters at the end of this run are used to start the 4 future runs: from January 1, 2001 to December 31, 2100. Results are obtained in the form of daily and mean monthly SIC fields per grid point, for each of the 5 runs.

Forcing data were obtained from the Canadian Centre of Climate Modeling and Analysis (CCCma). The output from the Coupled Atmospheric–Ocean Climate Model version 3.1/resolution T63 (CGCM 3.1 (T63)) (obtained at CCCma website http://www.cccma.ec.gc.ca) are used in the hindcast and forecasts. The atmospheric and oceanic forcing to run the model in the hindcast run (1954-2000) is the output from the CGCM 3.1 (T63) run based on the IPCC 20th century scenario 20C3M, and in the forecasts (2001-2100) is the output of

CGCM 3.1 (T63) runs based on IPCC 21th century scenarios: Committed, B1, A1B, and A2. The IPCC suggest a linear increase in the CO_2 concentration in each of the three scenarios. In B1, CO_2 concentrations increase from 380 ppm in 2001 to 550 ppm in 2100. In A1B, it increases from 380 ppm in 2001 to 720 ppm. In A2, it increases from 380 ppm in 2001 to 800 ppm. To be consistent with other studies, the forecasts have been named after the IPCC scenarios to reference the degree of warming.

The oceanographic outputs of CGCM 3.1 (T63)-Committed were unavailable, thus, the oceanic forcing from the CGCM3.1 (T63)-B1 was used in its place. This ocean forcing has mild warming that can affect the Committed simulation results with spurious melting at the bottom of sea ice. However, atmospheric forcing has a dominant role in the SIC trend in HB (Prinsenberg and Freeman, 1986, Wang et al., 1994b, Saucier and Dionne, 1998, Gough and Allakhverdova, 1999, Gough and Wolfe, 2001, Saucier et al., 2004, Joly et al., 2010) and in the Committed scenario the CO_2 concentrations are kept constant. Therefore, results from the Committed forecast are expected to be the most representative of present-day conditions in HB and are use as a control run to compare to B1, A1B and A2 forecasts.

Additionally, and to test the effect of different forcing data on the results of SIC, the model was run from 1973 to 2010 (hereafter NCEP-hindcast) using atmospheric forcing from the National Center of Environmental Prediction (NCEP)-National Center of Atmospheric Research (NCAR) (provided by

NOAA/OAR/ESRL PSD, Boulder, Colorado, USA, http://www.esrl.noaa.gov/psd/), and oceanographic forcing from the Polar Science Center of Hydrographic Climatology (PHC 3.1, University of Washington, Seattle, USA). The NCEP hindcast was initialized on January 1, 1973 using the same criteria as described above to prescribe initial sea ice parameters. For the first 6 years (until December 31, 1978) the model was forced with NCEP/NCAR reanalysis I (Kalnay et al., 1996), and from January 1, 1979 to December 31, 2010, the model was forced using NCEP-DOE reanalysis II (Kanamitsu et al., 2002).

3.2.4 Data processing and analysis

To compared the model results of SIC, monthly SIC fields from 20C3M and NCEP hindcast were compared to the Canadian Ice Service (CIS) SIC data from 1979-2000 (obtained from http://ice-glaces.ec.gc.ca). This helped isolate the model errors from the response of sea ice to different forcing.

The maximum SIC in HB is in spring, between March and April, this is also the most important hunting time for polar bears (Rode et al., 2010a, Hammill and Smith, 1991, Stirling and Øritsland, 1995). Therefore, predicting the mean spring SIC per year can provide insight into the impact of global warming on the access of polar bears to their prey, and the pattern and timing of total sea ice loss

within HB. Spring SIC maps from B1, A1B and A2 were compared to the Committed scenario.

Daily SIC outputs were used to measure the effects of warming on the timing of the seasonal cycle in WH. The break-up date (first day of 50% SIC) and a freeze-up date (first day of 10% SIC) are calculated each year. With these dates, I defined the start and the end ice-free period, respectively. The definition of the break-up and freeze-up dates based on the high correlation with the polar bear migration ashore and offshore are found in *Chapter 2*. Therefore the ice-free period corresponds to the length of the fasting period. The trend in the break-up date and the length of the ice-free period are calculated for each scenario: Committed, B1, A1B, A2. I focus on only these two parameters because of their significant ecological implications for polar bears (Molnár et al., 2010, Molnár et al., 2011). To isolate the effect of global warming, and to exclude possible errors introduced with the forcing data, the results are compared to the Committed scenarios and presented as the anomalies relative to Committed simulation: $An = X - Y$; where *An* is the anomaly, *X* is the result of either B1, A1B or A2, and *Y* is the result of the Committed simulation. The anomalies can be zero meaning no difference, positive, meaning an advance of the break-up date or a lengthening of the ice-free period, and negative, meaning delays in the break-up date or a shortening of the ice-free period (depending on parameter calculated). Freeze-up date is not explicitly shown because changes in the freeze-up date affect polar bear's survival in a manner equivalent to the lengthening of the ice-

free period. However, the general trend on the freeze-up day can be deduced from by comparing the ice-free period and the break-up date trends.

The frequency of critical break-up dates and critical length of the ice-free period per decade was calculated from the anomalies and defining them with the thresholds of 1 more advance in the break-up date and 180 days long ice-free period, respectively, predicted to cause significant declines in population growth and survival rate of polar bears in WH (Molnár et al., 2010, Molnár et al., 2011). Years in which either of the thresholds is reached are defined as critical years. The main assumption is that predictions in the Committed forecast resemble present-day sea ice conditions. The critical length of the ice-free period is calculated using a reference length of the ice-free period of 134 days long calculated with this model between 2001 and 2011 using NCEP forcing, as the simulation using CGCM 3.1 (T63) output was not as accurate.

3.3 Results

3.3.1 Effect of atmospheric forcing on model SIC results

The choice of forcing field had a strong influence on the model estimate of SIC in HB. Larger differences, ranging from 25 to 60%, were found in June, July, and December – February. During these months the 20C3M hindcast underestimated the SIC by about 25% compared to the CIS estimates, while the

NCEP simulation results were within 15%. From March to May and August to November the hindcasts results where similar and compared well with the CIS SIC estimates (within 20%; Figure 3.2). Regardless of the choice forcing field, the model simulates the interannual variability of the spring SIC from 1980-2000 similar to the CIS estimates (Figure 3.3).

3.3.2 21st Century Spring SIC in HB

The forecasts show decline in the spring SIC of ~20% between 2001 and 2010. In the Committed forecast there is no further loss in spring SIC, while in B1, A1B and A2 forecasts the SIC continue to decline after 2010 (Figure 3.4). The SIC declines at a similar rate in the three forecasts from 2001-2050: -1.95% per decade in B1, -3.10% per decade in A1B, and -2.71% per decade in A2. And between 2050 and 2100 this rate remain similar in B1 at -1.92% per decade, but significantly increased to -7.04% per decade in A1B, and -10.40% per decade in A2. In B1, the mean spring SIC by the end of the century (2090-2100) is of about 50%, a loss of about 30% compared to the Committed simulation; but in A1B, the mean spring SIC is reduced to 35% and in A2 the mean spring SIC is about 23% by the end of the century (Figure 3.4), a loss of 45% and 55%, respectively, compared to Committed.

The pattern of sea ice loss is similar in the three scenarios, but the timing and extension of the ice-free region is earlier and larger in A2 > A1B > B1

(Figure 3.5). According to B1, James Bay (JB) is predicted ice-free to be by 2080, but sea ice losses are not large in northern, eastern, or western HB. In A1B and A2, JB is predicted to be ice-free as early as 2050, and by 2060 the ice-free region extent north-east. In A1B, the ice-free area in 2060 extents from JB to Cape Henrietta Maria to Inukjuak, and in A2 it extents further north to Ivujivik, and after 2060 it expands northwest significantly affecting the sea ice extension and concentration in WH. Although the extension of the sea ice cover is similar in A1B and A2 from 2060-2080, the SIC per grid point is much lower in A2 than A1B (e.g., in 2080 the SIC per grid point ranges between 50 and 60% in A2, while in A1B it ranges from 70 to 80%). The largest changes are predicted from 2090-2100, where in A1B, sea ice is only found north of the 58ºN longitude and in SICs below 50%, except for a small area in the northwest (62ºN - 65ºN) where there is a maximum SIC of 80%. Conditions are exacerbated in scenario A2, where during the last decade HB is practically ice-free, with small amounts of sea ice only in the northwest, north of 64ºN, and with SIC that does not exceed 30% (Figure 3.5). In this scenario WH becomes ice-free in 2098, but mean SIC within WH is below 50% much earlier by 2080.

3.3.3 21st Century seasonal ice cycle in WH

Significant changes in WH seasonal cycle, especially after 2035 are predicted in the B1, A1B and A2 forecasts (Figure 3.6 and 3.7). Although, anomalies of the break-up date and length of the ice-free period show large

interannual variability, there is a clear and strong trend towards the advance in the break-up date and a lengthening of the ice-free period throughout the 21st century (Figure 3.6 and 3.7, Table 3.2 and 3.3). The rate at which each of parameter changes is function of the forcing data (e.g., the rate of change is faster and larger in A2 > A1B > B1). Before 2035 there is no detectable trend in the predicted break-up date or length of the ice-free period compared to the Committed simulation. However, from 2035-2100, there is a positive trend towards the advance of the break-up date of +0.2 days per decade in B1, +0.8 days per decade in A1B, and +1.5 days per decade in A2 (Figure 3.6). The break-up date advances by the end of the 21st century (2087-97) range from 2 weeks in B1 to 2 months in A2 (Table 3.2). At the same time, the ice-free period is predicted to lengthen by +0.2 weeks per decade in B1, +1.4 weeks per decade in A1B, and +2.5 weeks per decade A2 from 2035-2100 (Figure 3.7); and, compared to Committed simulations, the mean length of the ice-free period by the end of the century (2087-97) is predicted to be 1 month longer in B1, 2.2 months longer in A1B, and 4 months longer in A2 (Table 3.3).

The three warming simulations show that critical years can occur at any time during the 21st century, however, these are sporadic before 2040, and very frequent after 2050, especially in A1B and A2 (Figure 3.8 and 3.9). In the three simulations, the years in which the ice-free period is longer than 180 days are more common than those with a 1 month advance in the break-up date. For example, during the second half of the 21st century, 26% of the years meet the

criteria of a critical ice-free period length in B1, 66% in A1B, and 80% in A2, while years with critical break-up dates are only a 14% of the years in B1, 52% in A1B, and 66% in A2. In general, predictions indicate that after 2050, there will be usually 2 critical years per decade in B1, 5 to 7 critical years per decade in A1B, and 8 to 10 critical years per decade in A2.

3.4 Discussion

The contrasting results of the hindcast simulations is most likely a consequence of the different atmospheric forcing used, which emphasizes the dominant role of atmospheric forcing on the SIC field in HB (Maxwell, 1986, Saucier et al., 2004, Wang et al., 1994b). The 20C3M hindcast uses the outputs from a coarse resolution climate model, CGCM 3.1 (T63), while the NCEP hindcast uses the more realistic and higher resolution atmospheric fields of NCEP/DOE reanalysis II. A comparison of the two forcing fields conducted for the Arctic Ocean revealed large differences in the amplitude and direction of the 10 m wind fields (Hu, 2012). Similar observations are noted in Kwok, (2011), where CGCM 3.1 (T63) output fields of wind and sea ice drift differed clearly from those obtained using passive microwave satellite data (SSMI). In the same study, CGCM 3.1 (T63) simulated higher sea ice drift and misrepresented the location of the Beaufort Gyre (shifted southeast) compared to SSMI charts. Other

studies have shown that CGCM 3.0 and 3.1 are among the models predicting largest sea ice losses with global warming in the Arctic (Rampal et al., 2011) and HB (Gagnon and Gough, 2005a). The rapid losses of sea ice in this models could be a consequence of higher sea ice drift due to the stronger winds generated by CGCM 3.1 (Kwok, 2011). Supporting this hypothesis is the large difference between the Committed and B1 SIC simulation, which use the same oceanic forcing from CGCM 3.1 (T63)-B1, but different atmospheric forcing.

In contrast, in this model, the simplifications in the ocean dynamics makes the sea ice predictions conservative, especially towards the end of the 21st century, when there is a partial sea ice cover. Because of the simplifications, the mode does not consider the strengthening of the ocean currents with the sea ice cover declines (Prinsenberg, 1986a, Rampal et al., 2011), and the ocean currents in eastern HB have a significant contribution in the export of sea ice into Hudson Strait (Saucier et al., 2004, Wang et al., 1994c). In the model, sea ice drift is mainly driven by the winds which accumulates the sea ice in eastern HB (Wang et al., 1994c, Saucier et al., 2004). Therefore, one should look at the predictions with caution and note that sea ice conditions could be much worse for polar bears in HB.

The B1, A1B and A2 predictions are unlikely to affect polar bears in WH before 2040, because the SIC, the sea ice area, and the seasonal cycle in WH are not significantly affected before 2040. However, the three scenarios predict sporadic critical years during these 4 decades that could significantly affect the

survival of a population that is already in decline. Also, the three scenarios predict that sea ice will disappear from JB by 2040, which is a concern for the southern Hudson Bay (SH) population of polar bears that use this area (Peacock et al., 2010, Stirling et al., 2004).

In B1, changes in the sea ice area and SIC in spring after 2040 are mainly in eastern and southern HB. This could suggests that polar bears in WH may not be at risk, however, the seasonal cycle in WH is largely affected by the increase of the ice-free period with 1-2 critical years per decade, which could significantly affect the population that is already in decline. In A1B and A2 simulations, the sea ice area and concentration are predicted to rapidly decline after 2050. The predicted pattern of sea ice loss is from south-east to northwest, similar to the one predicted by (Joly et al., 2010) using the A2 scenario and a fully dynamic sea ice-ocean model for 2041-70.

The sea ice predictions in A1B and A2 threaten the persistence of the WH population. Although in A1B, the sea ice in spring does not disappear from WH in the 21st century, the predicted sea ice area and concentration in spring after 2080 are unlikely to support a polar bear population. The sea ice predictions for scenario A2 are the most alarming. In this scenario, the spring sea ice area in WH is reduced by more than half and the SIC is below 50% in every year after 2080. In WH, polar bears abandon sea ice for land when the SIC in the area reach 50% (*Chapter 2* and Stirling et al., 1999), which suggests that the spring sea ice habitat predicted with scenario A2 will not be suitable for polar bears in WH after 2080.

The low SIC predicted by both scenarios, A1B and A1, also suggests that the hunting success of polar bears could be significantly affected after 2080 (Krafft et al., 2007, Stirling, 2002).

The break-up date and the length of the ice-free period predicted in B1, A1B and A2 show alarming trends throughout the 21st century. The high frequency of critical years per decade after 2060, especially in scenarios A1B and A2, threaten the survival of polar bears in WH (Molnár et al., 2011, Molnár et al., 2010). Most years after 2050 will experience an exponential decline in the population due to the high frequency of years with critical ice-free period lengths. For example, using the last estimate of the population size of 935 polar bears in 2004 by Regehr et al. (2007), and assuming that half of the population are adult males (467), each year with a critical ice-free period length, 50% of the males will not survive the fasting period (Molnár et al., 2010). In a decade with 3 critical years (e.g., B1 after 2080, or A1B and A2 after 2050) the adult male population could be reduced to 58 males. Further, adult males were thought to be among the least affected group because they do not expend energy on growth or lactation (Molnár et al., 2010). Therefore similar or larger declines could be expected in all other age classes. This survival declines will combine with slow population growth after 2060 due to a significantly earlier break-up date is predicted to compromise females' reproductive ability by up to 100%.

Based on the predictions of SIC and critical years, WH region will likely become unsuitable habitat for a polar bears population near mid-century.

Although the frequency of critical years is much lower in B1 simulation compared to A1B and A2, only a few critical years per decade could result in major population declines. More research will be required to determine how resilient the polar bear population is, and how many critical years per decade can a population withstand, to more accurately assess the threat of each scenario. Results from this work could also presage the future challenges of polar bear populations at higher latitudes where the ice cover is expected to become a seasonal event (Koenigk et al., 2011, Rampal et al., 2011).

3.5 Conclusion

I used a high resolution finite element sea ice-ocean model to predict sea ice changes in Hudson Bay (HB) due to climate warming through the 21st century. The main focus was to assess the threat of global warming on the polar bear population in WH. I used atmospheric and oceanic forcing from global warming scenarios proposed by the IPCC: B1, A1B, and A2. From 2001-2040, sea ice predictions are similar in three scenarios, with no significant changes in the spring SIC in WH, however JB is ice-free by 2040. In B1, WH is not significantly affected by the loss of SIC in spring; however the seasonal cycle is affected by at least one critical year per decade after 2050. Although, impact of the sea ice changes on the population will depend largely on the resilience of the WH

population, even one critical year per decade could have devastating consequences to the WH population when added onto the existing demographic conditions. The sea ice predictions made for A1B and A2 after mid-century are most threatening to polar bears in WH. The two scenarios predict that HB loses more than half of the spring sea ice cover in most years after 2060, with the remaining sea ice confined to northwest HB in low SIC, and that the frequency of critical years per decade is high, < 5 in 2060-70 and < 7 after 2070. Such sea ice conditions suggest that WH will not be able to sustain a population of polar bear after 2060. However, current demographic trends of the population suggest that they may be significantly threatened with only one or two critical years per decade, and hence, the population in WH may be threatened much earlier than 2060.

A rapid and early sea ice loss from JB and eastern HB from 2001-2050, suggests that the SH population will be threatened earlier and endure significant climate change-impact before the WH population. However, currently this population is considered stable and no impact of climate change have been detected yet.

Although validation of the model showed good representation of SIC in HB, it is possible that this prediction underestimate the SIC in HB, especially in eastern HB and in years with partial sea ice cover when ocean currents become more important in exporting sea ice out of HB. Follow up research with a fully dynamic ocean model is recommended to determine if ocean currents will

strengthen in HB in association with the effects on SIC and sea ice loss patterns. Studies in the Arctic Ocean suggest that stronger ocean currents accelerate sea ice loss. Such studies would help increase the accuracy of estimates sea ice loss in SH due to global warming, and the threat to the polar bears. Further research in the field of dynamic energy budget models applied to polar bears could increase the understanding of how resilient are the polar bear populations, and how many critical years per decade can each population withstand. The application of these models to other polar bear populations will contribute to the identification of thresholds on each population that can be use to predict critical habitat conditions and obtain better understanding on the threat of climate change on each of the polar bear populations.

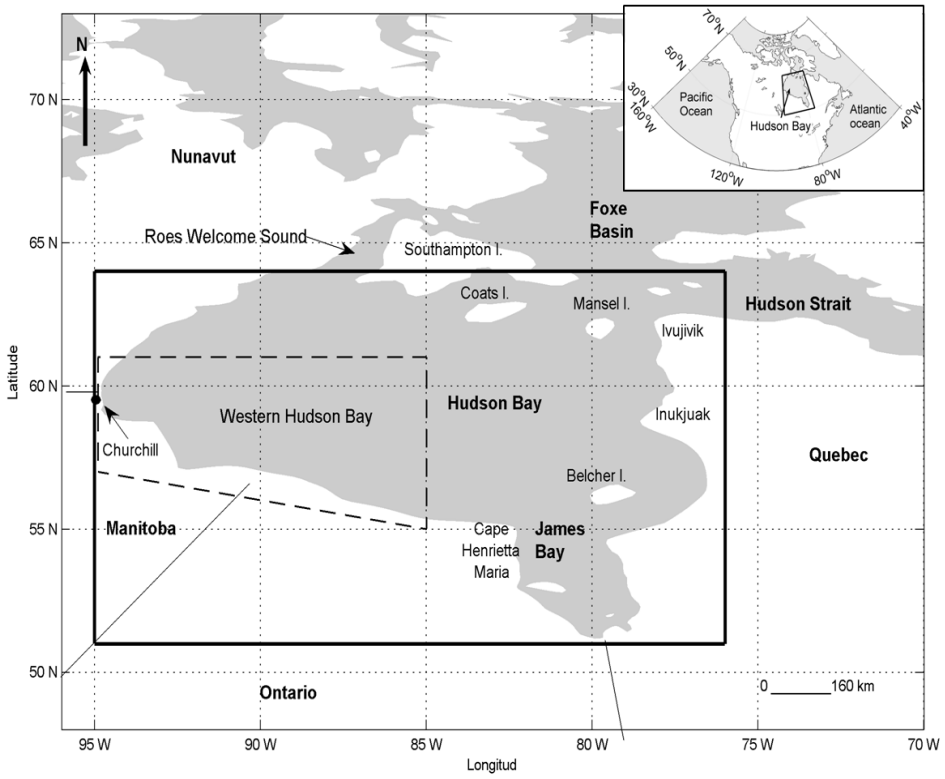

Figure 3.1 Study area location within the North American sub-continent (top-right corner). Hudson Bay area and Western Hudson Bay subsections are indicated by the solid rectangle and the dashed polygon, respectively. The Western Hudson Bay subsection is the minimum convex polygon defined by the 95% area used by polar bears in WH (2004-09).

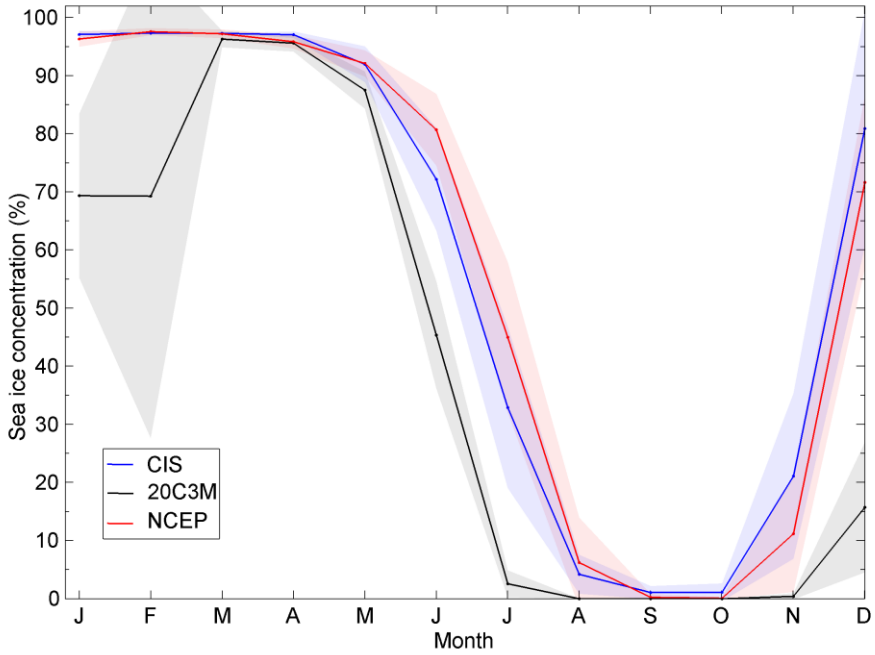

Figure 3.2 Mean monthly SIC in HB (solid line) and standard deviation (shaded area) for the period 1979-2000, calculated using CIS data (blue), and the model using two different atmospheric forcing fields: NCEP-DOE reanalysis II (NCEP; red), and CGCM 3.1 (T64) - 20C3M output (20C3M; balck).

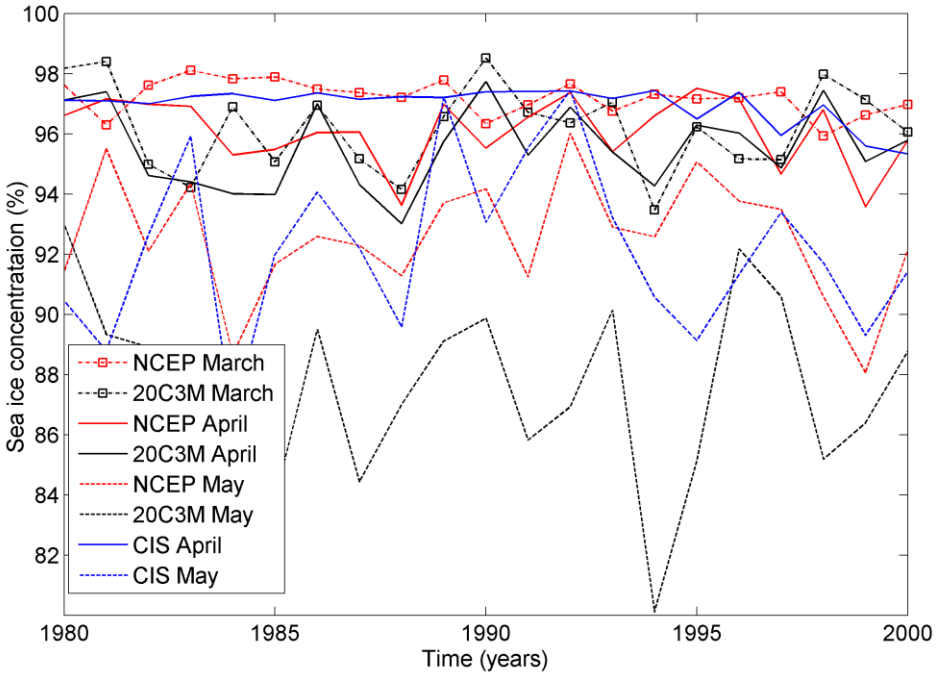

Figure 3.3 Interannual variability of the mean SIC in March (datched lines with squares), April (solid lines), and May (dotted lines without squares) for 1980-2000, and calculated using CIS data (blue), and the model using two different atmospheric forcing fields: NCEP-DOE reanalysis II (red), and CGCM 3.1 (T64) - 20C3M output (black). CIS missing data in March: no sufficient weekly charts were available to calculate a mean monthly SIC in March.

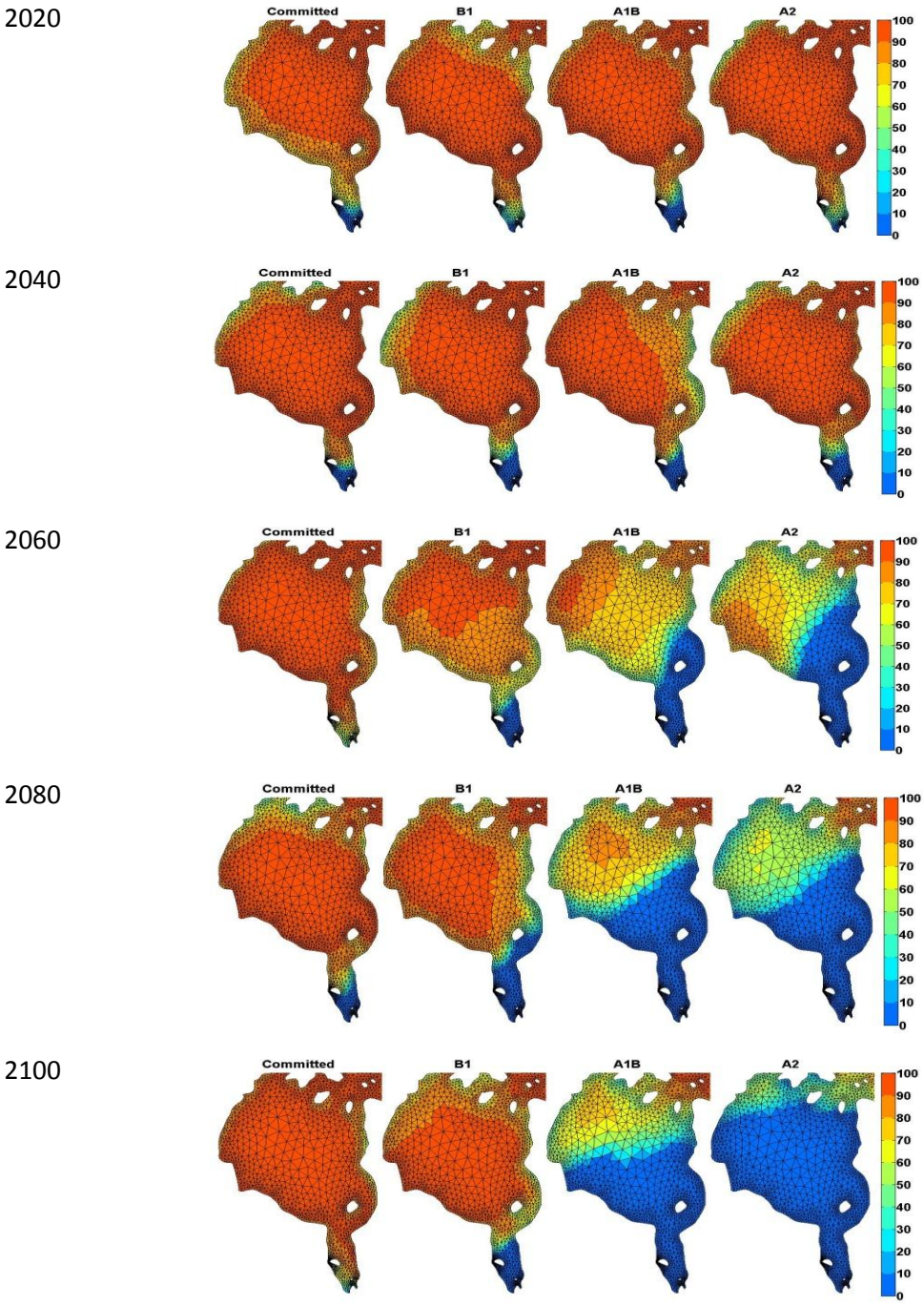

Figure 3.4 Predicted spring (mean March-May) SIC in HB for scenarios Committed (first column), B1 (second column), A1B (third column), and A2 (forth column).

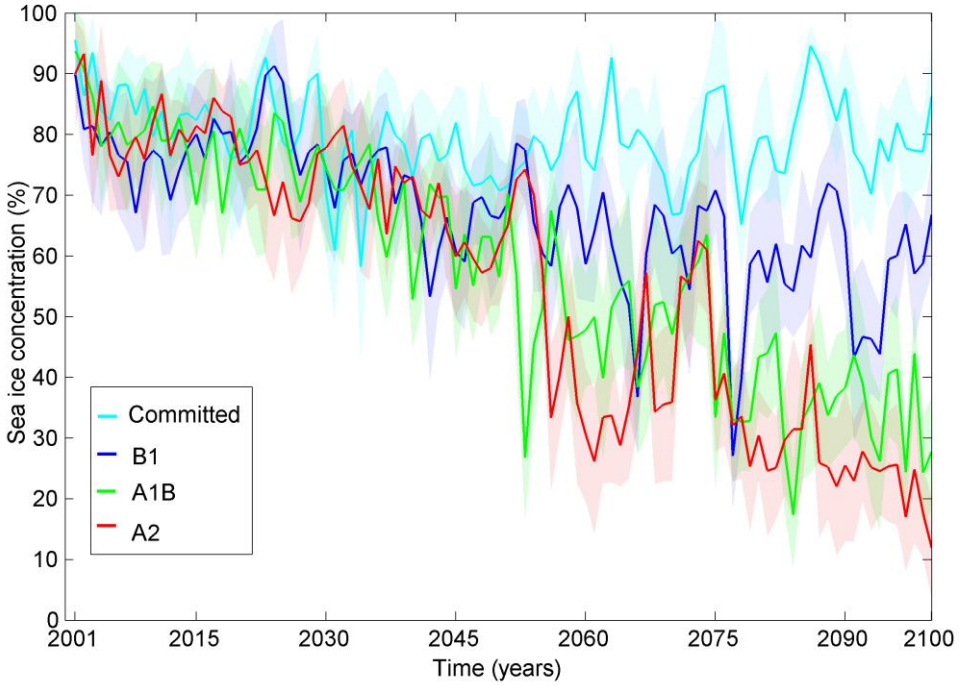

Figure 3.5 Trend in the mean spring (March-May) SIC in Hudson Bay (solid lines) through the 21st century (2001-2100) ± one standard deviation (shaded area). Predictions were produced with a high resolution finite-element sea ice-ocean model forced with atmospheric data from CGCM 3.1 (T63) -IPCC scenarios: Committed (light blue), B1 (blue), A1B (green), and A2 (red).

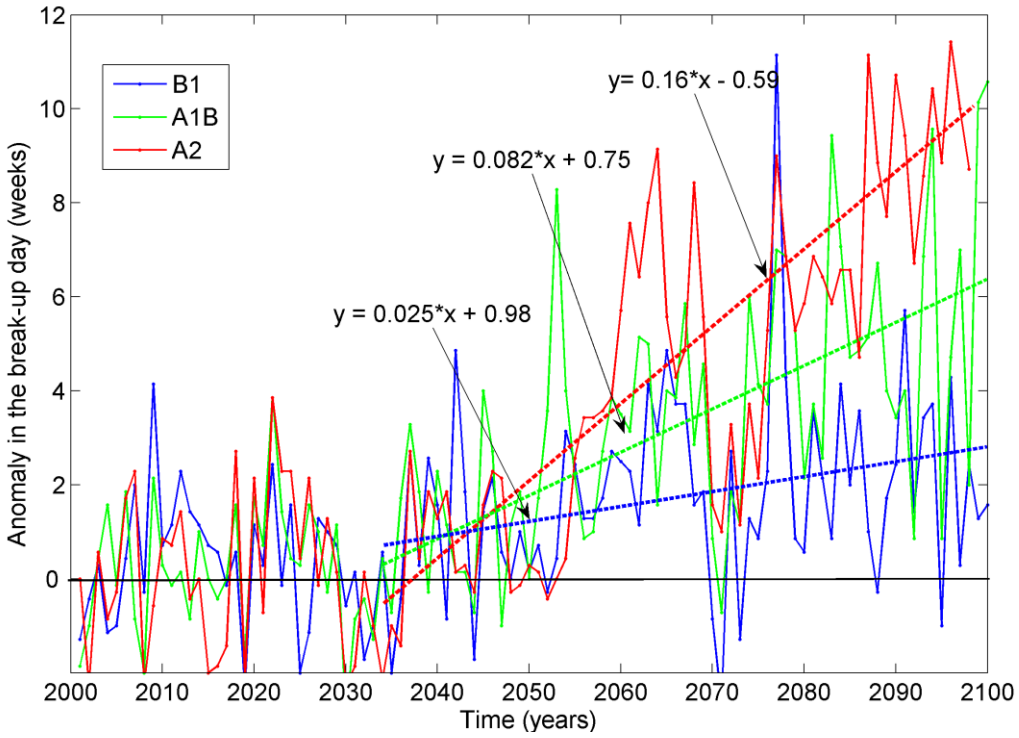

Figure 3.6 Trend in WH's break-up day anomalies* through the 21st century for IPCC scenarios: B1 (blue line), A1B (green line), and A2 (red line). Trends (dashed line) together with the corresponding linear equations are shown for 2035-2100 for each scenario. Predictions were produced with a high resolution finite-element sea ice-ocean model forced with atmospheric data from CGCM 3.1 (T63) for corresponding IPCC scenario. *Anomalies are calculated as: simulation (B1, A1B or A2) - Committed simulation.

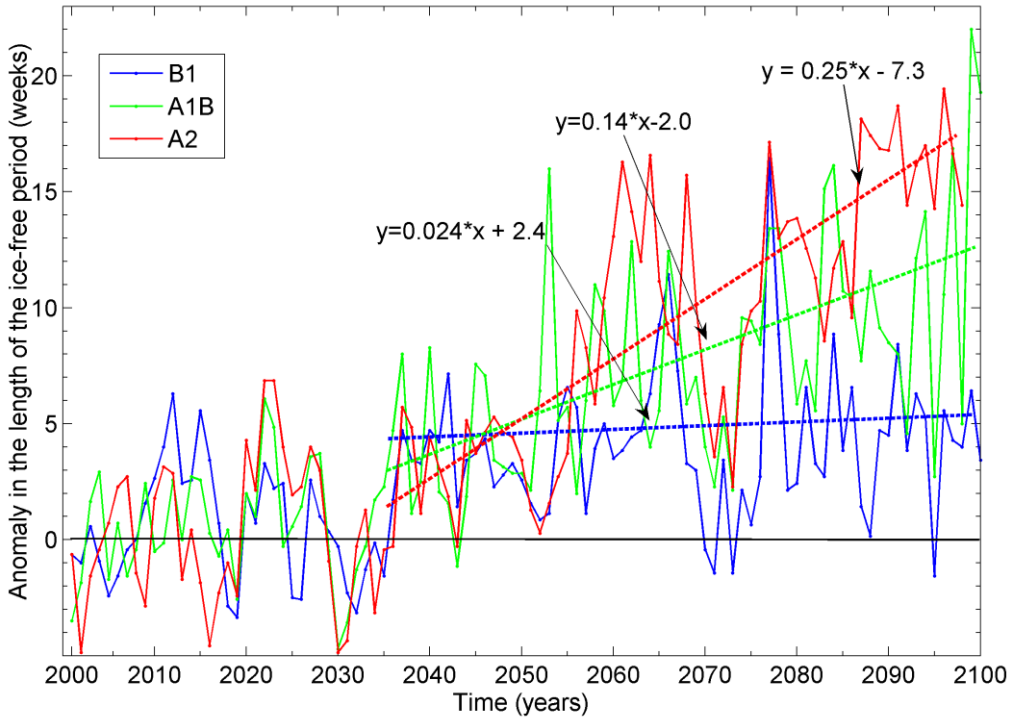

Figure 3.7 Trend in WH's length of the ice-free period anomalies* in throughout the 21st century for IPCC scenarios: B1 (blue line), A1B (green line), and A2 (red line). Linear trends (dashed line) together with the corresponding equations are shown for the period 2035-2100 for each scenario. Predictions were produced with a high resolution finite-element sea ice-ocean model forced with atmospheric data from CGCM 3.1 (T63) from the corresponding IPCC scenario.

*Anomalies are calculated as: simulation (B1, A1B or A2) - Committed simulation.

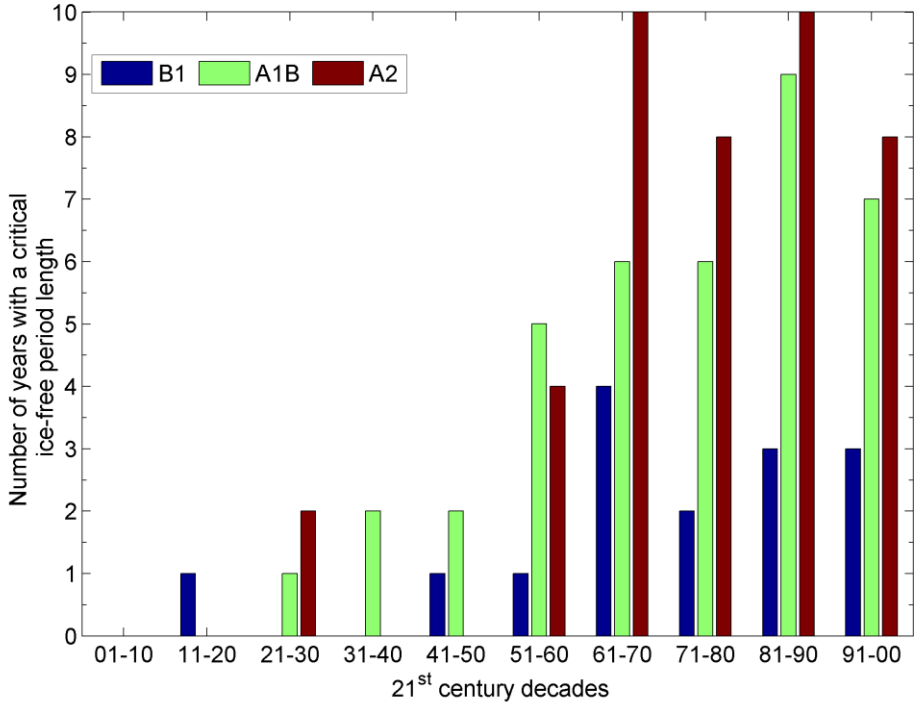

Figure 3.8 Frequency of critical years per decade in western Hudson Bay (WH) predicted by three warming scenario: B1 (blue), A1B (green) and A2 (red). A critical year is defined as a year with an ice-free period ≥180 days. An ice-free period length of 180 days is predicted to cause the death of 28-40% of adult males in WH (Molnár et al., 2010).

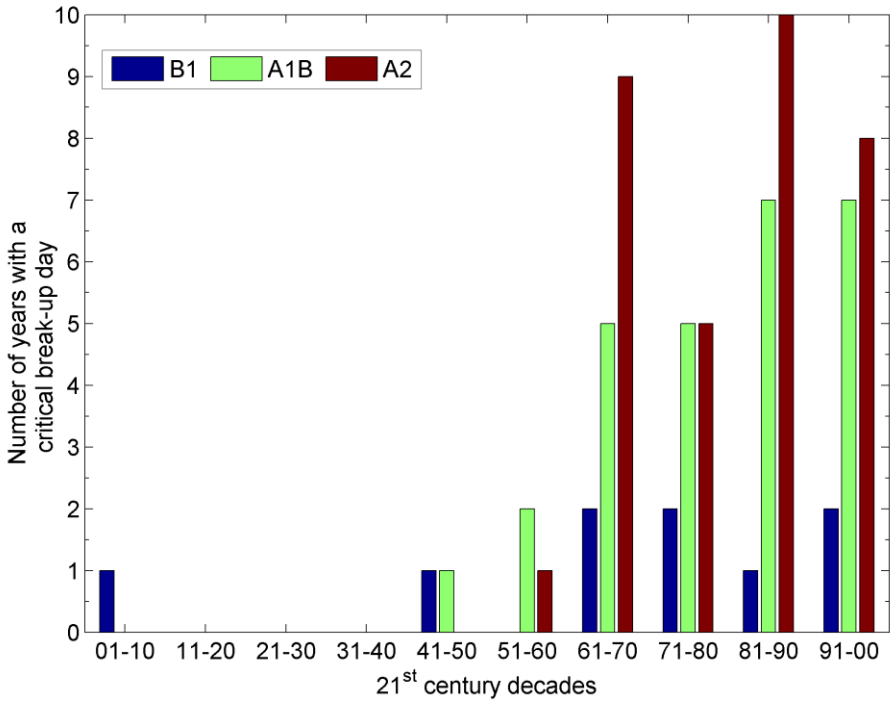

Figure 3.9 Frequency of critical years per decade in western Hudson Bay (WH) predicted by three warming scenario: B1 (blue), A1B (green) and A2 (red). A critical year is defined as a year in which spring ice break-up has advanced by ≥ 1 month relative to 1990s. Advances in the break-up date of 1 and 2 month are predicted to cause large female reproductive failure (40-73% and 55-100%, respectively) and to significantly reduce recruitment (22-67% and 44-100%, respectively) (Molnár et al., 2011).

Table 3.1 Selection of parameters and values used in the model run

PARAMETER	VALUE
Critical ice thickness	h_o= 0.05 m
Critical ice concentration	A_o= 0.15
Melting temperature	T_{Amelt}= 273.16 K
Stefan Boltzmann's constant	σ= 5.67e-8 W/m^{2}K^4
Thermal conductivity ocean-ice	K_{Oi}= 1.0e^{-3}
Thermal conductivity ice	K_i= 2.17 W / m K
Thermal conductivity snow	K_s= 0.31 W / m K
Albedo frozen snow $T_A \leq$ 273.16 K	α_{sd}= 0.85
Albedo melting snow $T_A \geq$ 273.16 K	α_{sw}= 0.73
Albedo frozen ice	α_{id}= 0.75
Albedo melting ice	α_{iw}= 0.66
Albedo sea water	α_O= 0.10
Water density	ρ_O=1025 kg/m^3
Ice density	ρ_i= 910 kg/m^3
Snow density	ρ_s= 290 kg/m^3
Air density	ρ_A= 1.3 kg/m^3
Volumetric heat capacity of water	CC=4.20e^6 j/m^{3}K
Volumetric latent heat of sea ice	C_i= 3.02e8 j/m^3
Specific heat capacity of air	C_{pA}=1004 J/kgK
Latent heat of evaporation	L_V= 2.500e^6 J/kg
Latent heat of sublimation	L_S= 2.834e^6 J/kg
Bulk sensible and latent heat transfer coefficients	C_{dS}=C_{dL}= 1.75e^{-3}
Heat transfer coefficient ocean-sea ice	γ_t= 1.0e^{-4}
Constant latent heat fluxes over ocean	Q_{SO}= 17.2694
Constant latent heat fluxes over ice	Q_{Si}= 21.8745
Latent heat over water	T_{QO}= 237.3 K
Latent heat over ice	T_{Qi}= 265.5 K
Drag coefficient of wind over ice	C_{DAI}= 1.32e^{-3}
Drag coefficient of wind over ocean	C_{DAO}= 1.0e^{-3}
Drag coefficient of ocean over ice	C_{DOI}= 3.0e^{-3}

Table 3.2 Mean anomalies* of the occurrence of the break-up day during the indicated decades in the 21st century for scenarios B1, A1B and A2.

TIME PERIOD	MEAN AND STANDARD DEVIATION IN DAYS FOR		
	B1	A1B	A2
2001-2011	2.9 (11.1)	0.2 (9.9)	-0.1 (10.2)
2050-2060	9.5 (8.0)	19.7 (16.4)	12.1 (12.4)
2087-2097	15.3 (14.3)	31.8 (19.4)	64 (9.9)

* Positive anomalies indicate an earlier break-up day. Anomalies are calculated as: simulation (B1,A1B or A2) - Committed simulation.

Table 3.3 Mean anomalies* of the duration of the ice-free period during the indicated decades in the 21st century for scenarios B1, A1B and A2.

TIME PERIOD	MEAN AND STANDARD DEVIATION IN WEEKS		
	B1	A1B	A2
2001-2011	0.5 (2.5)	0.5(2.4)	0.3(3.1)
2050-2060	3.4 (2.0)	6.6(4.2)	5.5 (4.2)
2087-2097	4.1 (2.7)	9.4 (4.2)	16.5 (1.7)

* Positive anomalies indicate an increase in duration of the ice-free period. Anomalies are calculated as: simulation (B1,A1B or A2) - Committed simulation.

3.6 References

Demaster, D. P. & Stirling, I. 1981. *Ursus Maritimus*. *Mammalian Species*, 145, 1-7.

Derocher, A. E., Lunn, N. J. & Stirling, I. 2004. Polar bears in a warming climate. *Integrative and Comparative Biology*, 44, 163-176.

Derocher, A. E. & Stirling, I. 1990. Distribution of polar bears (*Ursus maritimus*) during the ice-free period in western Hudson Bay. *Canadian Journal of Zoology* 68, 1395-1403.

Derocher, A. E. & Stirling, I. 1995a. Estimation of polar bear population size and survival in western Hudson Bay. *Journal of Wildlife Management*, 59, 215-221.

Derocher, A. E. & Stirling, I. 1995b. Temporal variation in reproduction and body-mass of polar bears in western Hudson Bay. *Canadian Journal of Zoology*, 73, 1657-1665.

Derocher, A. E., Wiig, Ø. & Andersen, M. 2002. Diet composition of polar bears in Svalbard and the western Barents Sea. *Polar Biology*, 25, 448-452.

Gagnon, A. S. & Gough, W. A. 2005a. Climate change scenarios for the Hudson Bay region: An intermodel comparison. *Climatic Change*, 69, 269-297.

Gagnon, A. S. & Gough, W. A. 2005b. Trends in the dates of ice freeze-up and breakup over Hudson Bay, Canada. *Arctic*, 58, 370-382.

Gough, W. A. & Allakhverdova, T. 1998. Sensitivity of a coarse resolution ocean general circulation model under climate change forcing. *Tellus Series a-Dynamic Meteorology and Oceanography,* 50, 124-133.

Gough, W. A. & Allakhverdova, T. 1999. Limitations of using a coarse resolution model to assess the impact of climate chance on sea ice in Hudson Bay. *Canadian Geographer,* 43, 415-422.

Gough, W. A., Cornwell, A. R. & Tsuji, L. J. S. 2004. Trends in seasonal sea ice duration in southwestern Hudson Bay. *Arctic,* 57, 299-305.

Gough, W. A. & Wolfe, E. 2001. Climate change scenarios for Hudson Bay, Canada, from general circulation models. *Arctic,* 54, 142-148.

Hammill, M. O. & Smith, T. G. 1991. The role of predation in the ecology of the ringed seal in Barrow Strait, Northwest Territories, Canada. *Marine Mammal Science,* 7, 123-135.

Hochheim, K. P. & Barber, D. G. 2010. Atmospheric forcing of sea ice in Hudson Bay during the fall period, 1980-2005. *Journal of Geophysical Research-Oceans,* 115.

Hochheim, K. P., Lukovich, J. V. & Barber, D. G. 2011. Atmospheric forcing of sea ice in Hudson Bay during the spring period, 1980–2005. *Journal of Marine Systems,* 88, 476-487.

Hu, X. January 2012. Personal comunication.

Hunke, E. C. & Dukowicz, J. K. 2002. The elastic-viscous-plastic sea ice dynamics model in general orthogonal curvilinear coordinates on a sphere-incorporation of metric terms. *Monthly Weather Review,* 130, 1848-1865.

JOLY, S., Senneville, S., Caya, D. & Saucier, F. J. 2010. Sensitivity of Hudson Bay Sea ice and ocean climate to atmospheric temperature forcing *Climate Dynamics,* 36, 1835-1849.

Kalnay, E., et al. 1996. The NCEP/NCAR 40-year reanalysis project. *Bulletin of the American Meteorological Society*, 437-470.

KAnamitsu, M., Ebisuzaki, W., Woollen, J., Yang, S., Hnilo, J. & Potter, G. 2002. NCEP-DOE AMIP II reanalysis (R-2). *Bulletin of the American Meteorological Society*, 1631-1642.

Koenigk, T., Doscher, R. & Nikulin, G. 2011. Arctic future scenario experiments with a coupled regional climate model. *Tellus Series a-Dynamic Meteorology and Oceanography,* 63, 69-86.

Krafft, B. A., Kovacs, K. M. & Lydersen, C. 2007. Distribution of sex and age groups of ringed seals (*Pusa hispida*) in the fast-ice breeding habitat of Kongsfjorden, Svalbard. *Marine Ecology-Progress Series,* 335, 199-206.

Kwok, R. 2011. Observational assessment of Arcitc Ocean sea ice motion, export, and thickness in CMIP3 climate simulations. *Journal of Geophysical Research*, 116, 1-8.

Lietaer, O., Fichefet, T. & Legat, V. 2008. The effects of resolving the Canadian Arctic Archipelago in a finite element sea ice model. *Ocean Modelling,* 24, 140-152.

Manabe, S., Ploshay, J. & Lau, N.-C. 2011. Seasonal variation of surface temperature change during the last several decades. *Journal of Climate,* 24, 3817-3821.

Markus, T., Stroeve, J. C. & Miller, J. 2009. Recent changes in Arctic sea ice melt onset, freezeup, and melt season length. *Journal of Geophysical Research-Oceans,* 114.

Maxwell, J. B. 1986. A climate overview of the Canadian Inland Seas. *In:* Martini, I. P. (ed.) *Canadian Inland Seas.* New York: Elsevier Science Publishers Company Inc, 79-99 pp.

Molnár, P. K., Derocher, A. E., Klanjscek, T. & Lewis, M. A. 2011. Predicting climate change impacts on polar bear litter size. *Nature Communications,* 2, DOI: 18610.1038/ncomms1183.

Molnár, P. K., Derocher, A. E., Thiemann, G. W. & Lewis, M. A. 2010. Predicting survival, reproduction and abundance of polar bears under climate change. *Biological Conservation,* 143, 1612-1622.

Mysak, L. A., Ingram, R. G., Wang, J. & Vanderbaaren, A. 1996. The anomalous sea-ice extent in Hudson Bay, Baffin Bay and the Labrador Sea during three simultaneous NAO and ENSO episodes. *Atmosphere-Ocean,* 34, 313-343.

Parkinson, C. L. & Washington, W. M. 2007. A large-scale numerical model of sea ice. *Journal of Geophysical Research,* 9527-9538.

Parks, E. K., Derocher, A. E. & Lunn, N. J. 2006. Seasonal and annual movement patterns of polar bears on the sea ice of Hudson Bay. *Canadian Journal of Zoology,* 84, 1281-1294.

Peacock, E., Derocher, A. E., Lunn, N. J. & Obbard, M. 2010. Polar bear ecology and management in Hudson Bay in the face of climate change *In:*

Ferguson, S. H., Loseto, L. L. & Mallory, M. L. (eds.) *A little less Arctic: Top predators in the world's largest northern inland sea, Hudson Bay.* London: Springer, 95-115 pp.

Prinsenberg, S. J. 1986a. The circulation pattern and current structure of Hudosn Bay. *In:* Martini, I. P. (ed.) *Canadian Inland Seas.* New York: Elsevier Science Publishers Company Inc, 187-204 pp.

Prinsenberg, S. J. 1986b. Salinity and temperature distribution of Hudson Bay and James Bay. *In:* Martini, I. P. (ed.) *Canadian Inland Seas.* New York: Elsevier Science Publishers Company Inc, 163-186 pp.

Prinsenberg, S. J. & Freeman, N. G. 1986. Tidal heights and currents in Hudson Bay and James Bay. *In:* Martini, I. P. (ed.) *Canadian Inland Seas.* New York: Elsevier Science Publishers Company Inc, 205-215 pp.

Rampal, P., Weiss, J., Dubois, C. & Campin, J. M. 2011. IPCC climate models do not capture Arctic sea ice drift acceleration: Consequences in terms of projected sea ice thinning and decline. *Journal of Geophysical Research-Oceans,* 116.

Ramsay, M. A. & Stirling, I. 1988. Reproductive biology and ecology of female polar bears (*Ursus maritimus*). *Journal of Zoology,* 214, 601-634.

Regehr, E. V., Lunn, N. J., Amstrup, S. C. & Stirling, L. 2007. Effects of earlier sea ice breakup on survival and population size of polar bears in western Hudson bay. *Journal of Wildlife Management,* 71, 2673-2683.

Rode, K. D., Amstrup, S. C. & Regehr, E. V. 2010a. Reduced body size and cub recruitment in polar bears associated with sea ice decline. *Ecological Applications,* 20, 768-782.

Rode, K. D., Reist, J. D., Peacock, E. & Stirling, I. 2010b. Comments in response to "Estimating the energetic contribution of polar bear (*Ursus maritimus*) summer diets to the total energy budget" by Dyck and Kebreab (2009). *Journal of Mammalogy,* 91, 1517-1523.

Saucier, F. J. & Dionne, J. 1998. A 3-D coupled ice-ocean model applied to Hudson Bay, Canada: The seasonal cycle and time-dependent climate response to atmospheric forcing and runoff. *Journal of Geophysical Research-Oceans,* 103, 27689-27705.

Saucier, F. J., Senneville, S., Prinsenberg, S. J., Roy, F., Smith, G., Gachon, P., Caya, D. & Laprise, R. 2004. Modelling the sea ice-ocean seasonal cycle in Hudson Bay, Foxe Basin and Hudson Strait, Canada. *Climate Dynamics,* 23, 303-326.

Semtner, A. J. 1976. Model for thermodynamic growth of sea ice in numerical intestigations of climate. *Journal of Physical Oceanography,* 6, 379-389.

Shein, K. A., et al. 2006. State of the climate in 2005. *Bulletin of the American Meteorological Society,* 87, S6-S102.

Smith, T. G. 1980. Polar bear predation of ringed and bearded seals in the land-fast sea ice habitat. *Canadian Journal of Zoology,* 58, 2201-2209.

Stirling, I. 2002. Polar bears and seals in the eastern Beaufort Sea and Amundsen Gulf: A synthesis of population trends and ecological relationships over three decades. *Arctic*, 59-76.

Stirling, I., Lunn, N. J. & Iacozza, J. 1999. Long-term trends in the population ecology of polar bears in western Hudson Bay in relation to climatic change. *Arctic*, 52, 294-306.

Stirling, I., Lunn, N. J., Iacozza, J., Elliott, C. & Obbard, M. 2004. Polar bear distribution and abundance on the Southwestern Hudson Bay Coast during open water season, in relation to population trends and annual ice patterns. *Arctic*, 57, 15-26.

Stirling, I. & McEwan, E. H. 1975. Caloric value of whole ringed seals (*Phoca hyspida*) in relation to polar bear (*Ursus maritimus*) ecology and hunting behavior. *Canadian Journal of Zoology*, 53, 1021-1027.

Stirling, I. & Øritsland, N. A. 1995. Relationships between estimates of ringed seal (*Phoca hispida*) and polar bears (*Ursus maritimus*) populations in the Canadian Arctic. *Canadian Journal of Fisheries and Aquatic Sciences*, 52, 2594-2612.

Stirling, I. & Parkinson, C. L. 2006. Possible effects of climate warming on selected populations of polar bears (*Ursus maritimus*) in the Canadian Arctic. *Arctic*, 59, 261-275.

Terwisscha van Scheltinga, A. D., Myers, P. G. & Pietrzak, J. D. 2010. A finite element sea ice model of the Canadian Arctic Archipelago. *Ocean Dynamics*, 60, 1539-1558.

Thiemann, G. W., Derocher, A. E. & Stirling, I. 2008. Polar bear (*Ursus maritimus*) conservation in Canada: an ecological basis for identifying designatable units. *Oryx,* 42, 504-515.

Timmermann, R., Danilov, S., Schroter, J., Boning, C., Sidorenko, D. & Rollenhagen, K. 2009. Ocean circulation and sea ice distribution in a finite element global sea ice-ocean model. *Ocean Modelling,* 27, 114-129.

Wang, J., Mysak, L. A. & Ingram, R. G. 1994a. A 3-Dimensional numerical-simulation of Hudson Bay summer ocean circulation- topographic gyres, separations and coastal jets. . *Journal of Physical Oceanography,* 24, 2496-2514.

Wang, J., Mysak, L. A. & Ingram, R. G. 1994b. Internal variability of sea-ice cover in Hudson Bay, Baffin Bay and the Labrador Sea. *Atmosphere-Ocean,* 32, 421-447.

Wang, J., Mysak, L. A. & Ingram, R. G. 1994c. A numerical-simulation of sea-ice in Hudson Bay. *Journal of Physical Oceanography,* 24, 2515-2533.

Watts, P. D. & Hansen, S. E. 1987. Cyclic starvation as a reproductive stratergy in the polar bear. *Symposia of the Zoological Sociaty of London,* 57, 305-318.

Chapter 4 . Conclusions

I conducted interdisciplinary research where I examined the performance of a recently developed sea ice-ocean model simulating the sea ice concentration (SIC) and seasonal cycle in Hudson Bay (HB). The model was intended to produce 21st century predictions of the mentioned sea ice parameters and highlighted the potential impact on polar bear (*Ursus maritimus*) populations in HB because sea ice declines have deleterious effects on recruitment and survival of bears. Monthly SIC fields were validated using the Canadian Ice Service (CIS) data; I also include in the validation the Passive Microwave Satellites (PMW) data because I needed daily fields of SIC. Results from this analysis showed that the model could produce accurate estimates of SIC, however it also revealed small overestimation during break-up and small underestimation during freeze-up. These comparison also showed that the PMW data had significant error during break-up, and thus the daily estimates could not be use to validate the seasonal cycle in HB. Therefore, to validate the seasonal ice cycle, I used GPS telemetry data from polar bears in Western Hudson Bay (WH). This is the first study in which polar bear telemetry data is used in this manner. The polar bear telemetry data suggested that the PMW data was significantly underestimated during break-up, and that the model was overestimating the sea ice extent however, mainly in eastern and southern HB. It also suggested a delay in the model sea ice formation. I also used the polar bear GPS data was to calibrate the model's seasonal cycle

with the migration of polar bears. The strong correlation between SIC and polar bear migration made possible this calibration. This was a necessary step to more accurate detect the potential effects of climate change on polar bear recruitment and survival in WH through the 21st century.

The 21st century sea ice conditions were predicted using warming proposed by the IPCC in scenarios Committed, B1, A1B and A2. In the Committed scenario CO_2 concentrations are maintain at 330ppm, while in B1, A1B and A2 CO_2 concentrations increase linearly from 330ppm in 2001 to 550ppm, 720ppm, and 800ppm, respectively, by 2100. To isolate the warming effects and avoid introducing errors with the atmospheric forcing data, I calculated the anomalies using the Committed as a control scenario. The future rate and magnitude of sea ice losses are highly dependent on warming whereby the rate of loss is faster and larger in A2 > A1B >> B1. In the three scenarios the spring SIC is significantly reduced, however only in scenarios A1B and A2 and after 2060, in scenario B1, the spring SIC in WH is not affected. The three scenarios however, predict that the WH seasonal ice cycle will be greatly affected by warming, with critical years becoming most abundant after 2070. In B1 there are only a few critical years per decade, but in A1B and A2, the frequency of critical years is high, with more than 5 critical years per decade. If these predictions for scenarios A1B and A2 are realized it is doubtful that a polar bears will survive in WH after 2060, without considering that the current trends in the population size, which indicates that even one critical years could have a

devastating effect on the population survival and recruitment that could threaten the population before 2040. The sea ice predictions in B1 for the next century are kinder than in A1B and A2, however, they are still threatening for polar bears. Regardless of the scenario, if the predictions are realized polar bear population survival in WH will be threatened.

The three scenarios predict the complete loss of the spring sea ice in Southern Hudson Bay (SH) by 2060, this suggests that the SH polar bear population will suffer from global warming earlier than the WH population. Currently this population is considered stable [PBSG 2011]. More rigorous monitoring of polar bears in this area may be necessary to assess the early trend in the population, and detect signs of decline.

This research has provided new information with application and importance in the fields of conservation biology, Arctic biology, and oceanography. A newly developed sea ice-ocean model is introduced and demonstrated to produce SIC in similar accuracy to observations by the CIS regardless of the simplifications of the ocean model. The overestimations in eastern HB, supports previous work that suggested that ocean currents have an important role in the advection of heat and sea ice in eastern HB. The inclusion of polar bear GPS data is a technique with potential applications in other regions of the Arctic where polar bear telemetry studies are conducted. The 21st predictions could contribute to the management and conservation of the polar bears in WH, and raise awareness on the need to develop and/or improve mitigation strategies

for communities and settlements in areas where polar bears habit in summer. In the years with longer ice-free period these communities are likely to experience higher number of polar bear-human interactions which may lead to negative outcomes for both parties. Improved mitigation techniques can help preserve the safety of the communities and reduced unnecessary problem kills.

Further analysis of the model in eastern HB using GPS data from polar bears in the SH population would be useful to estimate the magnitude of the delays in the melting of the sea ice in the east. A sensitivity study that measures the effect of restoring on model's performance could help identify the cause of the 4 day delay in the formation of the sea ice in northwest HB and nearshore. The application of the model in other polar bear-occupied regions could contribute to the identifications of strength and weakness of the model. Also, following-up this research with the fully dynamic ocean model could further help assess the effect of ignoring ocean dynamics in the simulation of SIC in HB and specifically in eastern HB. This type of research could help managers determining how many critical years per decade can a polar bear population withstand, and thus, more accurately assess the impact of the 21st century predictions made in this thesis.

Appendix 1. Model description

A. General details

The model is a Finite Element Sea ice Ocean Model (FESOM), however, it uses a slab-ocean model instead of a multilevel ocean model. The sea ice model is fully prognostic and is coupled to the slab-ocean model which has simplified dynamics. The model was made to focus and increase the understanding on the sea ice dynamics in the Arctic and subarctic and it was first described in Terwisscha van Scheltinga et al. (2010).

The model requires atmospheric forcing of daily air temperature (T_a), sea level geostrophic wind components, and monthly climatologies of relative humidity and total cloudiness. All calculations are preformed from the initial conditions where all fields are specified. The model includes two thickness categories: the actual thickness (h_r) and a thin sea ice thickness or newly formed sea ice (h_o = 0.05 m). The actual thickness is always greater than h_o. The sea ice is described by the velocity vector ($\boldsymbol{u}$), mean sea ice thickness (h) and mean sea ice concentration (A), where A is the proportion of ice of thickness h_r covering the grid cell area. The velocities are located at the edges of the triangular elements, while the scalar properties, h and A, are at the center of the elements and are constant within the grid cell.

B. Model Dynamics

The ice drift momentum equation consists of the force balance, per unit mass of ice, of all forces acting on the ice pack and integrated vertically through the ice thickness to obtain a 2-D equation (Eq1). There is controversy about which forces are most important in the calculations of ice drift, opinions vary among researchers and thus the ice dynamic formulation depends on researcher's view of which forces are most important (Parkinson and Washington, 1979, Lietaer et al., 2008, Hunke and Dukowicz, 1997). The most accepted view is that shown in Equation 1: the material derivative in left hand side decompose the acceleration term and the velocity components, and the right hand side (RHS) has: the wind stress (τ_a) and the water stress (τ_w), weighted by the ice concentration, the Coriolis force (2nd term in the RHS), the internal ice resistance ($\nabla.\sigma$), and the ocean dynamic height (4nd term RHS). The acceleration term is often neglected because it can be three orders of magnitude smaller than the terms in the RHS (Rothrock, 1975 *in* Parkinson and Washington, 1979) and (Hunke and Dukowicz, 1997)). The wind stress (Coon, 1980 *in* Hunke and Dukowicz, 1997) and the ice internal stress (Hibler, 1979, Parkinson and Washington, 1979) are thought to predominant in the balance of forces. While the ocean currents and dynamic height, are thought to be more significant over long periods (Hibler,1968 *in* Hunke and Dukowicz, 1997).

Equation 1. Time derivative of sea ice velocity per unit area of sea ice.

$$\rho h \frac{Du}{dt} = A(\tau_a + \tau_w) - \rho h f u \times k + \nabla . \sigma - \rho h g \nabla \varepsilon \quad (1)$$

ρh is the ice mass per unit area, A ice concentration, f coriolis parameter, u ice velocity, k is the unit vector normal to the surface, τ_a air surface stress, τ_w ocean surface stress, σ ice internal stress tensor, $\nabla\varepsilon$ gradient of sea surface height, $\frac{Du}{dt}$ material derivative of the ice velocity per unit of time, g acceleration due to gravity.

This sea ice-ocean model, however, uses a slab ocean that is assumed to have a constant sea surface height ($\nabla\varepsilon = 0$) and no ocean currents (U_w=0) such the tilt term disappear from (1) and the ocean stress (Eq.2a) is simplified to a drag of the ocean on the sea ice. In the model, the ocean acts as a frictional surface that could slow down sea ice drift. The wind stress (Eq.2b) is the main force giving sea ice momentum. A similar approach was taken in Lietaer et al. (2008). The ocean and wind stresses follow parameterization in Hunke and Dukowicz (1997) (Eq. 2a and 2b).

Equation 2. Ocean (a) and Wind (b) stress on sea ice.

$$\tau_w = \rho_w C_w |U_w - u|(u) \quad (2a)$$

$$\tau_a = \rho_a C_D |u_{10}|(u_{10}) \quad (2b)$$

U_w ocean velocity (set as zero), u ice velocity, u_{10} wind speed at 10 m, C_w water drag coefficient, C_D wind drag coefficient, ρ_w density of water, ρ_a density of air.

The model assumes that ice of thickens h_o has no internal strength ($\nabla . \sigma$=0) thus it is at free drift, but when the ice thickness is h_r the ice pack offers more resistance. To calculate the internal ice resistance, the model uses an elastic-viscous-plastic (EVP) rheology (Hunke and Dukowicz, 1997). More details on the application of this rheology are reviewed in several key publications (Hibler, 1979; Hunke, 1997; Parkinson, 1979).

In general, the EVP-rheology describes the same physical behavior of the sea ice as the viscous-plastic (VP) rheology (Hibler, 1979) however with greater numerical ease. The VP and EVP rheology algorithms allow the ice pack to diverge with little to no stress, but to resist compression and shearing under convergent conditions. In both rheologies, the sea ice is described as non-linear viscous-plastic material which absolute (η) and relative (ζ) viscosity increases with pressure (P) and decreasing strain rates ($\dot{\epsilon}$) as the following relation shows: $\zeta = \frac{P}{2\dot{\epsilon}}$ and $\eta = \frac{P}{2e^2\,\dot{\epsilon}}$, and assuming the elliptical yield curve axis ratio is e=2. Where the strain rate is a measure of the deformation of the material, and it is inversely related to the internal strength, and the internal strength increases with pressure and thickness. Numerical problems, however, arise in the limit of zero strain rate (large thickness) as the effective viscosity becomes infinitive. It is in the attempt to regulate this numerical problem that the two rheologies exist. The VP rheology (Hibler, 1979) applies a constant value for the viscosity when strain rates become very small, and the ice pack moves undergoing a very slow creep almost as a solid material, however, this regularization has numerical difficulties,

especially when applied to small mesh spacing (Hunke and Dukowicz, 1997). The EVP offers a much simpler numerical regulation to solve this limit, without significantly changing the ice behavior of Hibler's solution.

Once ice velocity components have been calculated, the sea ice in the grid cell is redistributed to the endpoint of the vector, maintaining thickness and compactness. Velocity components tangential to the coast are unaffected by continental boundary conditions, but velocity components leading onto land grid point are reduced to zero and the sea ice volume within the cell may increase as a result of convergence depending on the thickness and the previous time step.

C. Model thermodynamics

The thermodynamic approach in the sea ice-ocean model is similar to the one described in Lietaer et al. (2008) and Parkinson and Washington (1979) in that the model ignores density stratification of the ocean and uses a vertically homogeneous mixed layer of constant depth, H_{mxl}, equal to 30 m. The temperature and salinity of the ocean are calculated based on this depth and using prognostic equations for corresponding fluxes are used (Eq. 3 & 4).

Equation 3. Oceanic heat flux

$$Q_H + R_T = \rho_w \times C_{pw} \times H_{mxl} \times \frac{\delta T_w}{\delta t} \quad (3)$$

Equation 4. Oceanic freshwater flux

$$Q_S + R_S = H_{mxl} \times \frac{\delta S_w}{\delta t} = (S_0 - S_i)\frac{\rho_i}{\rho_w}\left(\frac{\delta h}{\delta t}\right)_{th} + S_0\frac{\rho_{sn}}{\rho_w}\left(\frac{\delta h_s}{\delta t}\right)_{th} \quad (4)$$

Q_S oceanic heat flux, Q_S oceanic freshwater flux, ρ_w density of the sea water, C_{pw} heat capacity of sea water, T_w temperature of the sea water, S_w salinity of the sea water, and α_w albedo of sea water, δt is a constant time step (= 95 s), H_{mxl} is the constant depth of the mix layer. R_T and R_S are the oceanic flux/restoring term and the salinity restoring term, respectively. S_0 ocean salinity. S_i sea ice salinity ($S_i = 5$g/kg), ρ_i density of sea ice, $\frac{\delta h}{\delta t}$ sea ice thickness time derivative. $\frac{\delta h_s}{\delta t}$ snow thickness time derivative. ρ_{sn} density of snow.

The ocean time step was 95 seconds. The freshwater flux (Q_S, Eq. 4) considers thermodynamic changes in the sea ice and snow, and differentiate the precipitation in either the form of snow or rain. Precipitation accumulates on the sea ice or fall in the ocean depending weather there is ice or not in the grid cell, respectively. The amount of precipitation is determined in the forcing data. The snow accumulation due to sea ice convergence or drift is not taken into account in the freshwater flux. The oceanic heat and freshwater fluxes are restored to the climatological temperature (T_{mxl}) and salinity (S_{mxl}) of the mixed layer by including the restoring terms, R_T and R_s, respectively. The model uses a relaxation time scale of 180 days and the set of equation 5.

Equation 5. Restoring terms for temperature (a) and salinity (b)

$$R_T = \rho_w \times C_{pw} \times H_{mxl} \times \gamma_t \times (T_{mxl} - T_w) \quad (5a)$$

$$R_S = H_{mxl} \times \gamma_t \times (S_{mxl} - S_w) \quad (5b)$$

H_{mxl} depth of the mix layer, $\gamma_t$is the relaxation constant ($6.43 \times 10^{-8} s^{-1}$). ρ_w density of sea water. C_{pw} heat capacity of sea water. T_w temperature of the sea water, S_w salinity of the sea water, T_{mxl} temperature of the mixed layer, S_{mxl} salinity of the mixed layer.

Thermodynamic calculations of sea ice thickness and concentration are based on energy balances at three interfaces: atmosphere-ice (A-I), ice-ocean (I-O), and atmosphere-ocean (A-O). Atmosphere energy fluxes are described below and their relation is shown in Equation 6. Energy fluxes from the mixed layer are determined by differences in temperatures between interfaces. The heat diffusion within the sea ice is based on a zero-layer model (Semtner, 1976), thereby sensible and latent heat storage within the ice are neglected.

Equation 6. Atmospheric fluxes

$$F_A + F_c = 0, \text{ where } F_A = (1 - \alpha) \times F_r + F_L + F_s + F_l \quad (6)$$

F_A net atmospheric flux (in the A-O interface $F_A = Q_H$), F_c conductive heat flux through ice, F_r parameterization of shortwave radiation, F_L parameterization of long wave radiation, F_s turbulent flux of sensible heat, F_l turbulent flux of latent heat, α surface albedo,

Atmospheric fluxes in (6) are computed using the empirical parameterizations in (Parkinson and Washington, 1979). The authors describe a parameterization for short wave radiation (F_r) that accounts for latitudinal variations, vapor pressure, and intrannual changes in cloud cover, using a solar constant of 1353 W m^{-2}. Our model includes a varying sea ice albedo depending on surface: water, melting ice, frozen ice, dry snow or wet snow. The long wave radiation flux (F_L) is modified by cloud cover, and it is a function of the 2-m atmospheric temperature (T_a), for this calculation the Stefan-Boltzmann constant is set at 5.67 x 10^{-8} W m^{-2} K^{-4}. The calculations of the sensible heat (F_s) and latent (F_l) heat required the input of the 5 m wind field and T_a. In addition, the latent heat flux parameterization depends on humidity fields from forcing data, and the use of the latent heat of vaporization or sublimation constants depend on the interface (A-O or A-I, respectively). Sensible and latent heat storage within the ice are neglected: heat diffusion within the sea ice is based on the zero layer model of Semtner (1976). For parameters values refer to Tables 2.1 and 3.1.

At the A-I interface the sea ice ablation at the surface of sea ice (S_{hr}^{su}) depends on the equilibrium between atmospheric surface temperature (T_a) and volumetric latent heat fusion of sea ice (L_i) (Eq 7a). If atmospheric fluxes are positive and predicted surface temperature is T_a > 0ºC, the T_a is lowered to the melting point (T_a = 0ºC) using the difference to warm and melt the sea ice. When T_a < 0ºC, T_a is increased to the melting point (T_a = 0ºC) and heat fluxes through

the sea ice are negative and sea ice thickness may increase. Therefore sea ice melting usually occurs when $S_{hr}^{su} < 0$ while sea ice formation may occur when $S_{hr}^{su} > 0$.

At the I-O interface the processes are to the A-I, however, at this interface the rate of sea ice ablation at the bottom of the sea ice (S_{hr}^{b}) depends on the balance between oceanic heat flux and the latent heat absorbed by sea ice (Eq 7b). If the oceanic heat flux is positive and larger than heat fluxes through the sea ice, then sea ice melts.

Equation 7. Thermodynamic changes in the sea ice thickness at the surface (a) and bottom (b)

$$S_{hr}^{su} = -\frac{F_A + F_c}{L_i} \quad (7a)$$

$$S_{hr}^{b} = \frac{F_c - Q_H}{L_i} \quad (7b)$$

The S_{hr}^{su} and S_{hr}^{b} are the sea ice changes at the the surface and bottom of sea ice, respectively. F_A is the net atmospheric flux, F_c is the conductive flux through sea ice, L_i is the volumetric latent heat of fusion of sea ice.

At the A-O interface positive energy fluxes into the mixed layer ($Q_H > 0$) act to increase the water temperature (T_w), while negative heat fluxes, $Q_H < 0$, decrease T_w. However T_w can only decrease to the freezing point (T_f), which depends on the salinity of the water; when energy fluxes reduced the temperature of the water such that $T_w < T_f$, then T_w is set to equal T_f and the excess energy is

used to freeze the water. The thickness of the newly formed sea ice is h_o. Therefore, for sea ice growth to occur $Q_H < 0$ and $T_w < T_f$. Sea ice formation is given by equation (8a), in which for the case of open water, A=0. The same reasoning is used in lead areas where the 0% < A < 100%. The energy input will result in the lateral formation or melting of sea ice through equation (8a) and (8b) for negative and positive Q_H respectively. The extension of the newly formed sea ice or the amount of melt depends on the balance between the atmospheric and oceanic heat fluxes shown in these equations.

Equation 8. Thermodynamic changes of the sea ice extent with freezing (a) and melting (b)

$$S_A^{acc} = -\frac{(1-A)Q_H}{L_i h_o} \quad (8a)$$

$$S_A^{abl} = -\frac{A}{2hr} \times [-(S_{hr}^{su} + S_{hr}^{b})] \quad (8b)$$

S_A^{acc} sea ice formation, A sea ice concentration, h_o constant thin sea ice thickness, L_i is the volumetric latent heat of fusion of sea ice, S_{hr}^{su} sea ice ablation at the surface and the bottom S_{hr}^{b} of sea ice of thickness *hr*, S_A^{abl} lateral melt of sea ice.

The total sea ice growth or melt is described using a linear combination of the fraction of thin ice and thick ice (Eq. 9).

Equation 9. Thermodynamic change of sea ice thickness

$$S_h = A \times (S_{hr}^{su} + S_{hr}^{b}) + S_A^{acc} \times ho + S_A^{abl} \times \left[hr + dt \times \left(S_{hr}^{su} + S_{hr}^{b}\right)\right] \quad (9)$$

hr is the actual sea ice thickness, A is the sea ice concentration, h_o thickness of newly formed sea ice, S_{hr}^{su} sea ice ablation at the surface and S_{hr}^{b} at the bottom, S_A^{acc} lateral sea ice formation, S_A^{abl} lateral melt of sea ice (Lietaer et al., 2008)

The sea ice concentration and thickness per grid cell are then calculated using continuity equations 10a and 10b, respectively.

Equation 10. Continuity equations for sea ice concentration (a) and mean sea ice thickness (b)

$$S_A = \frac{\delta A}{\delta t} + \nabla.(uA) \quad (10a)$$

$$S_h = \frac{\delta h}{\delta t} + \nabla.(uh) \quad (10b)$$

u is the velocity of the ice, h is the ice thickness, t is the time in seconds, A is the sea ice concentration which is constrained between 0 and 1 to account for mechanical redistribution of sea ice.

(A)

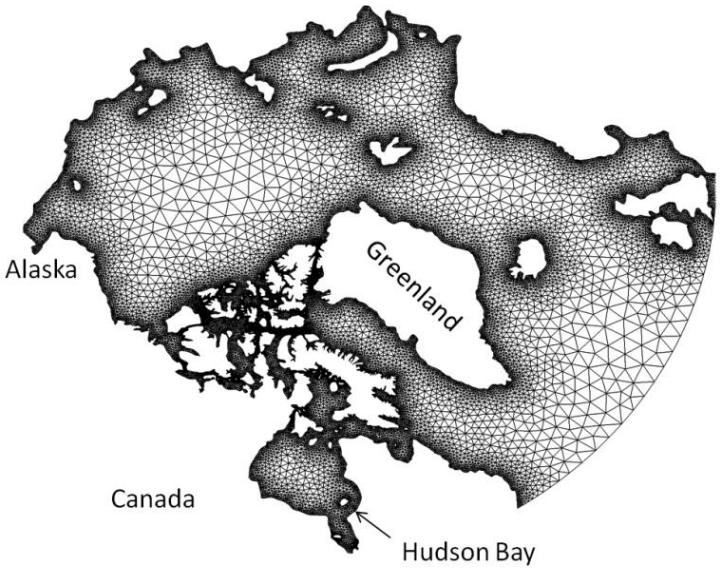

(B)

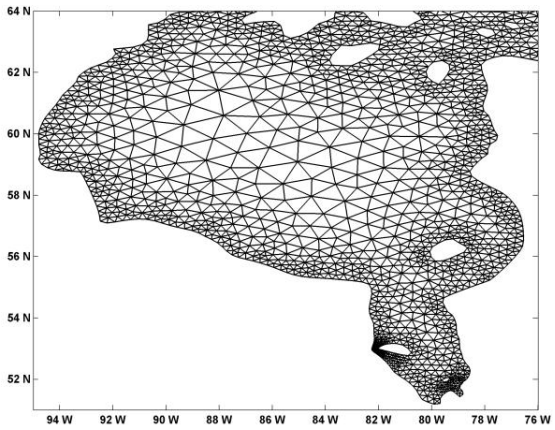

Figure 5.1 Finite element grid showing varying resolution in the full model domain north of the 50ºN (A) and zoom in Hudson Bay (B).

5.1 References

Hibler, W. 1979. A dynamic thermodynamic sea ice model. *Journal of Physical Oceanography*, 815-846.

Hunke, E. C. & Dukowicz, J. K. 1997. An elastic-viscous-plastic model for sea ice dynamics. *Journal of Physical Oceanography*, 27, 1849-1867.

Lietaer, O., Fichefet, T. & Legat, V. 2008. The effects of resolving the Canadian Arctic Archipelago in a finite element sea ice model. *Ocean Modelling*, 24, 140-152.

Parkinson, C. L. & Washington, W. M. 1979. Larege-scale numerical model of sea ice. *Journal of Geophysical Research-Oceans and Atmospheres*, 84, 311-337.

Semtner, A. J. 1976. Model for thermodynamic growth of sea ice in numerical intestigations of climate. *Journal of Physical Oceanography*, 6, 379-389.

Terwisscha van Scheltinga, A. D., Myers, P. G. & Pietrzak, J. D. 2010. A finite element sea ice model of the Canadian Arctic Archipelago. *Ocean Dynamics*, 60, 1539-1558.